2013-12-18

Carbonate Slope Morphology and Sedimentary Processes along Southwestern Great Bahama Bank

Andrew Jo
University of Miami, andrewyo97@gmail.com

UNIVERSITY OF MIAMI

CARBONATE SLOPE MORPHOLOGY AND SEDIMENTARY PROCESSES ALONG SOUTHWESTERN GREAT BAHAMA BANK

By

Andrew Jo

A THESIS

Submitted to the Faculty
of the University of Miami
in partial fulfillment of the requirements for
the degree of Master of Science

Coral Gables, Florida

December 2013

UNIVERSITY OF MIAMI

A thesis submitted in partial fulfillment of
the requirements for the degree of
Master of Science

CARBONATE SLOPE MORPHOLOGY AND SEDIMENTARY PROCESSES ALONG SOUTHWESTERN GREAT BAHAMA BANK

Andrew Jo

Approved:

_____
Gregor P. Eberli, Ph.D.
Professor of Marine Geology
and Geophysics

_____
Donald F. McNeill, Ph.D., P.G.
Scientist, Marine Geology
and Geophysics

_____
Mark Grasmueck, Ph.D.
Adjunct Associate Professor,
Marine Geology and Geophysics

_____
M. Brian Blake, Ph.D.
Dean of the Graduate School

JO, ANDREW (M.S., Marine Geology and Geophysics)
Carbonate Slope Morphology and Sedimentary Processes along Southwestern Great Bahama Bank (December 2013)

Abstract of a thesis at the University of Miami.

Thesis supervised by Professor Gregor P. Eberli.
No. of pages in text. (102)

High-resolution multibeam bathymetry and sub-bottom profile data from offshore Great Bahama Bank, covering an area of 6,500 km^2, allow an assessment of the evolution of the slope and basin environment. The data reveal a substantial variability in the slope morphology. Three different sedimentary processes (downslope mass gravity flows, margin collapse, and contour currents) control this variability in slope morphology. The deposits that result from these processes produce a consistent facies distribution along the slope, consisting of four morphofacies: 1) a steep upper slope with an onlapping sediment wedge, 2) a toe-of-slope with redeposited carbonates, 3) a basin floor covered with pelagic sediments, and 4) an elevated seafloor with pockmarks.

The margin and uppermost slope is steep and cemented, with declivities ranging from 20° to 70°. The steep slope is onlapped by a sediment wedge that reaches a thickness of 100 m and extends >5 km basinward. The lower slope and toe-of-slope is dominated by coarse-grained sediments and debris from mass-gravity flows. Most of the coarse-grained sediment is funneled through closely spaced gullies on the middle slope and deposited as turbidite beds at the toe-of-slope.

These turbidite deposits are arranged in lobes and apron system. In this area fine-grained sediment is largely winnowed away by ocean currents.

Margin and slope instability add to the strike variability. Four segments of the platform margin collapse have been identified. Margin collapse features are characterized by crooked and convex bankward morphology. The smallest collapse margin scar is 3 km long and the largest scar is more than 20 km long. The 20 km long scar eroded bankward more than 350 m and produced an extensive megabreccia on the adjacent slope and basin floor that extends tens of kilometers from the margin.

Contour currents that flow in the Old Bahama Channel transport drift sediment to the basinal are of this study where they interfinger with bank-derived the toe-of-slope deposits. The surface of the drift deposit is littered by thirty pockmarks generated by water and gas escape. The close proximity of these pockmarks to the Cuban fold and thrust belt indicates that the degassing is related to overpressure from by tectonic activity.

Keywords: multibeam bathymetry, carbonate slope, variability, density current, contour current, margin collapse, deep-water.

TABLE OF CONTENTS

LIST OF FIGURES

LIST OF TABLES

CHAPTER 1. INTRODUCTION

OVERVIEW

The slope environment is an important component of a carbonate platform. Understanding slope deposition is important for stratigraphic correlation because it links the shallow- and deep-water environments (Blomeier and Reijmer, 2002). In addition, the lateral expansion of a carbonate platform relies on slope progradation (e.g. Eberli and Ginsburg, 1989).

The platforms of the Bahamas archipelago are some of the best-studied modern carbonate platforms. This research has been driven by the need to understand processes that control platform development, to have modern analogs for subsurface characterization, and help understand climatic history. Unlike the shallow-water environment, the slope and its adjacent basin floor in the modern settings are relatively under-explored due to their limited accessibility (Playton et al., 2010). New geophysical technology has, in recent years, provided extensive seafloor topographic maps and extensive sub-bottom profiles that have added to the understanding of the processes that control the variability of carbonate slope and its adjacent basin. These new data will ultimately be able to aid prediction and help develop better reservoir models for carbonate reservoirs in a slope and basin setting. This study relies on such a new data set. The aim of this research is to delineate the sedimentary processes that control the variability of carbonate slope and basin floor morphology on the leeward side of Great Bahama Bank. The study area is located between southwestern Great Bahama Bank and the north coast of

Cuba (Figure 1.1). The data sets consist of high-resolution multibeam bathymetry, sub-bottom profile data, and multi-channel seismic data of two vintages.

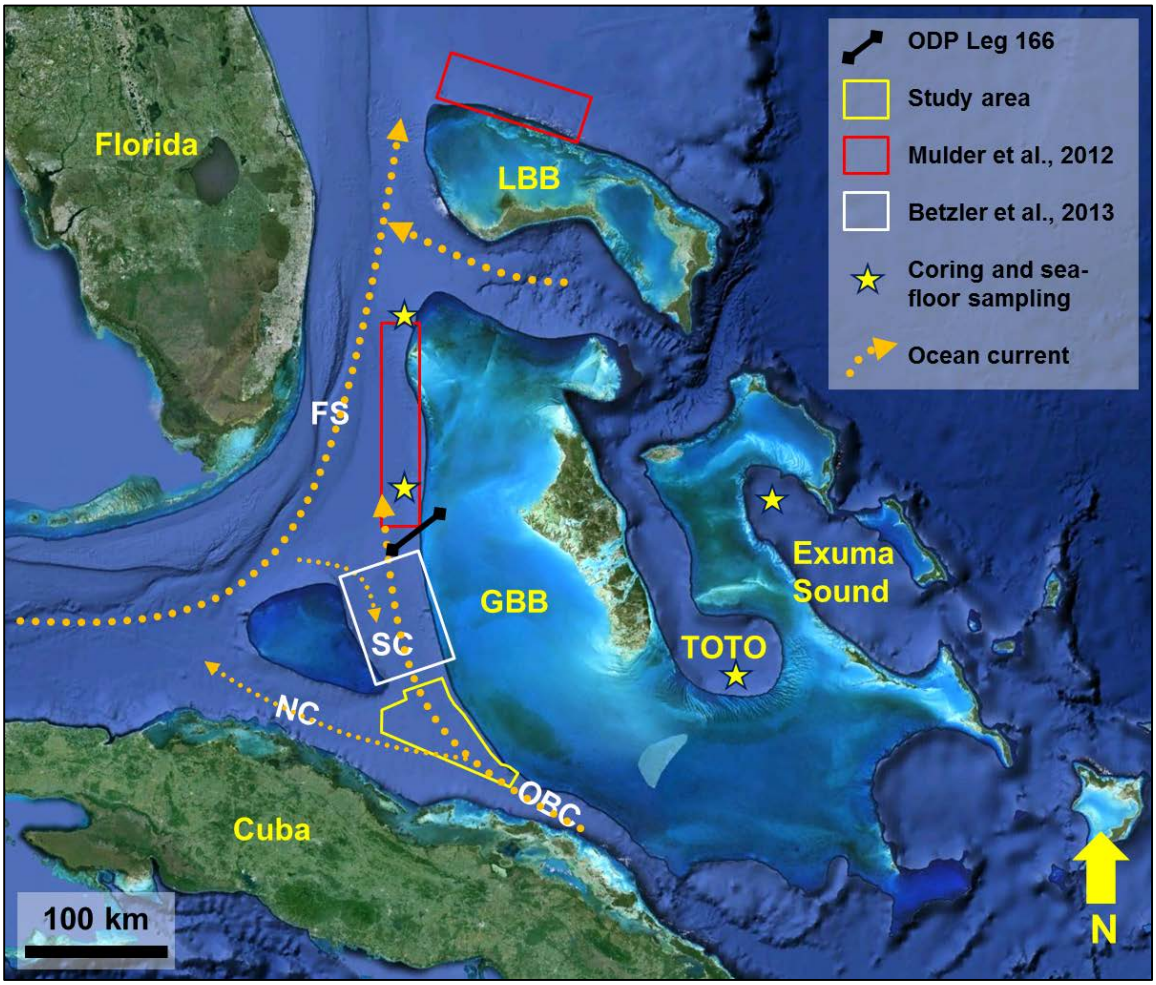

Figure 1.1. Overview of the Florida-Bahamas region with the locations where the slope and basin environments had been explored. Three deep-water areas were surveyed using high-resolution multibeam bathymetry: Santaren Channel, northwestern Great Bahama Bank, and northern Little Bahama Bank. This study area in the southwest corner of Great Bahama Bank is outlined in yellow. Yellow dashed lines represent the ocean currents. The portion of the cores drilled for the Bahamas Transect (Bahamas Drilling Project and ODP Leg 166) is in black. FS=Florida Straits, SC=Santaren Channel, NC=Nicholas Channel, and OBC=Old Bahama Channel.

North of the study area, multibeam bathymetry data show a steep margin with occasional slope failures onlapped by a sediment wedge (Mulder et al. 2012). At the point of onlap (~180 m) these sediments form a well-defined, continuous moat of up to 30 m deep (Betzler et al., 2013). Gullies and channels dissect part of the upper slope sediment wedge. These gullies funnel slope material to the basin floor where it is deposited in small lobes and fans. In these northern areas, slope failure is common on the lower slope, where large lithified slabs of the slope break loose and slide several kilometers basinward (Mulder et al., 2012a). These observations and the new data from this study area refine some of the existing slope models.

EXISTING SLOPE MODELS

A carbonate slope is markedly different from its siliciclastic counterpart, particularly in regards to the slope angle. Carbonate systems can maintain a high angle of repose of up to 55˚ (for loose material), depending on the size and roughness of the slope material (Schlager and Camber, 1986; Kenter, 1990). In addition, outward and upward biological growth of the margin and slope, and rapid submarine cementation contribute to the steep slopes of carbonate platforms. Schlager and Ginsburg (1981) proposed that as the height of the slope and its declivity increase, the slope evolves from depositional, to by-pass, to erosional (Figure 1.2). As a consequence of this steepening, the primary depositional process would change from slumping and gravity flows to turbidity currents.

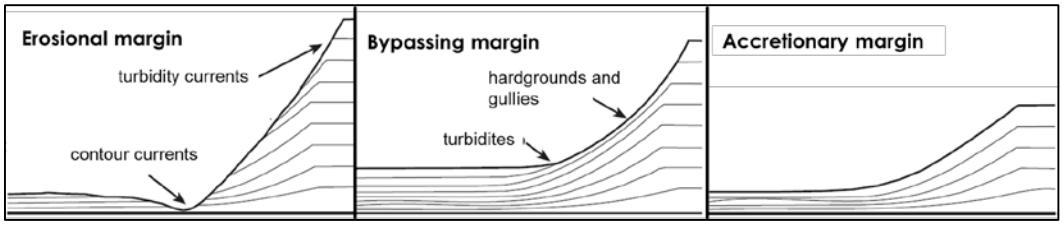

Figure 1.2. The three types of carbonate slopes: erosional, bypass, and accretionary margin proposed by Schlager and Ginsburg (1981).

The sediment transport mechanism from shallow water to deeper water is also different for carbonates and siliciclastics. Carbonate platform margins and shelves are a line source for redeposition whereas in siliciclastic systems usually a channel forms a point source for sediment dispersal into the basin (Schlager and Chermak, 1979; Mullins et al., 1984). The result of the line source is an extensive slope apron composed of grainy debris embedded in muddy matrix (Playton et al., 2010). However, margin and slope instability can lead to collapses that shed slope breccias to the toe-of-slope and basin floor. Irregularities in the slope morphology can focus sediment transport and erosion to promote channelization on the slope, and transport shallow water derived material downslope to mix with basinal carbonate in a basinal fan apron (Enos, 1973; Payros and Pujalte, 2008; Playton et al., 2010).

The morphology and architecture of carbonate slopes and the adjacent basins are controlled by numerous processes: sea level, tectonics, climate, oceanographic setting (windward or leeward), diagenesis, and sediment fabric (Schlager and Ginsburg, 1981; Mullins et al., 1984; Kenter, 1990). On the large scale, there are two recognizable carbonate slope geometries: escarpment (bypass) and accretionary (depositional) margin (Figure 1.3, McIlreath and James, 1978). These

geometries are controlled by the ability of the sediment to modify the slope profile (Playton et al., 2010). Carbonate slopes vary along the strike. Playton et al. (2010) provide a comprehensive review of the whole spectrum of variability, including both strike-continuous and strike-discontinuous deposits which are mainly controlled by margin instability.

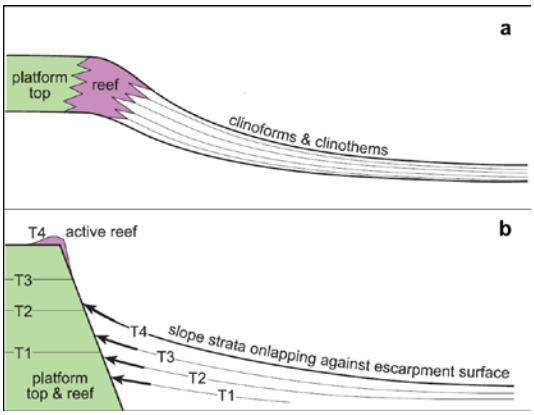

Figure 1.3. Two end members of slope profiles: a) Accretionary margin where the platform top sediments interfingers with the slope sediments, b) escarpment margin where platform top sediments are separated from the coeval slope deposits by a surface of non-deposition. (Modified from McIlreath and James,1978).

MODERN SLOPE OF THE BAHAMAS

The morphology and facies of modern Bahamian slopes have been the subject to numerous investigations: Little Bahama Bank (Mullins and Neumann, 1979; Mullins et al., 1984; Austin et al., 1988; Harwood and Towers, 1988; Mulder et al., 2012b; Rankey and Doolittle, 2012), western Great Bahama Bank (Eberli et al., 1997a; Mulder et al., 2012a), Tongue of the Ocean (Schlager and Chermak, 1979; Grammer and Ginsburg, 1992; Grammer et al., 1993) and Exuma Sound (Crevello and Schlager, 1980; Austin et al., 1988; Grammer et al., 1999). The focus of these studies and the type of data and methodology were different, however these

studies complement each other to form an integrated picture of the slope environment.

Northern Little Bahama Bank

Off of the Little Bahama Bank, an AUV was used to image the slope to a depth <300 m (Rankey and Doolittle, 2012). The uppermost slope is characterized by a gently dipping (<6˚) rocky surface at water depth <60 m, which then changes to a steep escarpment of 30-50˚ in the un-rimmed margin and 16-30˚ in the rimmed margin slope (Rankey and Doolittle, 2012). At 90-230 m water depths, the inclination decreases to 10-15˚ in the un-rimmed margin and 18-25˚ in the rimmed margin slope.

Further downslope, the slope is dissected by numerous canyons (Mullins et al., 1984; Mulder et al., 2012b). The canyons occur at >400 m water depth and initiated as slope failures and developed further through headward erosion (Mulder et al., 2012b). It was suggested that the degree of submarine cementation controls the occurrence of slope failures and the extent of canyon head erosion (Mullins et al., 1984; Harwood and Towers, 1988).

The lower slope (900-1300 m water depths) is the depocenter for the bypassed sediment. It is divided into two zones: the proximal apron and the distal apron. The proximal apron contains thick mud-supported debris-flow deposits and thick coarse-grained turbidites. The distal apron contains thinner turbidites, both coarse- and fine-grained, and grain-supported debris flows (Mullins et al., 1984). The lithoclasts incorporated in the gravity flows are resedimented lithified slope

sediment and deep-water corals, and lack shallow-water sediment (Davis, 1983). Both proximal and distal facies are interbedded with peri-platform ooze.

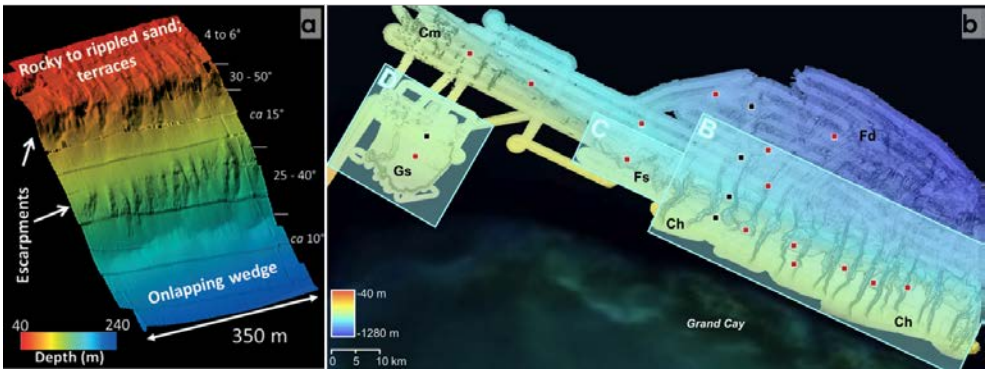

Figure 1.4. Bathymetry data of northern Little Bahama Bank show: a) uppermost slope (<300 m water depth) is characterized by a steep escarpment onlapped by a sediment wedge (Rankey and Doolittle, 2012). b) The middle and lower slope is dissected by numerous canyons that transport sediment to the basin floor (Mulder et al., 2012b).

Western Great Bahama Bank

A recent multibeam bathymetry survey conducted in northwestern slope of Great Bahama Bank (Figure 1.5) provides new insights into the slope morphology (Figure 1.5a, Mulder et al., 2012a). One of the most spectacular features is the formation of erosive furrows that are perpendicular to the margin and bend southward at their terminations (Figure 1.5b, Mulder et al., 2012a). Slope failures, kilometers in length, and their associated mass transport complexes are also common in the area. These failures start at ~450-550 m water depth on the lithified slope (Figure 1.5c, Mulder et al., 2012a). On the toe-of-slope, debris that were produced by the slope failure become the substrate for the growth of deep-water coral colonies (Figure 1.5.d, Correa et al., 2012b). The slope also contains channel-levee complexes that resemble those in siliciclastic turbidite systems (Figure 1.5e).

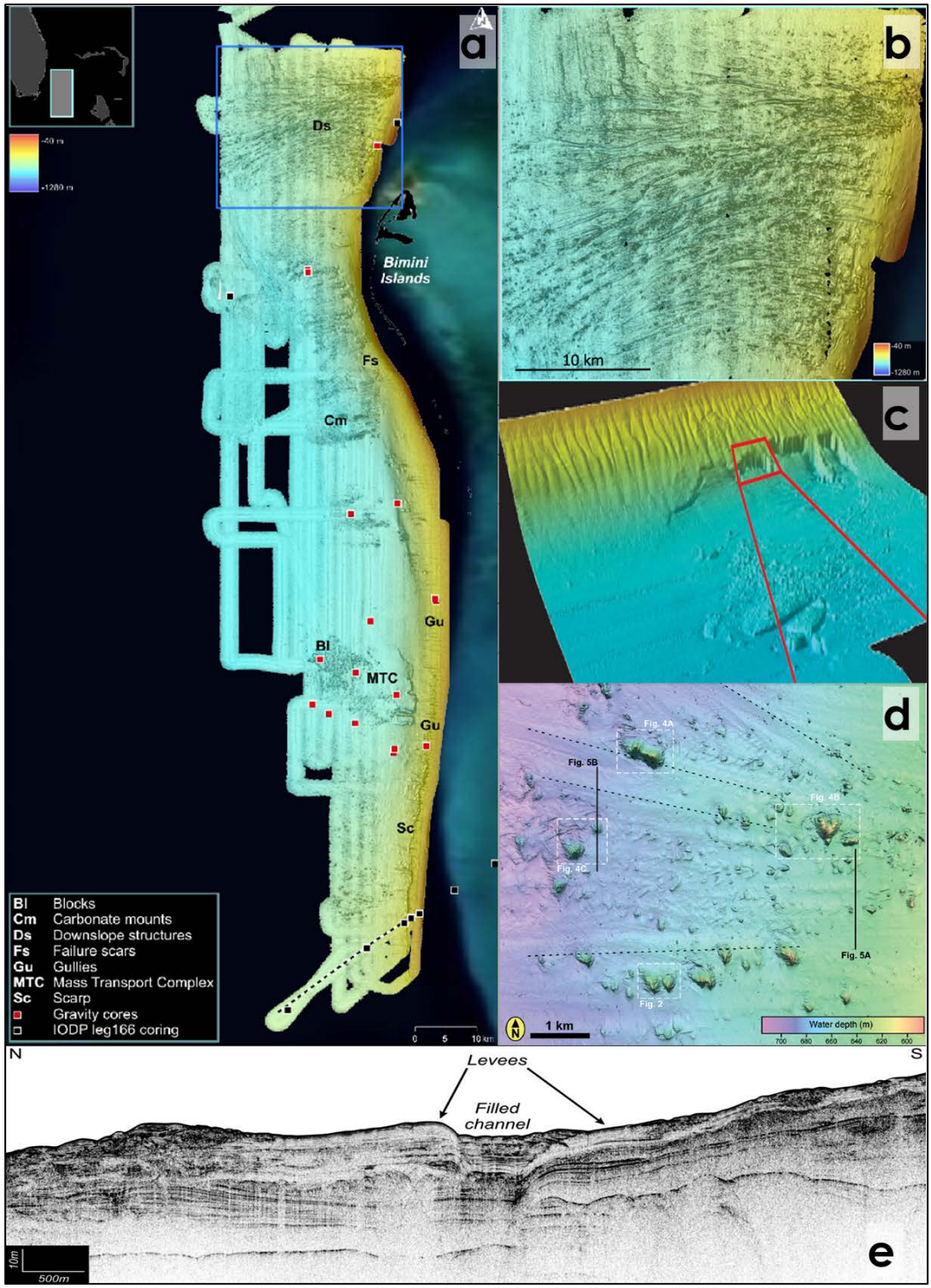

Figure 1.5. a) Multibeam bathymetry data from northwestern Great Bahama Bank show numerous features: b) erosive furrows, c) slope failures, d) blocks and debris that colonized by deep-water corals, and e) a channel-levee complex. Images a, b, c, e taken from Mulder et al. (2012a), d from Correa et al. (2012b).

Tongue of the Ocean (TOTO)

In the Tongue of the Ocean, the deep-water environment is divided into three facies belts: slope, basin margin, and basin interior (Figure 1.6.a, Schlager and Chermak, 1979). The uppermost portion of the slope consists of a near vertical (70-90˚) wall from 60-140 m water depth (Grammer and Ginsburg, 1992; Grammer et al., 1993). The wall changes to a cemented slope with slope angles of 35-45˚ at ~120 m depth. The cemented slope contains scattered large talus blocks and boulders, and lenses of coarse-grained sediments derived from the wall and platform top. Rock fall, grain flow, slumping, and grain creep are the main depositional processes in this part of the slope (Grammer et al., 1993). Below ~250 m water depth, the slope is onlapped by a sediment wedge with slope angles from 25-28˚. The point of onlap is deeper on the windward side, at >360 m depth than the leeward side. The sand fraction within the sediment wedge indicates a provenance from the outermost margin while the mud is transported from the platform interior. The lower slope is covered with peri-platform ooze and dissected by gullies in which sand and gravel occur (Schlager and Chermak, 1979). Downslope, coarse-grained turbidites and debris flow deposits transition to fine-grained turbidites in the basin interior. Slumps and debris flows are less common in TOTO than in other Bahamian basin (Schlager and Chermak, 1979).

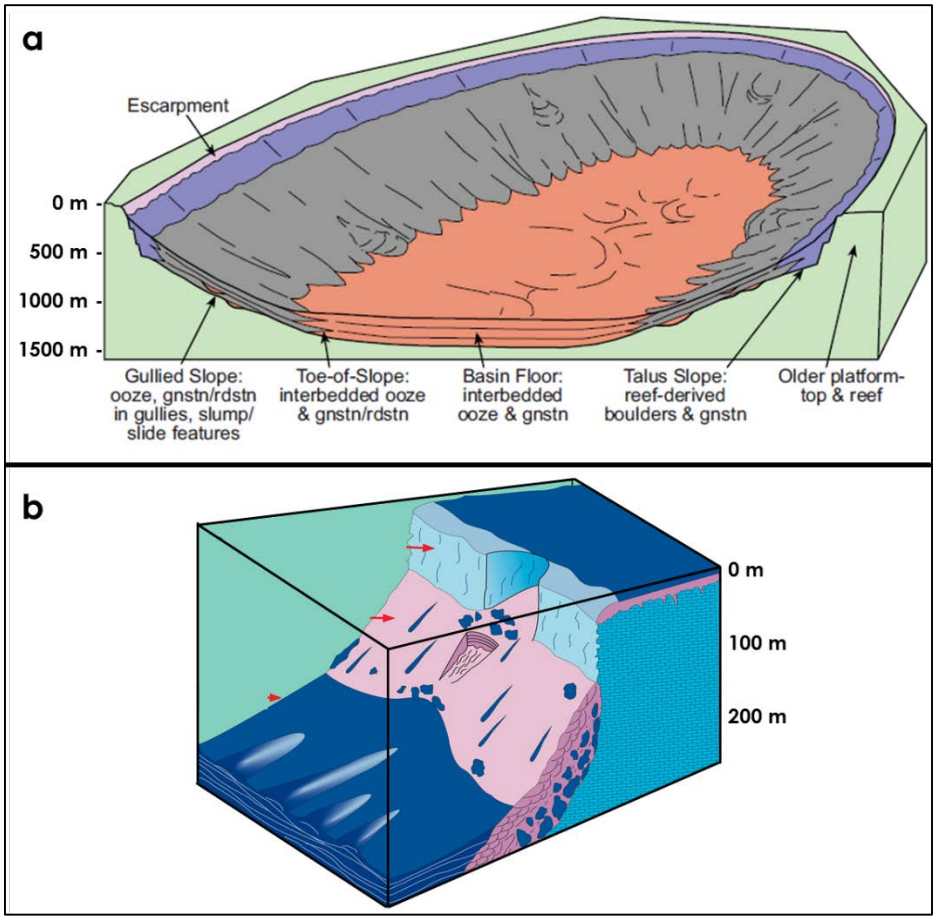

Figure 1.6. a) The Tongue of the Ocean is divided into three facies belts: slope with gullies, basin margin with coarse-grained redeposited carbonates, and the fine-grained basin interior (Schlager and Chermak, 1979). b) The uppermost portion of the slope is characterized by a steep wall. The wall transitions into a cemented slope that is onlapped by a sediment wedge (Grammer et al., 2001).

Exuma Sound

The Exuma Sound is also differentiated into three physiographic environment: gullied slope, basin margin, and basin floor (Crevello and Schlager, 1980). The lower slope and basin floor is dominated by debris flows and turbidite deposits arranged in an extensive sheet and tongue morphology respectively (Figure 1.7).

The turbidites sequence contains platform sediment, whereas the debris sheet has a mix of platform and slope materials (Crevello and Schlager, 1980).

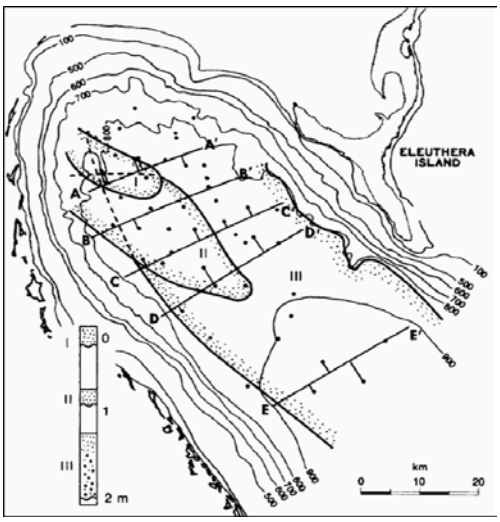

Figure 1.7. Tongues of turbidite and debris flows that were mapped using shallow coring in the Exuma Sound. These deep-water deposits are composed of platform-derived debris and were interpreted as produced by margin collapse. Image taken from Crevello and Schlager (1980).

OVERVIEW OF THE STUDY AREA

Regional Geology

The Bahamian archipelago lies between latitudes 20° and 28° N and longitudes 72° and 80° W and is one of the largest tropical carbonate platforms. Seismic data from northwestern Great Bahama Bank shows that present day Bahamas bank morphology is a result of repeated tectonic segmentation that started in the Middle Cretaceous. Subsequently, a number of these smaller platforms coalesced to form the modern GBB (Eberli and Ginsburg, 1987). Southern Great Bahama Bank underwent three major events: extension during Early-Middle Jurassic, reactivation of Jurassic faults during Middle Cretaceous caused by subsidence, and wrenching associated with Late Cretaceous to Middle Tertiary collision between Caribbean and North American plates, which cause fragmentation of the

Cretaceous platform in the south. The collision ceased in Middle to Late Eocene but active faults in the younger sequences suggest that some deformation was ongoing during the Neogene (Masaferro and Eberli, 1999).

Oceanographic processes

The Florida-Bahamas region is influenced by several ocean currents (Figure 1.1). The clockwise Loop Current originating from the Yucatan Channel circulates in the Gulf of Mexico and together with Old Bahama Current, they form the Florida current which has a mean transport of 31.7 Sv (Leaman et al., 1987). This current is the onset of Gulf Stream, which flows along the continental shelf of eastern North America. The Florida Current is responsible for basinal drift deposits and sediment waves structures in the Santaren Channel west of Great Bahama Bank (Anselmetti et al., 2000; Bergman, 2005). However, the benthic currents in the Straits of Florida consist of counter-currents, cyclones and internal tides. For example, at 600-800 m water depth along the slope of GBB, an AUV survey recorded tidal bottom current flowing in north and south direction, changing every 6 hours (Grasmueck et al., 2006).

Seasonal heat flux variations on the Bahama Banks create hyperpycnal water flows (Wilson and Roberts, 1995). These dense bank-top waters flow downslope until they reach a density compensation level. This process has been termed density cascading by Wilson and Roberts (1995). This mechanism is probably important for fine-sediment shedding from the platform to the slope and basin, for erosion by associated turbidity currents, and transport of sand to the deep basin (Wilson and Roberts, 1995).

WORKING HYPOTHESIS

The geophysical data from southwest Great Bahama Bank allows the testing of three hypotheses in regards to slope and basin development. They are:

a. The morphology of the carbonate slope along southwestern Great Bahama Bank varies along the strike and dip directions because of different sedimentary processes.

b. Large margin collapses create convex bankward morphology and shed large debris blocks to the toe-of-slope and basin floor.

c. The occurrence of pockmarks in the Santaren channel is related to shallow gas migration and controlled by regional tectonics.

TESTING OF WORKING HYPOTHESIS

In order to test the working hypotheses three main approaches are used:

a. Describe and map the morphological features of the slope and basin floor using multibeam bathymetry and sub-bottom profile data. In addition, seismic facies analysis is performed to interpret the depositional facies. This analysis is based on the internal reflection character and external morphology of the multichannel seismic data.

b. Map and quantify the margin failures and their associated debris deposits on the toe-of-slope. To estimate the extent of the margin collapse feature (i.e. convex bankward morphology) beyond the coverage of the multibeam bathymetry data, a visual inspection on the satellite imagery is performed.

c. Describe the morphology of pockmarks from multibeam bathymetry and sub-bottom profile data. An analysis of the regional multichannel seismic data is presented to interpret the genesis and controlling factors on the distribution of these pockmarks.

DATA

Multibeam bathymetry and backscatter data

The surface morphology of the slope and basin floor is characterized by multibeam bathymetry data and backscatter data acquired by Fugro Geoservices in 2011 and made available by the Bahamas Petroleum Company (BPC). These data cover an area of about 6,500 km^2 on southwest Great Bahama Bank (Figure 1.1). The bathymetry data was collected using a Reson SeaBat 8160 59 kHz Multibeam Echosounder (MBES) system, which also recoded the backscatter data. The depth range of the study area is from 20 to 670 m water depth. The surface bin resolutions for multibeam bathymetry data are 15 m in the standard survey area and 10 m in selected high resolution areas. The data set was originally intended to image sea-bottom seeps as part of a hazard assessment.

Sub-bottom profile

The high-resolution single-channel seismic survey was acquired concurrently with the multibeam bathymetry data using a GeoPulse 5430A sub-bottom profiler system that is able to transmit at frequencies from 2 to 12 kHz. The dominant frequency of the sub-bottom profile data is 3.5 kHz. The depth of penetration depends on the acoustic properties of the seabed, reaching up to 35 ms (TWT) in relatively fine-grained sediments.

Multichannel seismic data (BPC 2011 and 1981 vintage)

The top one second of nine multi-channel seismic lines are made available by BPC within the study area. The lines provide subsurface imaging useful for the analysis of the slope geometry and surface features. Several deeper 2D lines from 1981 vintage were also analyzed.

ODP Leg 166

Seven boreholes drilled during Ocean Drilling Project (ODP) Leg 166, five of which were positioned on the slope (Sites 1003, 1004, 1005, 1008, and 1009) and one on the toe-of-slope (Site 1007) and one on the drift deposit within the Santaren Channel (Site 1006). The borehole locations are shown in Figure 1.8. The ODP Leg 166 boreholes are situated north of this study area, but the nearest boreholes are Sites 1008 and 1009, ~8 km from the multibeam bathymetry data location.

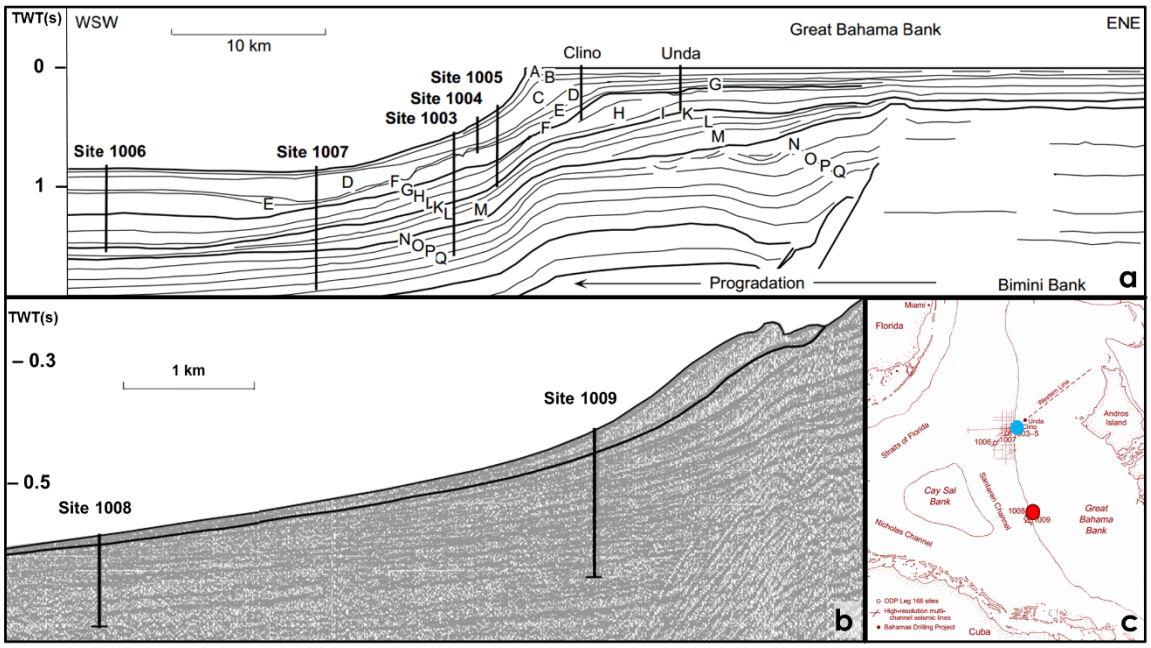

Figure 1.8. a) Location of boreholes in ODP Leg 166 Sites 1005, 1004, 1003, 1007, and 1006, b) Sites 1008 and 1009, c) the map location of transect (a) in blue and (b) in red. Modified from Eberli et al. (1997a)

METHODOLOGY

Morphology and sedimentary processes

Fledermaus and *ArcMap 10.1* software were used to analyze the multibeam bathymetry data. The slope is subdivided into 3 segments: upper, middle and lower, and the declivities were measured. Dimensions of different sedimentary features were quantified: length, width and thickness, together with the distance from platform margin and water depth.

The interpretation from the multibeam bathymetry data is compared with subsurface data from Ocean Drilling Project (ODP) Leg 166, sub-bottom profile data and industrial 2D seismic lines. These data were analyzed using the *Petrel (Schlumberger)* interpretation software.

Sediment composition and distribution

Some physical characteristics of sea floor sediment can be estimated based on backscatter data. Backscattering strength is a function of surface roughness and volume inhomogeneity (Chakraborty et al., 2000). In the Straits of Florida, multibeam backscatter texture correlates with three sediment types: muddy sediments, coarse sands, and coral rubble (Grasmueck et al., 2006). This information is used as a calibration to interpret backscatter data. The acoustic properties of the sediments can be inferred from sub-bottom profile as well. Borehole data from ODP Leg 166 is also incorporated in the interpretation of slope facies.

Volume of sediments transported from margin and slope to the basin floor

The amount of material transported from the margin and slope is estimated from the geometry of failure scar and also derived from subsurface data. The extent and thickness are measured from bathymetry and sub-bottom profile.

OUTLINE OF THESIS

The thesis contains five chapters, which include an introductory chapter, three chapters that discuss the result of this work, and a conclusion chapter. Chapter 1, this chapter, provides a general overview of the study area and previous studies of Bahamian carbonate slopes. In addition the data that are available for this research are outlined, the hypotheses are formulated, and the methodology that are used to analyze the data are described.

Chapter 2 discusses the variability of the slope morphology off southwestern Great Bahama Bank. This chapter includes a detailed description of the slope morphology and depositional features along strike, and the interpretation on the controlling sedimentary processes.

Chapter 3 focuses on the margin collapse features and their associated mass transport complexes. This chapter also provides a quantitative analysis of the margin collapse morphology and discusses the timing and the possible triggering mechanisms.

Chapter 4 documents the drift deposit and the occurrence of mega-pockmarks in the study area. In addition, this chapter evaluates the influence of regional tectonics to the formation and distribution of the pockmarks.

Chapter 2 through 4 are written in a paper format, so there will be some repetition in the introduction and methodology sections.

Chapter 5 summarizes and discusses the implication of this work.

CHAPTER 2. VARIABILITY OF CARBONATE SLOPE MORPHOLOGY ALONG SOUTHWESTERN GREAT BAHAMA BANK

OVERVIEW

Over the past 30 years the geology of carbonate slopes is of increasing interest. Numerous efforts have been made to characterize and classify the spectrum of the depositional settings and the controlling processes by using both ancient and modern examples. However, the main challenges in research on carbonate slope are the availability of good outcrops and accessibility to the modern environments (Playton et al., 2010).

The slopes and basins of the Bahamas are one of the best studied in modern settings. Using seismic and high-resolution biostratigraphy data, previous workers showed that the slope architecture of western Great Bahama Bank (GBB) is controlled by sea-level fluctuations and ocean current dynamics (Eberli and Ginsburg, 1987; Anselmetti et al., 2000). A steep and cemented wall forms the margin and the uppermost slope, which is onlapped by a sediment wedge (Wilber et al., 1990; Grammer and Ginsburg, 1992). Recent multibeam bathymetry surveys from western GBB and northern Little Bahama Bank (LBB) improve the understanding of the more distal slope morphology. On the northern slope of LBB, there are a series of long slope canyons through which turbidite are funneled to the basin. The entire system resembles the siliciclastic counterpart (Mulder et al., 2012b). Along western GBB the slope is variable, in some areas the sediment wedge is dissected by regularly spaced gullies, in other areas numerous

bifurcating channels run from the upper slope to the basin floor (Mulder et al., 2012a). In some areas the slope failed, resulting in large slump scars and associated mass transport deposits (Mulder et al., 2012a). This study documents the slope variability in an area further south along western GBB than from Mulder et al. area (Figure 2.1).

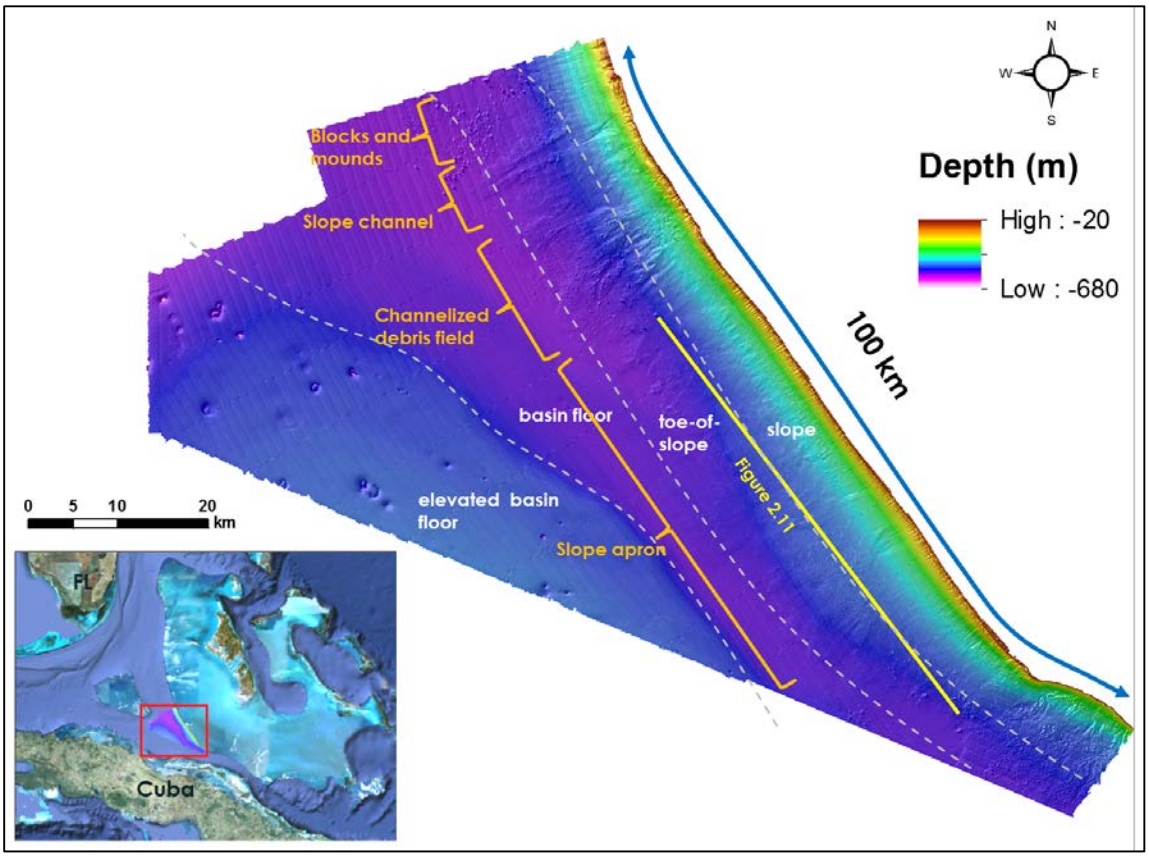

Figure 2.1. Location of multibeam bathymetry dataset and BPC seismic lines in southwestern Great Bahama Bank. The study area is divided into four physiographic environments: slope, toe-of-slope, basin floor and elevated basin floor.

The purpose of this study is to characterize the slope morphology and document its spatial heterogeneity. The analysis was done on high-resolution multibeam bathymetry, sub-bottom profile, and backscatter data from offshore southwest

GBB. The data show that the slope variability is controlled by different sedimentary processes related to with eustatic sea-level changes and ocean currents.

GEOLOGICAL SETTINGS

Study area

The study area is located along the southwestern edge of GBB, at the intersection between the Santaren and Old Bahama Channel Channels (Figure 2.1). It is bordered by Cay Sal Bank (CSB) in the northwest and Cuba to the south. The water depth in the survey area ranges from 21 to 670 meters. The axis of basin floor deepens towards the north.

Evolution of the Bahamas platform

The Bahamian archipelago lies between latitudes 20° and 28° N and longitudes 72° and 80° W and contains numerous carbonate platforms. GBB is the largest platform of the archipelago and also the world's largest tropical carbonate platform. Vertically, the thickness of GBB exceeds 5 km. The Great Isaac well, drilled on its northwestern corner of the bank penetrated the entire carbonate bank and encountered siliciclastics at ~5.4 km depth (Meyerhoff and Hatten, 1973). The Doubloon Saxon-1 well, which is the closest one to the study area bottomed out in Lower Cretaceous carbonates in more than 6 km depth (Walles, 1993). Based on the seismic data, the southern GBB is estimated to be more than 10 km thick. There is evidence that during the Early Cretaceous an even larger mega-carbonate platform existed that extended from the Florida peninsula to the Bahamas (Ladd

and Sheridan, 1987). Subsequently, the megabank was tectonically segmented and coalesced into the present day basin and bank morphology (Eberli and Ginsburg, 1987).

Tectonics

Southern Great Bahama Bank underwent three major tectonic events: extension during Early-Middle Jurassic, reactivation of Jurassic faults during the Middle Cretaceous caused by increased subsidence, and wrenching associated with Late Cretaceous to Middle Tertiary collision between the Caribbean and North American plates, which caused the fragmentation of the Cretaceous platform in the south (Masaferro and Eberli, 1999). The collision ceased in Middle to Late Eocene, but faults in the younger strata indicate deformation was still active during the Neogene (Masaferro et al., 1999).

Oceanographic setting

The seaway along western GBB is mainly influenced by the ocean current that flows from the Lesser Antilles into the Old Bahama Channel and further north into the Santaren Channel before it merges with the Florida Current in the Florida Straits (Atkinson et al., 1995). The Florida Current itself is a complex system that has a mean transport of ~31.7 Sv (Leaman et al., 1987). The contributions to the Florida Current are mainly from ~2 Sv from the Old Bahama Channel and ~1 Sv from Northwest Providence Channels (Atkinson et al., 1995; Hamilton et al., 2005). The maximum current speed in the Old Bahama Channel is found between 50 and

250 m of water depth and reaches up to 193 cm/s, but decreases to an average of 26 cm/s near the sea floor (Atkinson et al., 1995).

During a recent survey with an Autonomous Underwater Vehicle, Grasmueck et al. (2006) measured bottom currents off western Great Bahama Bank that change direction (north-south) every 6 hours. This current has sustained peak speed of 20 cm/s and is decoupled from the surface Florida Current.

An Acoustic Doppler Current Profiler (ADCP) measurement in the Santaren Channel, between CSB and GBB, reveals a water mass that flows south and is confined to the west side of the channel, whereas the eastern portion is dominated by a northward flowing current (Betzler et al., 2013).

METHODOLOGY AND DATASET

The surface morphology of the slope and basin floor is provided by multibeam bathymetry data and backscatter data acquired by Fugro Geoservices. They cover an area of about 6,500 km^2 in southwest GBB and were originally intended to image sea-bottom seeps and as a hazard assessment. The bathymetry data were collected using Reson SeaBat 8160 59 kHz Multibeam Echosounder (MBES) system which also recoded the backscatter data. The bin resolution for the multibeam bathymetry data is 15 m in the standard survey area and 10 m in the high resolution area. The NNW/SSE acquisition track direction produces artifacts seen on the multibeam bathymetry data.

A high-frequency single channel seismic survey was acquired concurrently with multibeam bathymetry data using a GeoPulse 5430A Sub-Bottom Profiler system (2-12 kHz frequency range). The dominant frequency of the sub-bottom profile data is 3 kHz. The depth of penetration depends on the acoustic properties of the sea-bed, reaching up to 35 ms (TWT) in acoustically soft sediments.

RESULTS

The slope environment is divided into three zones: upper, middle, and lower and toe-of-slope (Figure 2.2). Each of these zones is described in the following sections.

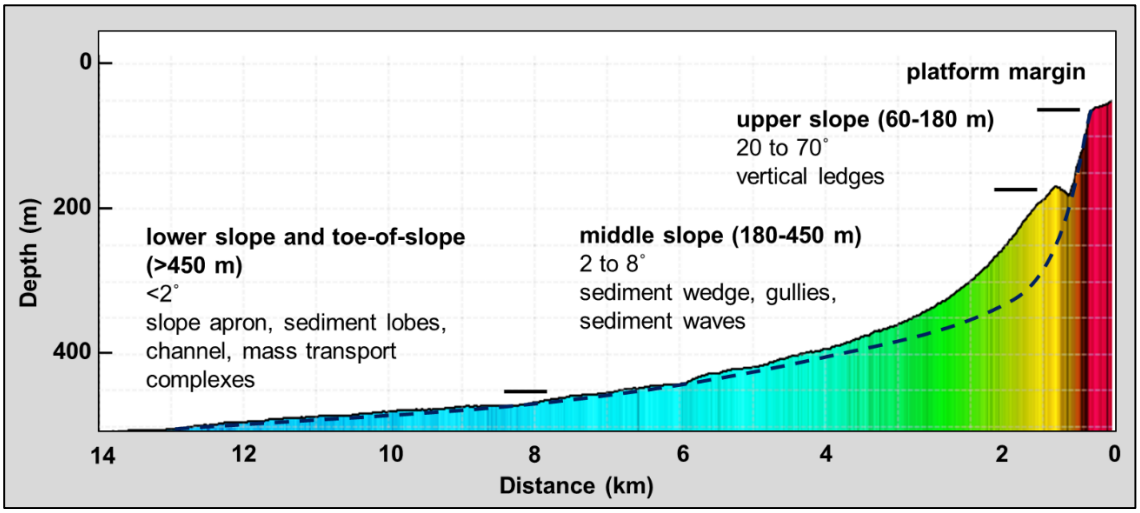

Figure 2.2. Detailed zonation of the slope off southwestern GBB. The slope can be divided into upper, middle, lower, and toe-of-slope. Blue dashed line indicates the inferred Pleistocene surface. (VE=10x)

Upper slope (65 – 180m)

The upper portion of the slope is characterized by a gently inclined bank margin top (~3˚) that changes abruptly at ~60 m water depth. It becomes a steeply inclined wall (25-40˚) which extends to ~100 m water depth. Below that depth, the declivity decreases to ~10-25˚. This slope profile extends to an average depth of 165-180 m, where it is onlapped by a sediment wedge (Figure 2.3A). The surface of the steep upper slope is not smooth; it is rugged and contains numerous vertically incised scars. These scars are commonly recessed by 50-100 m and are 30-200 m wide, but can reach up to 300 m in depth and 800 m in width (Figure 2.4). The vertical scars are regularly spaced (200-500 m); they initiate at the platform top and narrow downslope.

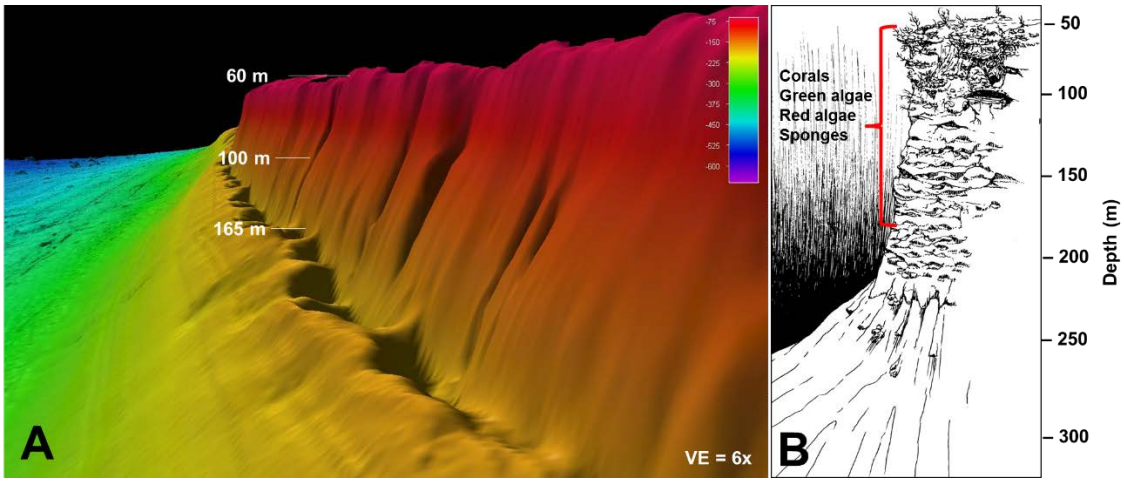

Figure 2.3. A) The upper slope is steep, carved by vertical scars, and onlapped by a sediment wedge. The vertical scars in this figure are ~30-70 m wide and incise ~50 m deep, B) similar steep wall morphology from the Tongue of the Ocean that is built by deep reefs, calcareous algae, and sponges (image modified from Ginsburg et al., 1991)

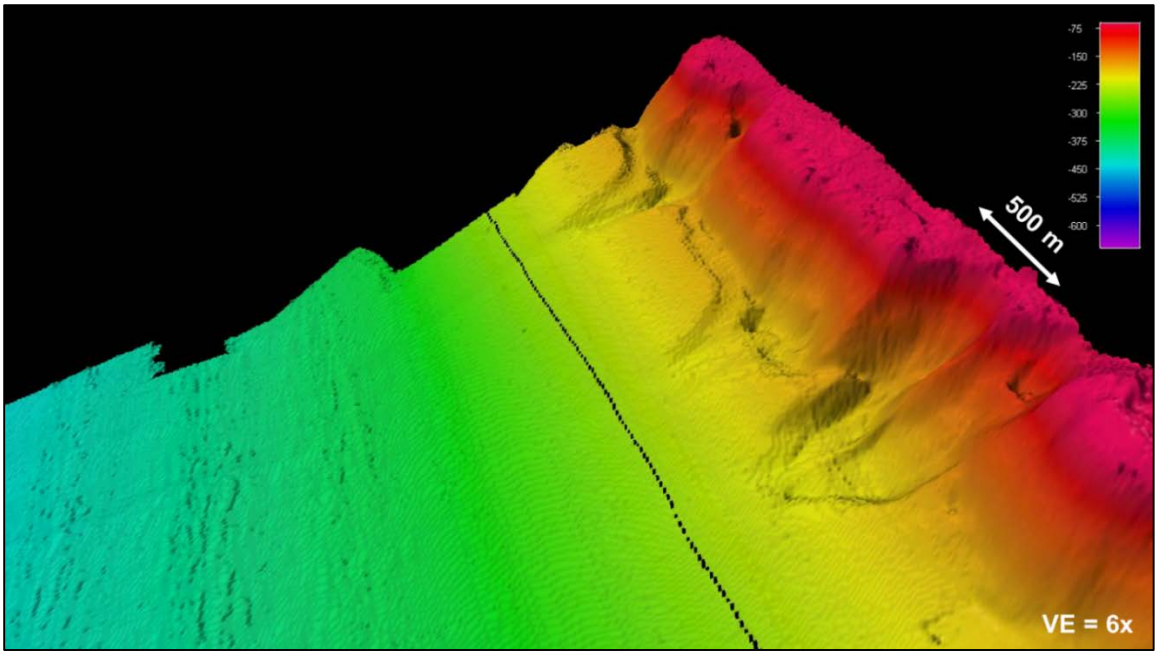

Figure 2.4. Eroded upper slope that is approximately 500 m wide and cuts more than 300 m deep into the platform margin. These reentrants act as a conduit for downslope currents that form gullies, which dissect the sediment wedge.

Middle slope (180 – 450 m)

Sediment wedge

The steep upper slope is onlapped by a sediment wedge. The wedge has a declivity of 8˚ in the upper portion and gently decreases to 1˚ in the lower portion. The morphology of the upper sediment wedge is variable along strike. At the point of onlap at ~160 m water depth, a moat of up to 40 m deep is found between the cemented slope and the basinward ridge (Figure 2.5). The moat has an undulating floor of 5-30 m relief, thus creating isolated pockets behind the ridge. The pockets are often connected to the vertical scars of the upper slope or to circular depressions on the basinward flank of the ridge.

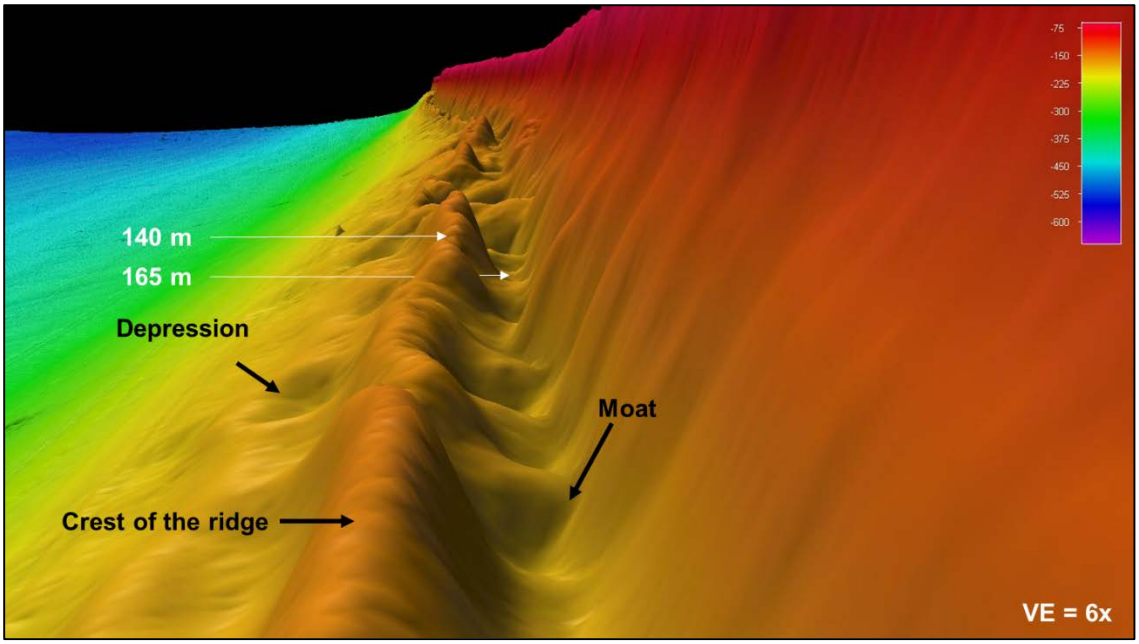

Figure 2.5. Morphology of the approximately 25 -40 m deep moat on the upper end on the sediment wedge. The undulating depth of the moat forms small sub-basin between the crest of the sediment wedge and the slope. Basinward of the ridge up to 4 m deep depression form.

The linear ridge is not uniformly developed. The crest of the ridge itself has an undulating surface of 5 to 40 m topography with >400 m spacing and is located 300-400 m from the platform margin. In some areas, it is breached and the sediment wedge is cut, forming ~10-20 m deep, v-shaped incisions that then act as conduits for gullies (Figure 2.4 and Figure 2.8).

In the northern part of the study area, the moat and ridge are not very well developed; instead, the sediment wedge directly onlaps to the rugged rock surface. A similar morphology is also encountered at the southern part of the study area, where there is a 220˚ bend in the margin. There, the onlapping sediments create a low relief moat and ridge morphology that is ~5 m at the deepest (Figure 2.6).

From the sub-bottom profile data, the thickness of the wedge is up to 100 m, and thins to barely nothing at ~5-7 km basinward from the margin (Figure 2.7).

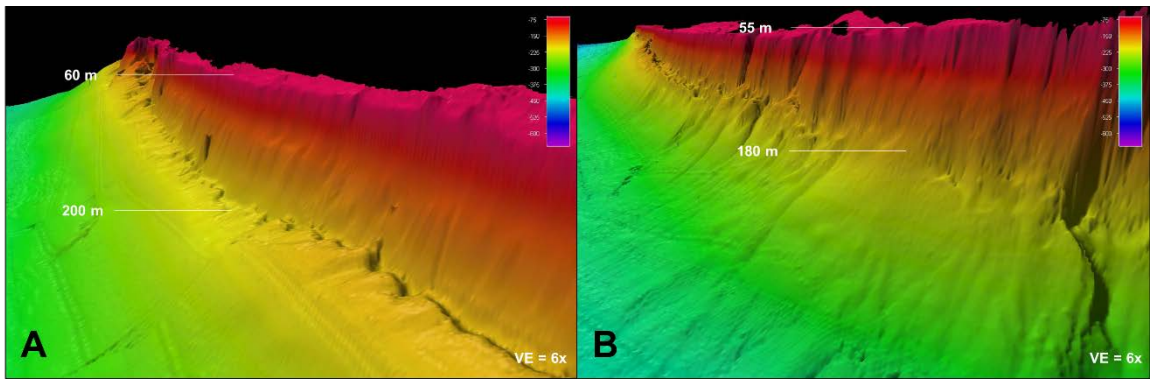

Figure 2.6. Examples of the onlapping sediment wedge where it lacks the ridge and moat morphology from A) northern and B) southern part of the study area.

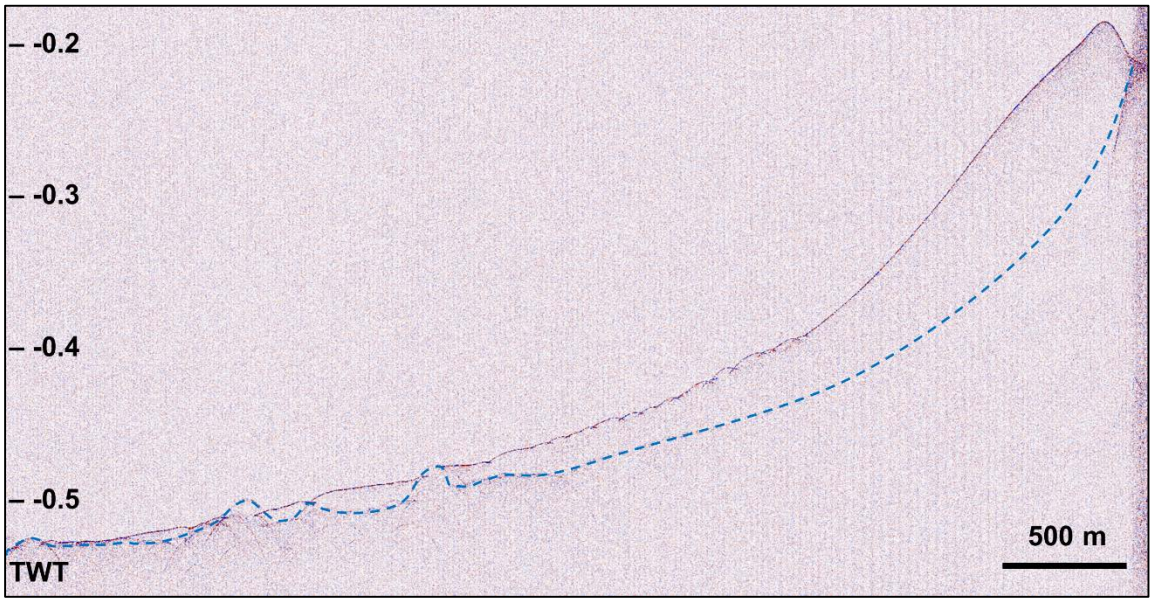

Figure 2.7. Sub-bottom profile of transparent Holocene sediment wedge, displaying the thinning of the wedge in a basinward direction.

Gullies

The sediment wedge is dissected by regularly spaced gullies that run perpendicular to the platform margin to the basin. V-shaped incisions on the crest

of the sediment wedge mark the beginning of the gullies. The gullies are 0.5-2 m deep and from 1 to more than 3 km in length. They run from 180 to 430 m water depth (Figure 2.8). They are regularly spaced, 100 to 300 m apart from each other. In most cases, the connections between the gullies and the v-shaped incisions are very subtle, and might be near the resolution limit of the multibeam bathymetry data.

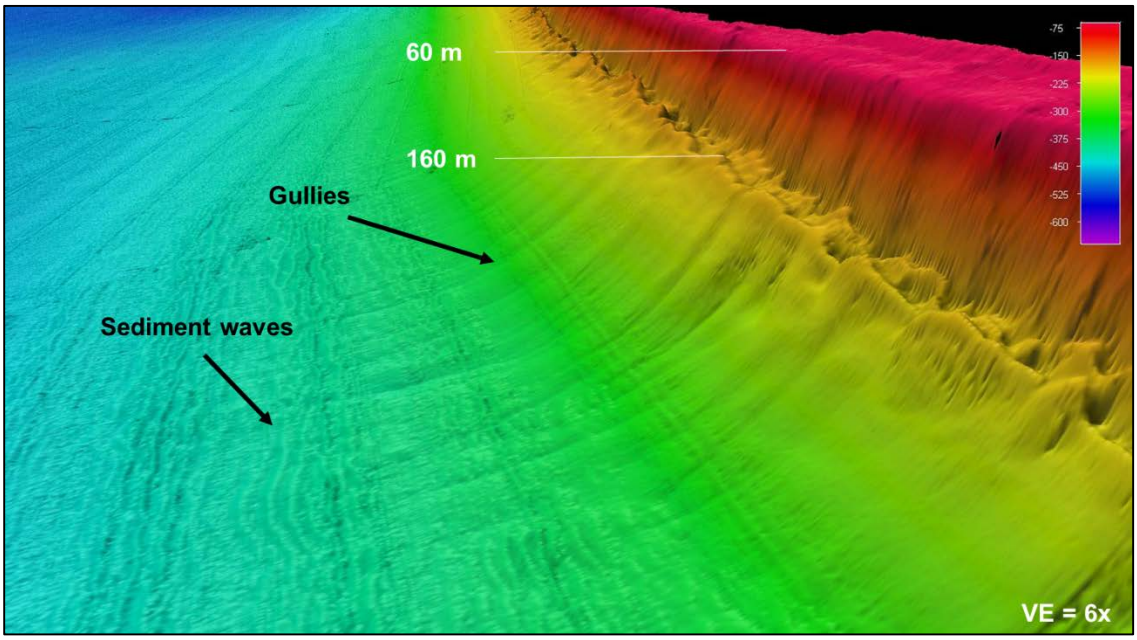

Figure 2.8. Shallow gullies originating from the crest of the sediment wedge and carve the wedge for more than 3 km basinward.

Sediment waves field

On the lower portion of the sediment wedge between 310-460 m water depth (middle slope), low-relief sediment waves are observed. The sediment waves lie ~2 km from the margin, where the slope declivity is ~2˚. They are oriented parallel to the bank margin and are almost continuously distributed along strike. The sediment waves have wavelengths of ~60-120 m and amplitudes ~2.5 m. The

wave crests are slightly sinuous (Figure 2.8). The waveform is asymmetrical, being steeper in the upslope face (Figure 2.9A). Sub-bottom profiles also image the sediment waves on the slope that is inferred to be Pleistocene in age (Figure 2.9B). However, the wavelength of these buried waves is longer than the modern waves (Figure 2.9B).

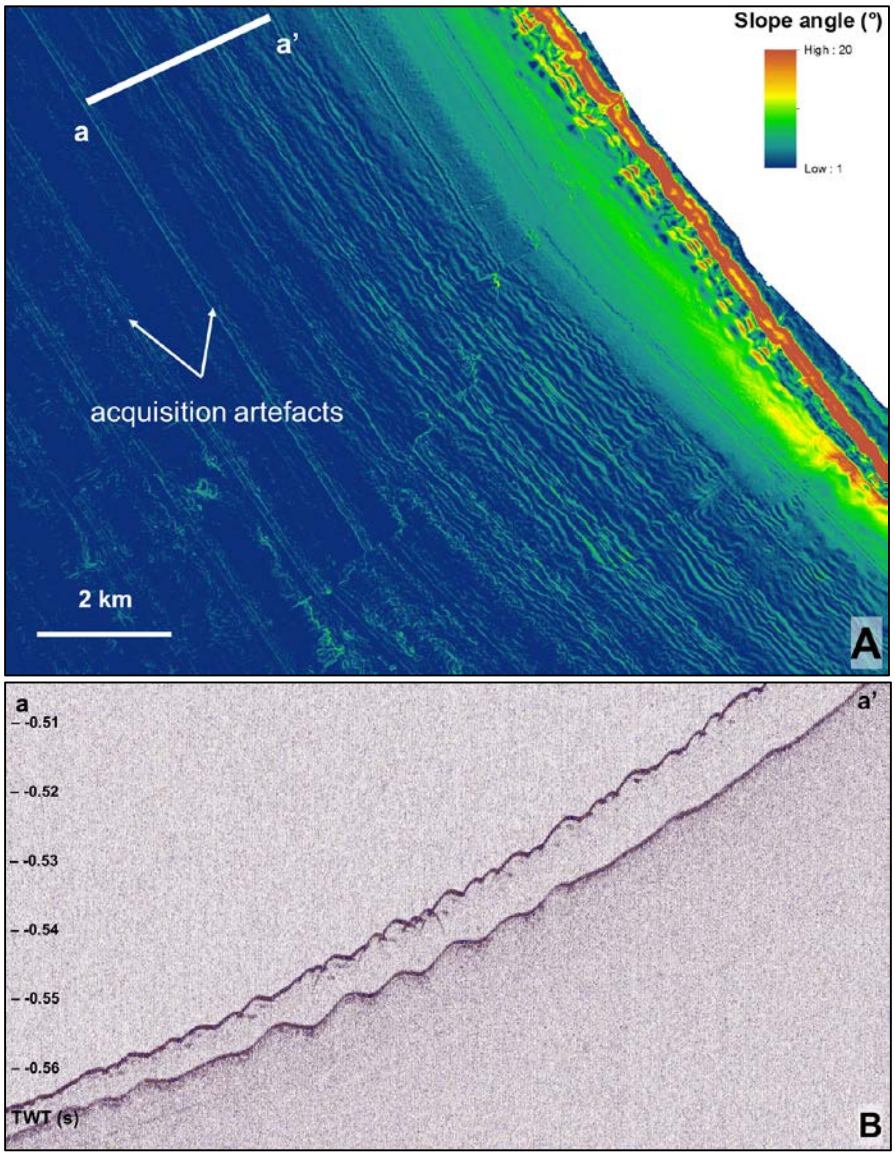

Figure 2.9. A) Slope angle display of the multibeam bathymetry data illustrate the sand wave field on the sediment wedge by delineating the steeper sides of the sand waves (in green) on the blue slope. B) Sub-bottom profile a-a' images the Holocene sand waves and also Pleistocene sand waves.

Lower slope and toe-of-slope (>450 m)

Proximal lobes and slope apron

The slope apron is a major physiographic feature along strike of the slope, and constitutes approximately 50% (by length) of total 100 km of margin. The apron is comprised of three parts: proximal lobes, a sediment sheet, and debris deposit which extends up to 16 km out from the platform margin (Figure 2.10). The whole deposit creates a ~50 m high, mounded relief and extends for 50 km in a strike direction (Figure 2.11).

The multibeam bathymetry data show that between water depths of 340-430 m small lobes are deposited between the gullies (label b in Figure 2.10). The lobes are 400-700 m wide and create ~5 m relief (Figure 2.12.a). The lobes and gullies form on the sediment wedge and overlie older strata with laterally variable thickness (Figure 2.12.a). The thickness of this older strata reaches a maximum of ~8.5 m (10 ms TWT) and up to 1 km wide. The topmost portion of the buried strata has semi-parallel to wavy bedding that changes to a seismically transparent facies. The topographic low of this buried strata creates preferential flow pathways for gullies on the sea floor.

In the distal portion, the slope apron is devoid of the transparent sediment cover. It forms tongues of sediments at its termination, which is 17 m (10 ms TWT) thick (Figure 2.12b). Several sediment lobes occur at the toe-of-slope and form part of the slope apron.

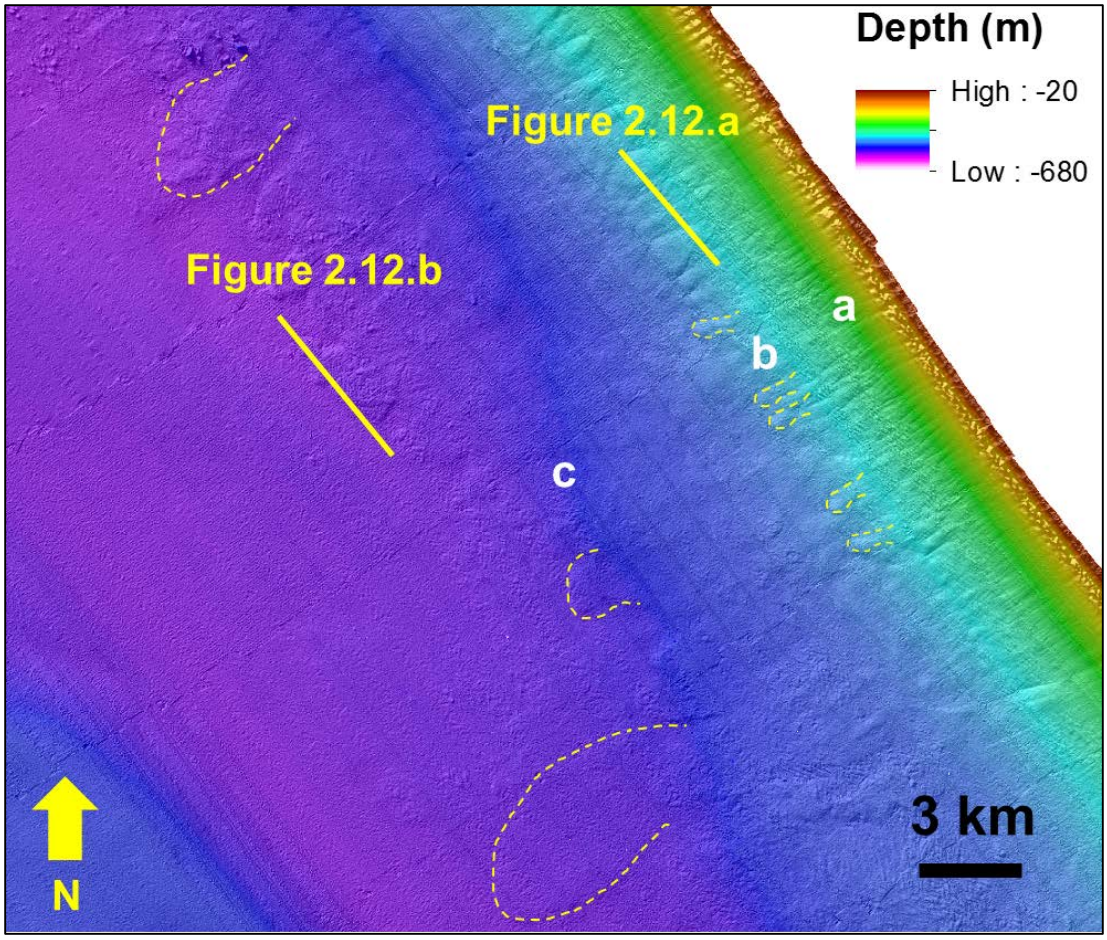

Figure 2.10. (a) Sediment wedge dissected by gullies that feed sediment downslope (b) small but discrete proximal lobes at ~420 m water depth of the sediment funneled through the gullies, (c) larger lobes are deposited further basinward, forming an apron that reaches 13 km out in the basin floor. Some of these sedimentary feature are outlined in yellow dashed lines.

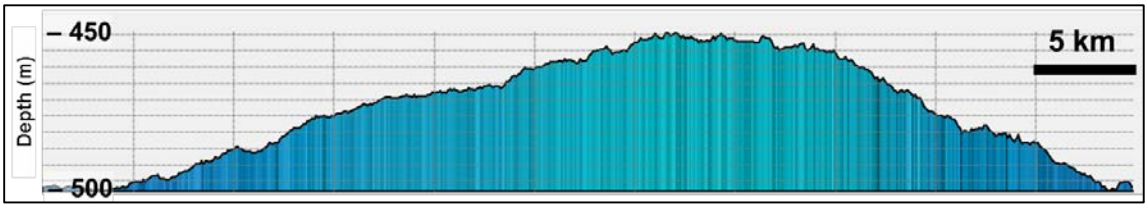

Figure 2.11. The seafloor topography of the bypassed sediments that are deposited an apron. This deposit has a ~50 m high, mounded morphology (see Figure 2.1 for location).

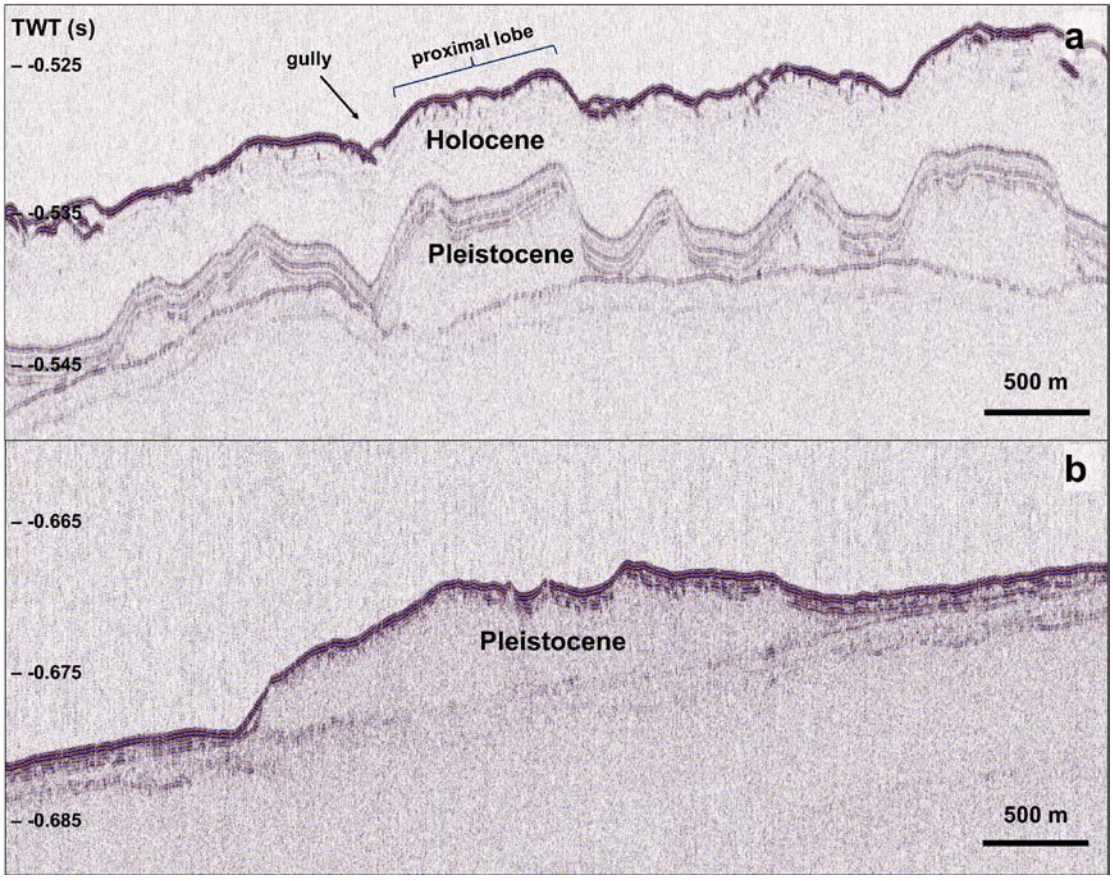

Figure 2.12. a) The sub-bottom profile of the middle slope that is carved by gullies. b) Cross-section through a lobe in distal portion of the slope apron (see Figure 2.10 for location).

Slope creep

The largest lobe on the slope apron is ~12 km wide (label B in Figure 2.13). The proximal portion of most lobes is littered by several large blocks (~400 m wide, ~3 m high) that are partly buried. The deposit extends seaward ~18 km from the platform margin. Upslope, the sediment lobes are linked to a reentrant that has been buried by Holocene sediments (Figure 2.14). The reentrant is 2.2 km wide, 10 m deep (10 ms TWT), and ~5 km long. The reentrant funneled sediments downslope, which created a lens shaped deposit that is 7 m wide and 10 m (12 ms

TWT) thick. This deposit has an irregular basal contact (Figure 2.14d). The middle slope sediment wedge that buries the erosional reentrant is cut by several gullies. These gullies are several kilometers long and ~1 m deep (label A in Figure 2.13).

The proximal part of the sediment lobe at 450 m water depth has an undulating morphology. The slope at this location has an inclination of only 0.1˚. The portion of the slope with undulating sediments is approximately 3 km wide and oriented radially downslope. The wavelength of the undulating features ranges from 60 m up to 190 m and are quite symmetrical (Figure 2.15). They gradually form a chevron pattern in the basinward direction.

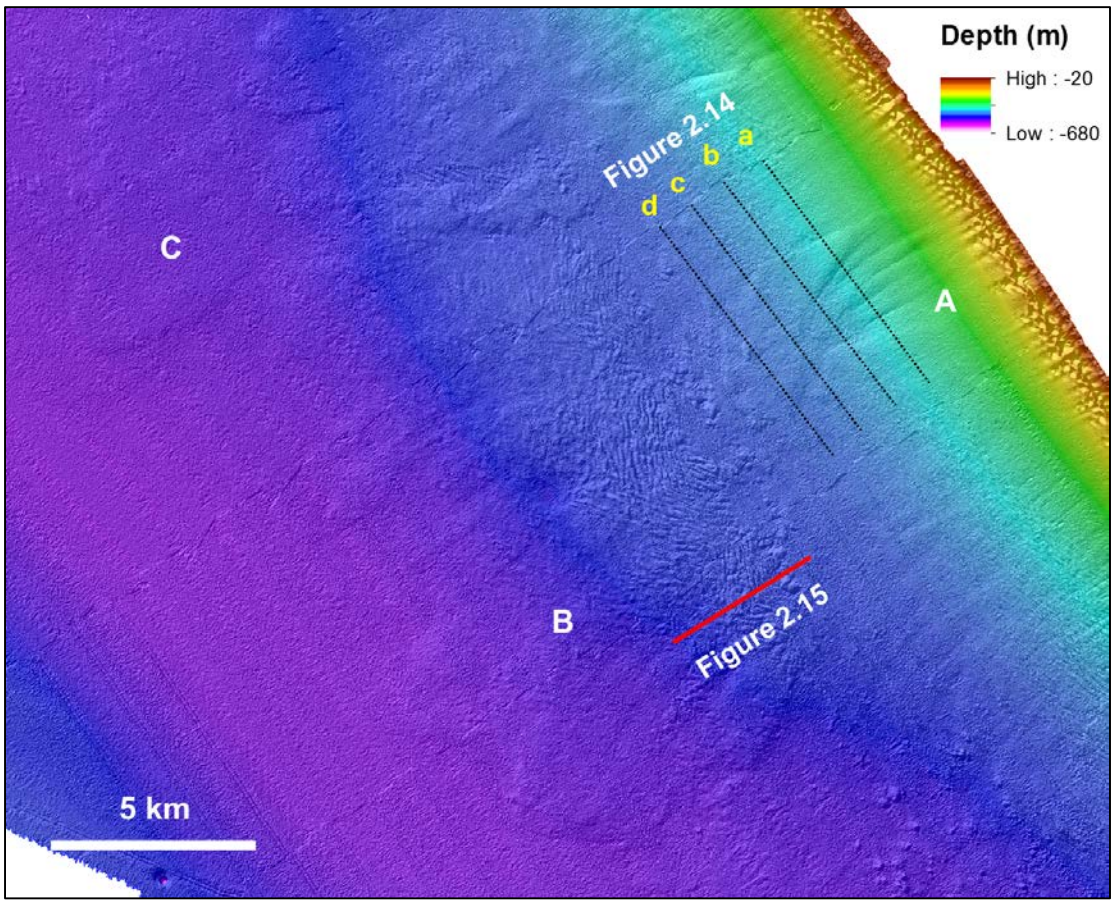

Figure 2.13. Several gullies (A) on the middle slope transition into a sediment lobe with an undulating surface in the proximal portion (B). On the left, another large sediment lobe (C).

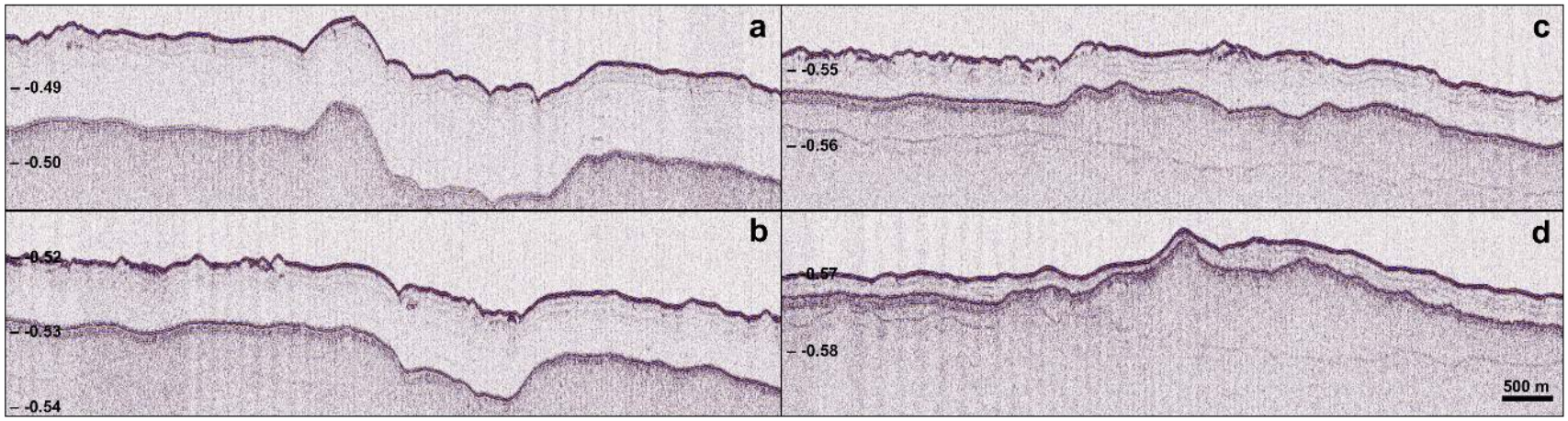

Figure 2.14. A buried reentrant on the middle slope. This reentrant was likely a slump scar. Figure a to d show downslope evolution of the mass movement. This downslope mass transport likely exert pressure on the sediment and produces folds (see Figure 2.13 for the location)

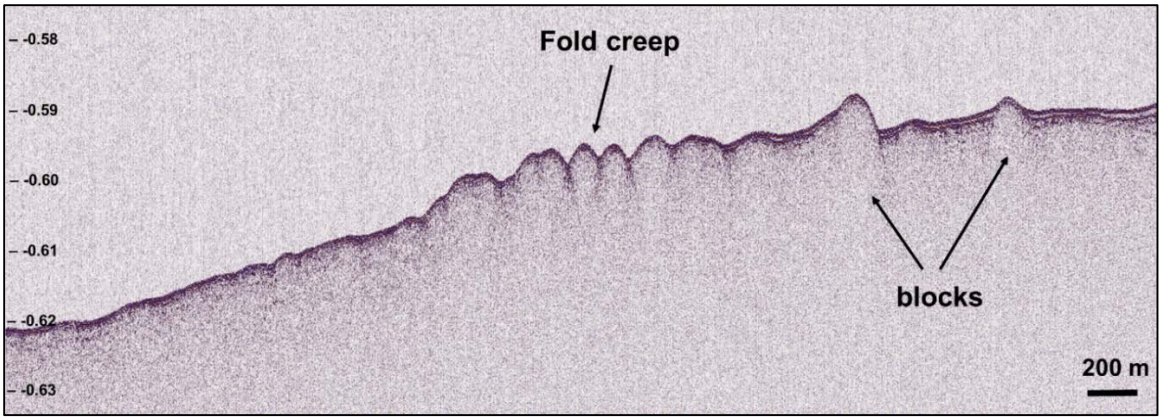

Figure 2.15. Undulating sediment surface on the proximal part of the sediment lobes.

Block and mound fields

Blocks -

The seafloor in the northern part of the study area has many scattered blocks and mound fields in 450-550 m water depth (Figure 2.16). Blocks are deposited in a more proximal position in 450-540 m water depth, and have a square to rectangular morphology (Figure 2.17). The blocks are up to 30 m high, 300-600 m long, and 200-300 m wide. They do not follow any particular orientation. Some are partly buried, others have scours of up to 15 m adjacent to the blocks along their northeastern side. In the south, some of the blocks are onlapped by sediments creating a more gently dipping side, whereas others have 5-10 m deep moats that encircle them (Figure 2.17). Sub-bottom profiles indicate there are internal layers within some of the blocks (Figure 2.18b).

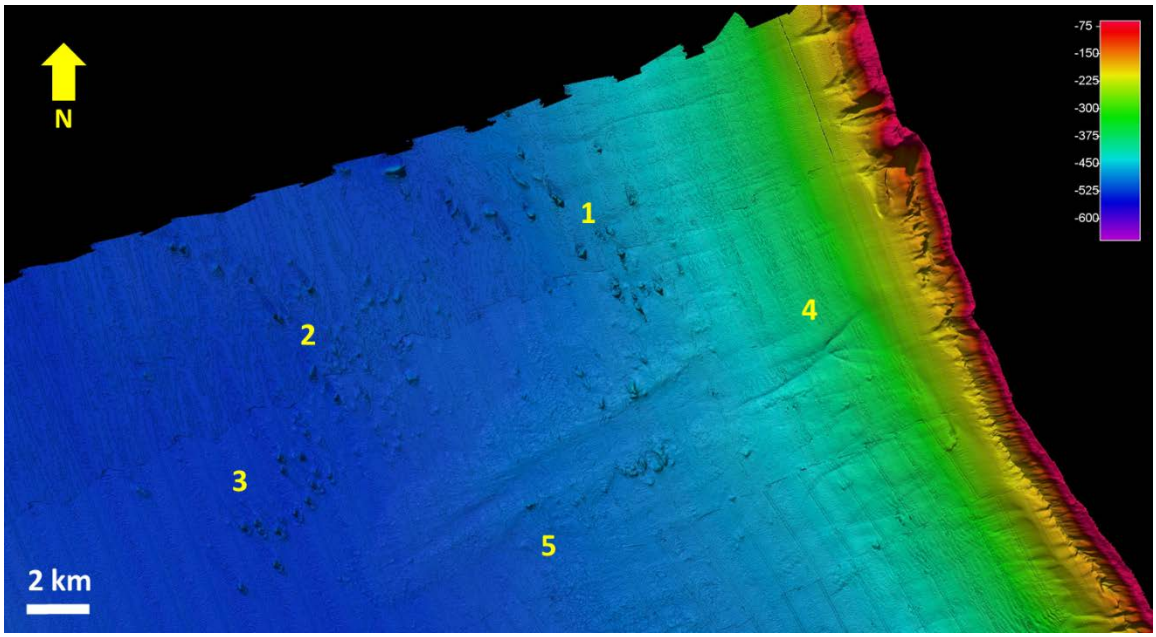

Figure 2.16. The middle and lower slope contains several morphological elements: 1) blocks, 2) buried mounds, 3) mounds, 4) gullies, and 5) a slope channel and fan complex.

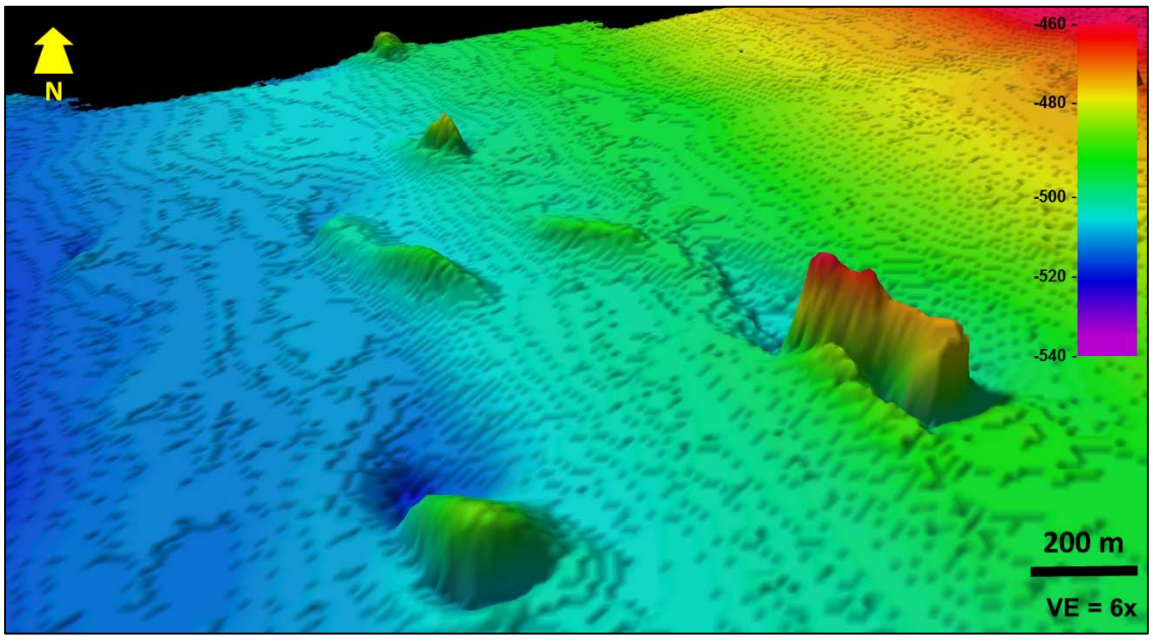

Figure 2.17. Blocks of different sizes and shapes are partly buried by slope sediments. Along some of the blocks (foreground) a moat occurs on the northwestern side (location of blocks is labeled as 1 in Figure 2.16)

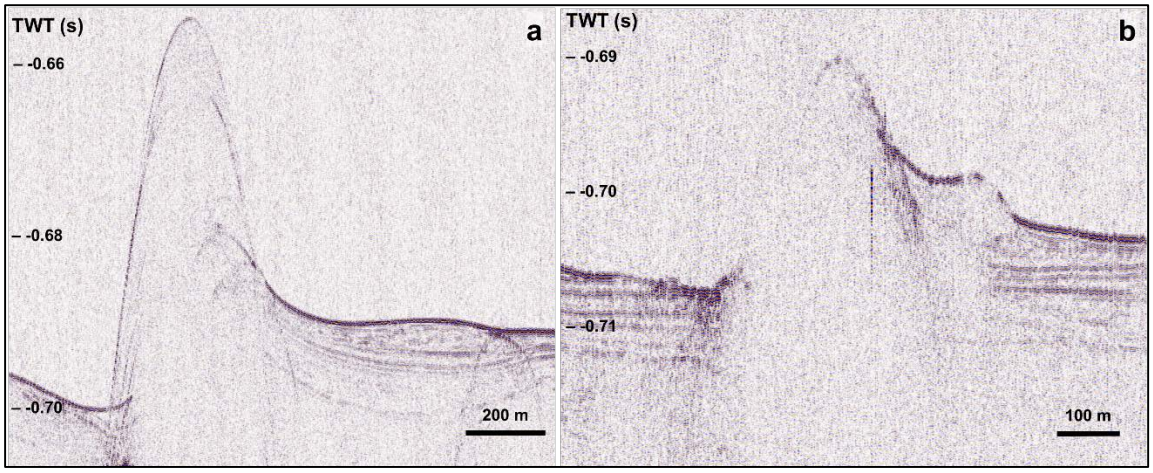

Figure 2.18. Sub-bottom profile of a) a block which has diffraction suggesting there are layers within it, and b) a mound with an onlapping package at its side. Truncation on the left side of the mound suggests an erosional feature.

Mounds -

Further downslope, a cluster of semi-conical buildups and mounds are observed in ~540 m water depth approximately 20 km from the bank margin (Figure 2.19). Their morphology is quite distinctive from the blocks and debris deposited in the more proximal slope. The mounds are slightly elongated in NW-SW direction and are up to 30 m high, 250-300 m long, and 200 m wide. The southwestern flanks of the mounds are onlapped by sediments that can form up to 10 m of relief. The mounds have chaotic to transparent seismic facies on sub-bottom profiles (Figure 2.18b). On the northeastern sides, ~3 m deep NW-SW elongated scours (up to 1 km long) are observed adjacent to the mounds (Fig. 2.18). Sub-bottom profile data show that some of the mounds are partially buried, and others are completely buried. The reflectors at the base of the mounds are not imaged, so the true height of the mounds is not known.

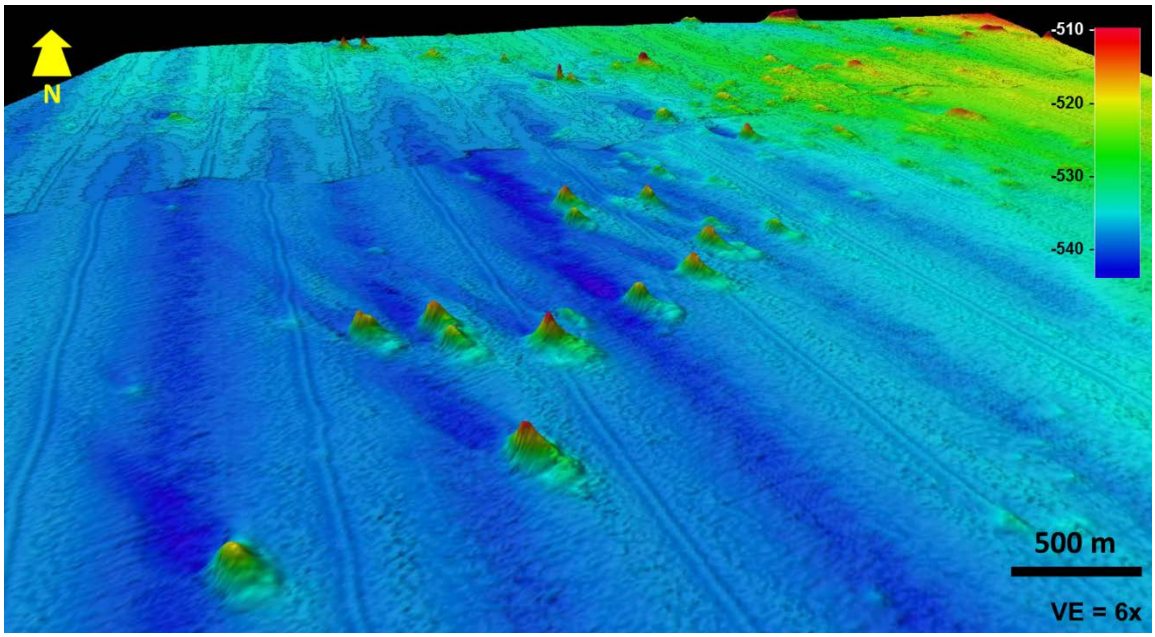

Figure 2.19. Conical mounds interpreted as cold-water coral colonies in water depth of ~540 m. They have scour mark in the NW direction (location of mounds is labeled as 3 in Figure 2.16)

Slope channel

An 18 km long channel system occurs immediately south of the debris and mound fields (Figure 2.16). The proximal part of the channel is buried by Holocene sediment that thins out 6 km from the margin. The partly filled channel is about 30 m (25 ms TWT) deep and 2 km wide. Basinward, the channel becomes shallower and narrower (Figure 2.20 and Figure 2.21). At the top of the channel fill, several ~2-5 m deep, 1.5 km long gullies incise the middle slope and converge into a 3 km long gully. This series of gullies conveys sediment toward the basin.

At 465 m water depth, the gullies terminate and a channel levee system starts. The channel is 1.5 km wide and narrows to ~500 m at its termination at ~530 m water depth. Levees flank both sides of the channel. Large blocks ~300 m long and up

to 20 m high are deposited on the proximal part of the levee and are more sparsely scattered distally. The levees are not symmetrical, being boarder and resembling a lobe on the north down-current side, whereas the south side is narrower. The channel terminates in a basal fan deposit which is 3.3 km wide and approximately 17 m thick (Figure 2.22).

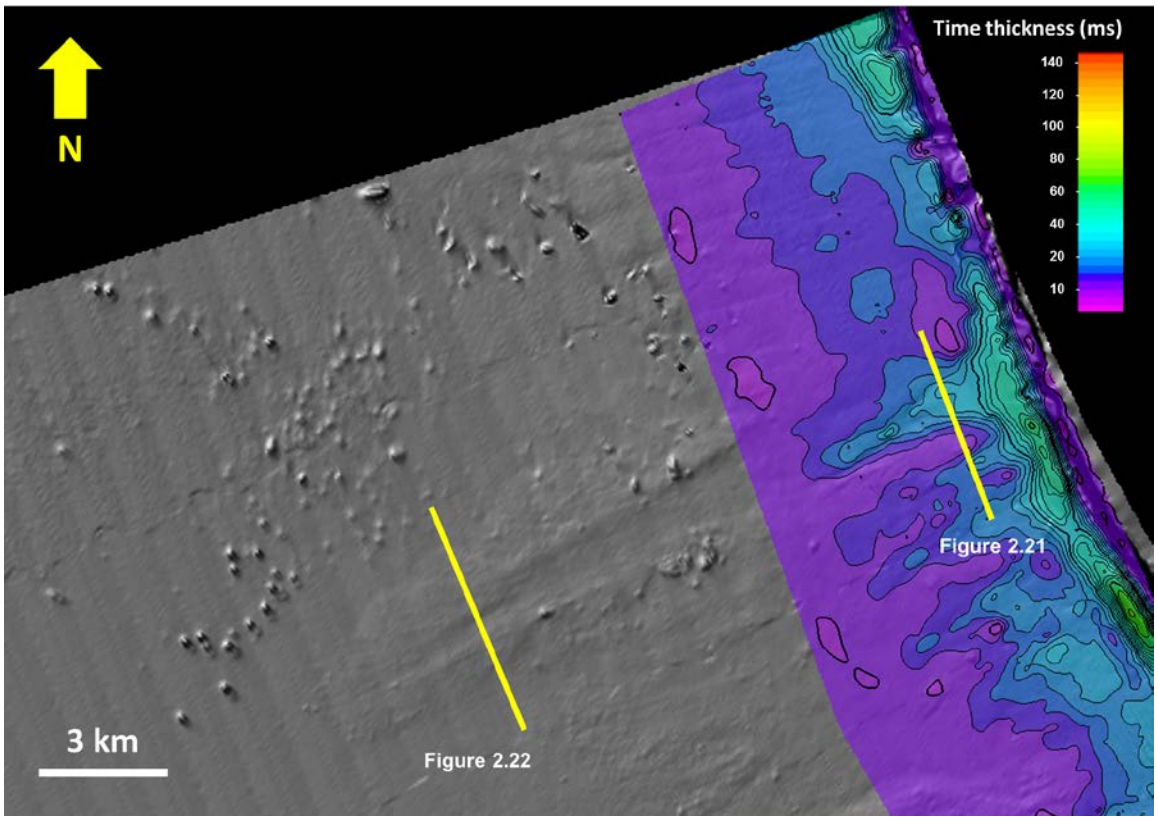

Figure 2.20. Isopach of Holocene sediment that buries the proximal portion of the slope channel and the debris field, overlies the shaded relief map.

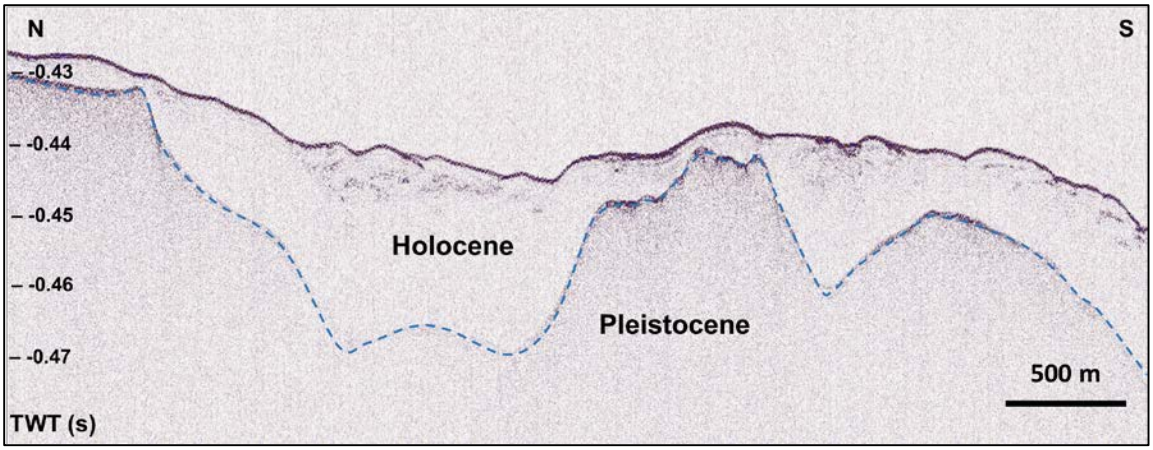

Figure 2.21. Pleistocene topography underneath the proximal portion of the channel lobe covered by the Holocene sediment (see Figure 2.20 for location).

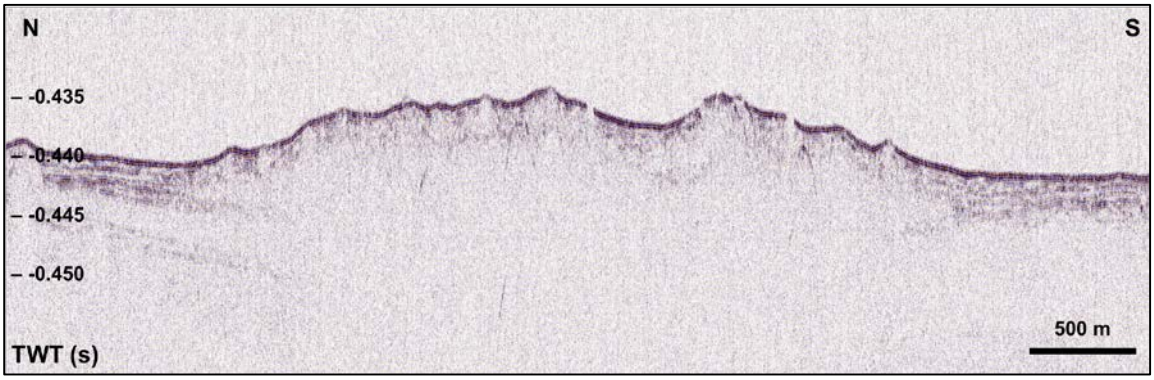

Figure 2.22. Cross-sectional view of the fan deposit at the termination of the channel (see Figure 2.20 for location).

Channelized debris field

A 13 km-wide debris field extends for 17 km from the middle to the toe-of-slope, at 300 to 540 m water depth (Figure 2.23). The field consists of large blocks 100-400 m in diameter and up to 20 m high. Sub-bottom profile data show that the blocks are located within 7 km from platform margin and are (partially) buried by the Holocene sediment wedge (Figure 2.7).

The debris field has a mounded morphology with ~10 m of relief relative to the surrounding sea floor. The large blocks are incorporated in finer matrix sediment and the deposit is cut by several channels ranging from 800-1000 m wide, 2-5 km long, and 4-8 m deep.

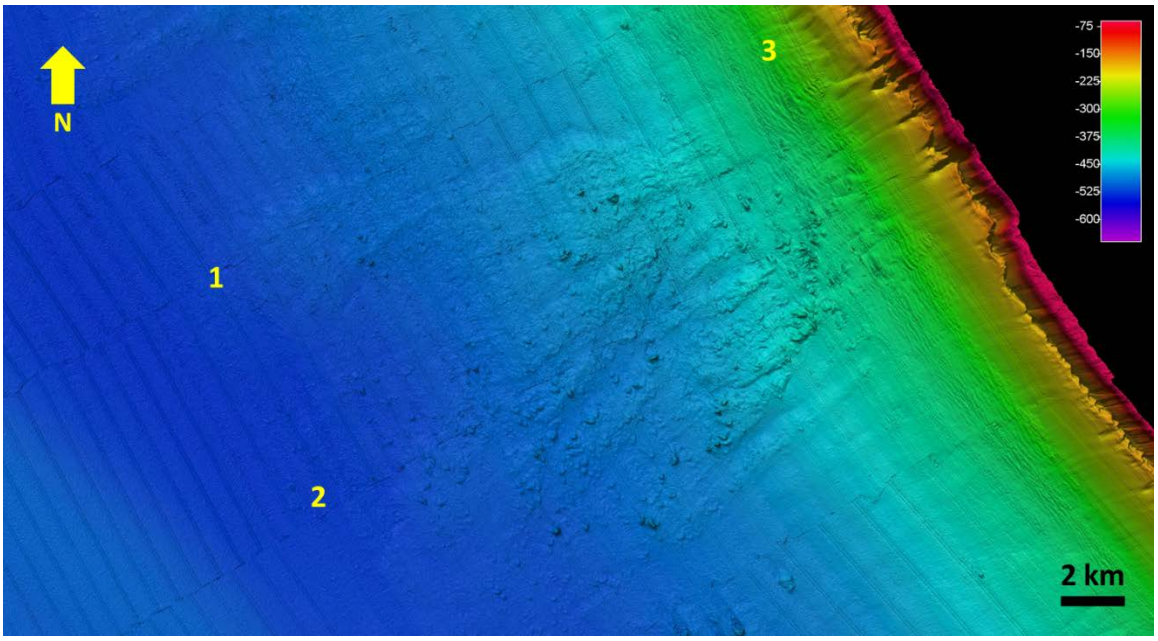

Figure 2.23. A part of the slope that displays 1) a sediment lobe, 2) a channelized debris field, and 3) a sediment wave field on the Holocene sediment wedge.

Slope sediment properties

Slope sediment properties were ascertained for the study area with the use of multibeam backscatter data. The backscatter survey were compared to the one that had been calibrated with the ground truth during a deep-water coral expedition using core samples and drop camera data (Grasmueck et al., 2006). They were able to classify three different facies: coarse sand, rubble, and soft mud.

The multibeam data from the slope and basin southwest of GBB shows a consistent pattern based on the physiographic environment (Figure 2.24). The upper and middle slopes have low backscatter values that indicate homogeneous Holocene sediment. High backscatter value are indicative of heterogeneous sediment grain size. High backscatter values form a linear band along the toe-of-slope that is continuous along the strike. This high backscatter band is composed of carbonate debris flows and turbidites that are sourced from the upper slope and margin.

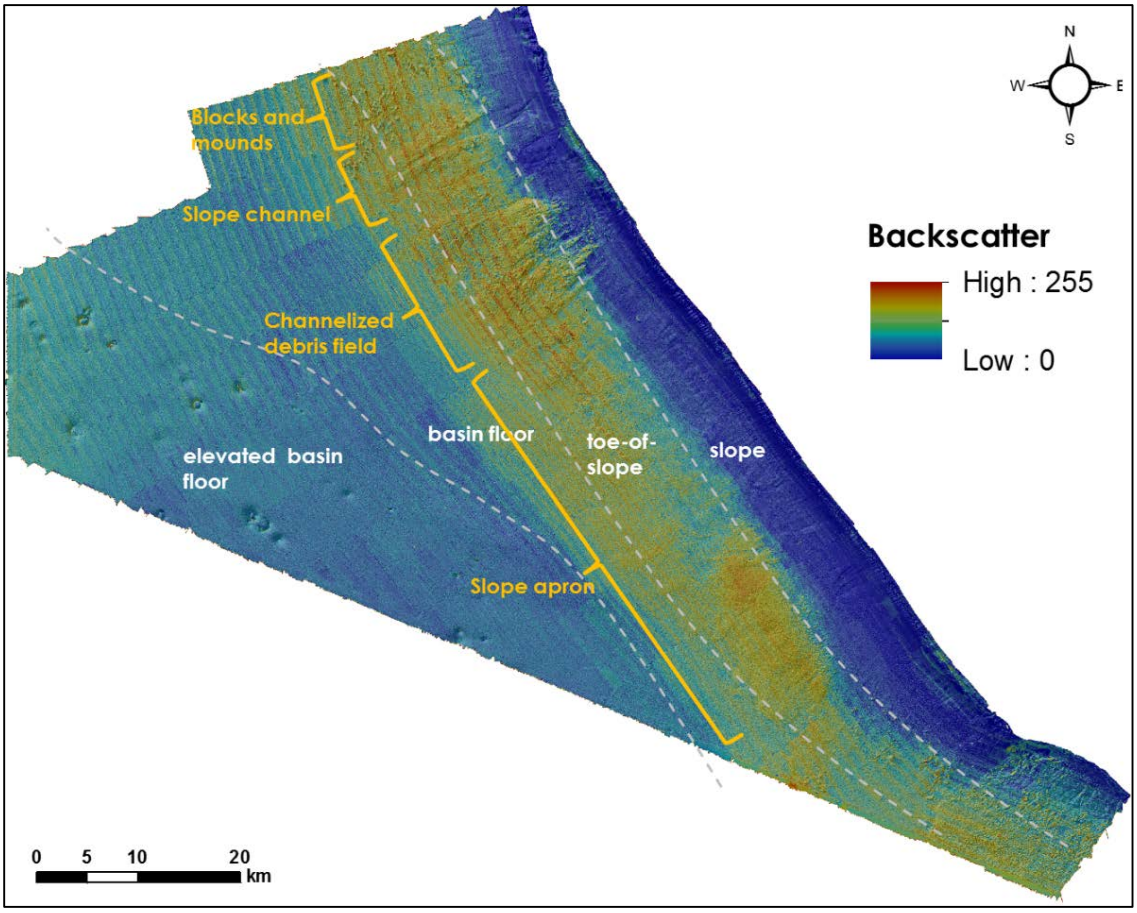

Figure 2.24. Backscatter data along southwestern GBB. The upper and middle slope exhibit a strike-continuous homogeneous signature. The toe-of-slope consists of a heterogeneous signature, typical of redeposited carbonates.

In contrast to a deep-water siliciclastic model, in which relatively coarse sediments are arranged in large upper slope submarine fans, coarse materials in the carbonate setting mostly bypass the upper slope and are deposited along strike at the toe-of-slope.

DISCUSSION

Major sedimentary processes

Carbonate sediments are mostly produced in the shallow water setting and can be transported off-bank to deep water by different mechanisms. Suspension settling, resedimentation, and bottom currents are important in both deposition and erosion of slope sediment (Coniglio and Dix, 1992). During highstands, the carbonate platform top produces abundant sediment, some of which is exported off-bank, a process that is often referred to as highstand shedding (Droxler and Schlager, 1985; Schlager et al., 1994). This phenomenon has been observed in both in modern and ancient platform settings (Schlager et al., 1994). Highstand and lowstand of sea level are related to the orbital driven climate changes and the associated waxing and waning of ice sheets. These climate cycles are reflected in both the mineralogy and grain types of the sediment exported to the slope (Droxler et al., 1983; Rendle and Reijmer, 2002).

The off-bank sediment is deposited on the slope as a seismically transparent wedge, for example, along northwestern GBB (Wilber et al., 1990). Wilber et al. (1990) found that the sediment wedge is composed mostly of aragonite mud

transported from platform top and is veneered by muddy sand. The radiocarbon dating of the base of the sediment wedge from a borehole in northwestern GBB yielded 7230 year BP (Roth and Reijmer, 2004), which coincides with the onset of platform flooding since the last glacial period, corroborating the highstand shedding notion.

The composition and dip variation of the sediment wedge was analyzed during ODP Leg.166 (Eberli et al., 1997a). The late Pleistocene to Holocene strata consists of several coarsening upward cycles, predominantly peloidal mudstone/wackestones to packstone separated by hardgrounds and harder layers. The hardgrounds form during the sea-level lowstands when no sediment is transported off-bank and ocean currents remove the pelagic deposits on the upper slope (Kenter et al., 2001; Malone et al., 2001). The Holocene unit is composed of shallow-water platform grainy materials: peloids, planktonic and benthic forams, pteropods, gastropods, *Halimeda* debris, shell fragments, and coral debris, together with muddier material made of aragonite needles, nannofossil ooze, and micritic matrix. Particles <63 μm (mud size) are the most abundant, ranging from 85-88% of the total sediment (Rendle and Reijmer, 2002). The sedimentary processes (i.e. suspension settling, downslope turbidity current, and contour current) that act on the slope and basinal settings leeward of GBB are discussed in the next sections.

Suspension settling

Despite the notion that carbonate sediments are autochthonous, the slope environment receives most of its sediments from elsewhere. They are sourced from both the overlying water column and the platform top. Observation on the LBB shows that during winter storms, muddy sediments are suspended and swept off into the deeper water by the ebb tide (Neumann and Land, 1975). The contribution of shallow bank components and planktonic materials to the slope varies through time and space (Pilskaln et al., 1989). Sediment trap experiments on the slope in Northwest Providence Channel (NWPC) during storm-free periods showed 61% of the carbonate flux is contributed by planktonic sources, while the remainder is shallow-bank components (Pilskaln et al., 1989). However, grab samples from the same area show that ~80% of total sediment is derived from the shallow bank (Boardman and Neumann, 1984), suggesting significant amount of the off-bank transport is aided by storm-related cold front (Pilskaln et al., 1989).

Downslope turbidity current

Seasonal heat flux variation on the Bahama banks can create hyperpycnal water that may flow off bank (density cascading) (Wilson and Roberts, 1995). The dense water may entrain sediment and move downward to a density compensation level (~450-800 m) depending on temperature. Once these fluids reach their density equilibrium, they then spread laterally (Wilson and Roberts, 1992). This mechanism is likely important for fine-grained sediment transport to the slope and basin, enhanced erosion by induced turbidity currents, and transfer of sand to the basin (Wilson and Roberts, 1995). There is some debate as to whether the density

cascading process is depositional or erosional. Wilber et al., (1993) suggest that the density cascading current is an erosional agent as evident from the “plunge pool” or the pockets on the top of the sediment wedge. They also argue that the deposition of periplatform sediment is largely controlled by along-slope currents, but this mechanism is downplayed by Wilson and Roberts (1993) in favor of the density current.

Furrows observed on the margin and upper slope likely focus the downslope sediment transport. The erosive nature of the downslope current can be seen by the occurrence of gullies on the sediment wedge. These gullies act to bypass sediment to the turbidite sheets on the lower slope. Similar features and basinal deposits were all described in both, the Tongue-of-the-Ocean and Exuma Sound, intraplatform basins (Schlager and Chermak, 1979; Crevello and Schlager, 1980). Similarly, ODP Leg 166 cores from western Great Bahama Bank show that turbidites bypassed the upper slope and were deposited on the lower slope and toe-of-slope (Eberli et al., 1997b). Because of highstand shedding, this process yields higher sedimentation rates during highstands, as recorded as thicker turbidite packages (Bernet et al., 2000).

The presence of slope parallel sediment wave field along the lower slope might be an additional indication of the downslope turbidity currents. Sediment waves in the deepwater environment are commonly associated with bottom current process or turbidity currents (Wynn and Stow, 2002). Sediment waves formed by bottom current usually have crests aligned oblique to the regional contour, while turbidity current deposits are normally elongate slope parallel (Wynn and Stow, 2002). The

downslope turbidity currents on the western slope of GBB largely flow as an unconfined sheet in the absence of channel and levee complex. Sediment waves could form in such condition based on the antidune model proposed by Normark et al. (1980).

Contour current

Along-slope currents play an important role in deep water carbonate sedimentation. Currents can winnow slope sediments and promote submarine cementation (Mullins et al., 1980a; Mullins et al., 1980b; Mullins et al., 1984). Contour currents also carry sediment and redistribute it in drift deposits. A study on the western flank of GBB by Anselmetti et al. (2000) shows that carbonate slope architecture is controlled by both platform derived sediments and deposition by ocean currents. To the north, the Florida Current and Northwest Providence Currents contribute to the deposition of large drifts at the northwest corner of GBB (Mullins et al., 1980b). The drift deposits are composed of sand-sized planktonic and pelagic materials, and fine-grained off-bank sediments (Mullins et al., 1980b; Anselmetti et al., 2000).

The intensity of ocean current can change through time. During the middle Miocene, Florida Current in the Florida Straits was strengthened due to the closure of Isthmus of Panama. The ocean current strengthening in the Miocene was recorded as an expansion of the drift deposit (Bergman, 2005). A lowering of sea level can also promote the strengthening of bottom currents (Richardson et al., 1969).

In the study area, contour current deposits were identified using multichannel seismic data. This deposit has a mounded morphology and extends 200 km in the Old Bahama Channel. This drift deposit interfingers with the slope sediments from western flank of GBB. Detail description of this deposit is given in Chapter 4. Bottom current flow is also indicated by the linear scour behind mounds and blocks in the northern portion of the study area (see Figure 2.19). Analysis of sediment samples from the onlapping sediment wedge by (Wilber et al., 1990) shows that the surface sediments contain less than 30% mud while the subsurface sediments has up to 96% aragonite mud, signifying the winnowing process by the ocean current.

Slope depositional model and evolution

Great Bahama Bank has evolved from a ramp morphology in the Miocene to a steep margin buildup today (Eberli and Ginsburg, 1987, 1989). Despite the classification of the leeward side of GBB as an accretionary slope (Playton et al., 2010), its upper margin exhibits a >100 m high escarpment margin. By definition, such an escarpment margin is separated from the coeval slope and basin by a bypass surface (Playton et al., 2010). This morphology is evident from the Holocene sediment wedge that onlaps the Pleistocene rocky surface at ~180 m water depth. However, the incision on the sediment wedge by closely spaced gullies, which act as line source for downslope transport indicates bypass of sediment. Hence, three margin architectures, i.e. accretionary, bypassing, and escarpment (McIlreath and James, 1978; Schlager and Ginsburg, 1981), co-exist in western slope of GBB.

A dense grid of sub-bottom profile data allows reconstruction of the slope morphology during late Pleistocene. Despite of the lack of core and borehole data from the study area, the age of major surfaces can be tied to seismic lines in the northern portion of GBB (see Wilber et al., 1990; Rendle and Reijmer, 2002; Slowey et al., 2002). The Holocene isopach map shows that the Pleistocene slope is cut by channels, which are perpendicular to the margin (Figure 2.25). They were more extensive in the north.

The presence of a channel-levee and fan system on the lower slope suggests turbidity currents are active in depositing the sediments. Submarine channels in an isolated carbonate system have no river input from the platform top. Off northern LBB, slope canyons are initiated by slumps, which eroded their way upslope (Harwood and Towers, 1988; Mulder et al., 2012b). The formation of channel in southwestern GBB probably has the same mechanism, judging from the breadth and the rectangular shape of the proximal incision in plan-view (Figure 2.20). Any irregularities on the slope may focus the downslope currents and enhance erosion that may contribute to slope channelization. The channels might be long-lived, initiated during past sea-level highstands when off-bank sediment transport was active. Subsequent platform-top exposure during sea-level lowstand slowed the channel deposition; this non-deposition may have promoted hardground formation. During the last interglacial maximum, the proximal portion of the channel is buried by off-bank sediment. Simultaneously however, several deep gullies incise into the buried portion of the channel (reactivation of the

channel). This cut and fill morphology is similar to the slope canyons documented in the Pliocene strata of western GBB (Anselmetti et al., 2000).

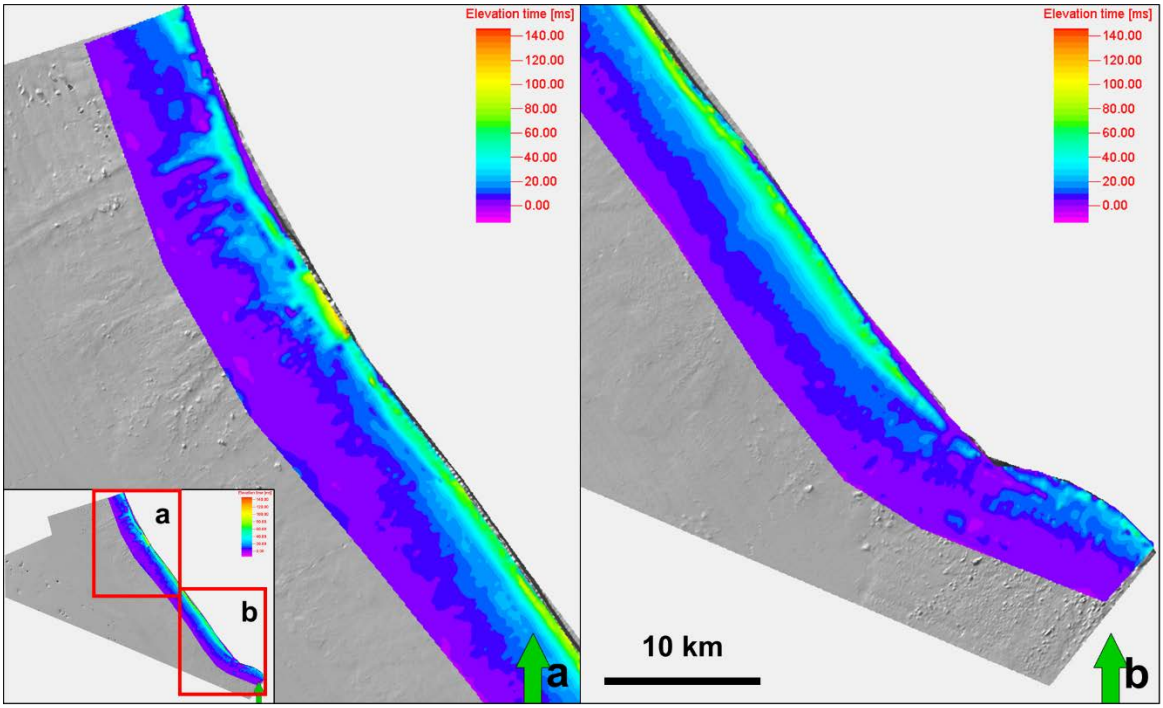

Figure 2.25. Isopach of Holocene sediment mapped from sub-bottom profile data. Warmer colors indicate thicker sediment cover. This map shows that the Holocene sediment wedge thins out approximately 5-7 km from the platform margin.

CONCLUSIONS

The slope of southwest Great Bahama Bank has a great variability in the strike and dip direction. The upper slope is characterized by a steep and furrowed wall. In the Tongue of the Ocean, a similar steep wall is built by plate-like corals, red and green algae, and sponges (Grammer and Ginsburg, 1992). It is onlapped by a sediment wedge, largely produced on the platform-top during sea-level highstand, which mainly consists of mud and peloidal sand. Most of the coarse-grained sediments bypass the upper slope through gullies and redeposit on the

lower slope as a turbidite lobes, which was also demonstrated by the boreholes from slope to basin transect of ODP Leg 166 (Eberli et al., 1997a). The slope is dissected by channel-levee and fan complex suggesting a complete turbidite system, similar to what was observed in northwestern GBB by (Mulder et al., 2012a). Megabreccia complexes occupy a significant portion of the lower slope. This type of deposit has been observed in many ancient examples, e.g. Devonian carbonates of western Canada (Cook et al., 1972) and Devonian limestone in Canning Basin (Playford, 1980).

The ability to map out the base of the Holocene sediment wedge gives an insight into the slope evolution from the late Pleistocene. The slope experiences more erosion, which is shown by numerous reentrants and channels, during the last sea-level lowstand. In the Holocene, the slope is mainly progradational due to sediments transported from the bank top.

The recognition of spatial variability of a carbonate slope and its controlling processes are crucial. The understanding of those variables has the application in hydrocarbon exploration, where discoveries were made in the slope and basinal settings e. g. Poza Rica, Mexico (Janson et al., 2011) and Tengiz, Kazakhstan (Collins et al., 2006).

CHAPTER 3. MARGIN COLLAPSE AND SLOPE FAILURE IN SOUTHWEST GREAT BAHAMA BANK

OVERVIEW

Steep embayments along carbonate platform margins have been observed in many ancient outcrop and subsurface examples (e.g. Cook et al., 1972; James, 1981), but a modern analog is not very well documented (Mullins et al., 1991). The term 'scalloped margin' was coined by Mullins and Hine (1989) to describe a convex bankward embayment observed in the west Florida Shelf and the eastern Bahamas region caused by platform margin collapse. This morphology has been linked to the deposition of breccias and megabreccias on the slope and basin floor (Playford, 1980; Mullins et al., 1986; Mullins et al., 1991; Hine et al., 1992; Morsilli et al., 2002). Isolated large blocks in the debris field can easily be mistaken as bioherms (Cook et al., 1972). In the absence of multibeam bathymetry data, the relation between margin collapse and their depositional products is not easy to establish. Several multibeam surveys in the Bahamas now provide the first regional data of modern slope and margin failures. For example, a large slope failure and mass transport complex (MTC) on the modern slope was imaged in northwest Great Bahama Bank (GBB) (Mulder et al., 2012a).

The study area is located at southwestern GBB, in the northern edge of the Cuban-Bahamas collision zone (Figure 3.1). Four margin and upper slope failures have been identified using multibeam bathymetry data. These failures have shed large debris blocks to the toe-of-slope and basin floor some tens of kilometers from the

platform margin. Debris blocks and boulders from mass transport events also provide substrates for deep-water coral communities (Mullins et al., 1984; Correa et al., 2012a; Correa et al., 2012b). This current study is focused on defining the distribution, geometry, and morphology of mass transport complexes on the carbonate slope and their relation to the upper slope morphology.

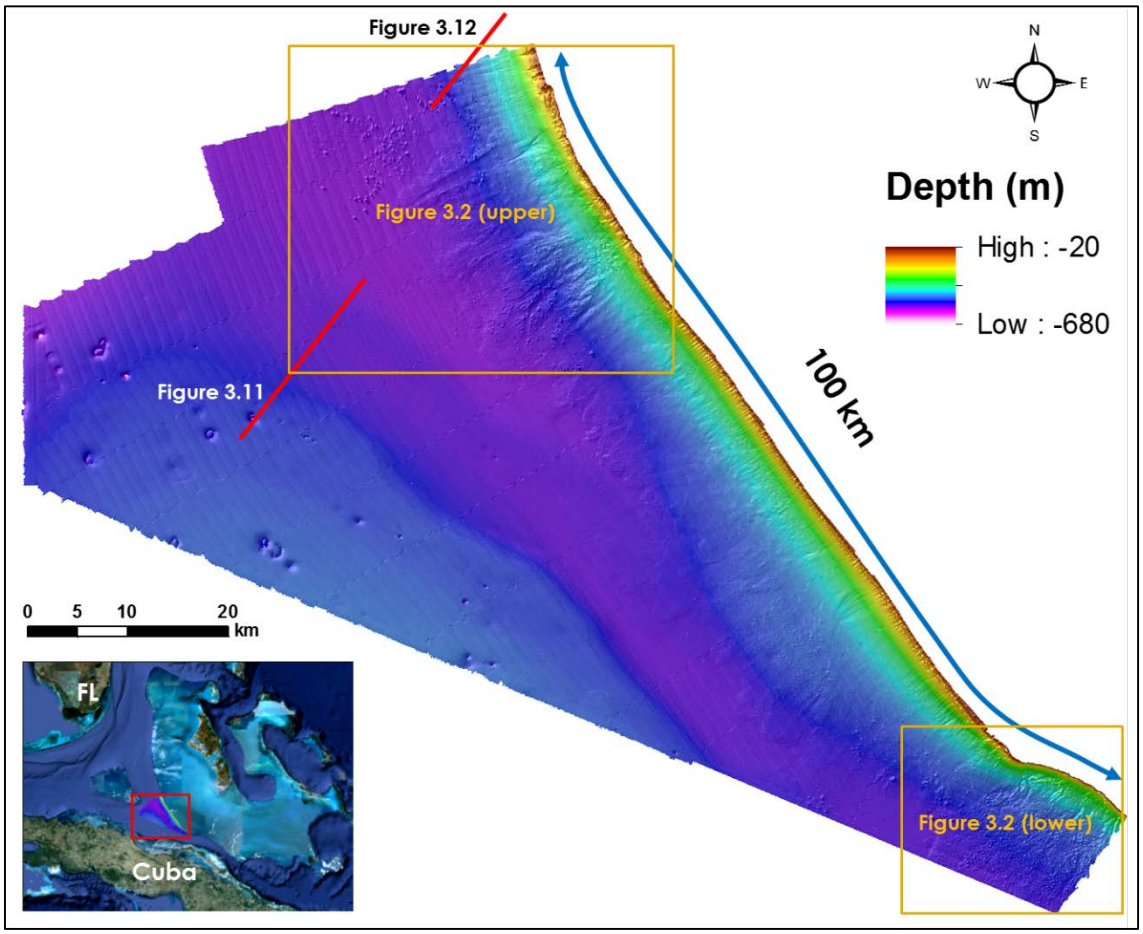

Figure 3.1. Multibeam bathymetry data from the study area.

RESULTS

Margin and upper slope morphology

Within the study area, the platform edge is not continuous but is interrupted by crooked and convex bankward morphology. There are four segments with such a morphology along the ~100 km margin length, two in the north (segments *a* and *b*) and two in the south (segments *c* and *d*). The four zones are identified by their shape and accentuation in steepness (Figure 3.2). Table 1 summarizes the margin collapse dimension and the associated mass transport complex.

Table 1. Summary of the margin collapse segment *a* to *d* with their associated mass transport complex.

Segment	Length of margin scar (km)	Upper slope angle (°)	Deposits on lower to toe-of-slope	Lower slope failure	Volume of eroded slope est. (km^3)
a	6	~50	mound field, block field, a slope channel-fan complex	No	N/A
b	6	~50	channelized debris field	No	N/A
c	3	~30	blocks	No	N/A
d	23	>70	debris field, a channel	Yes	30

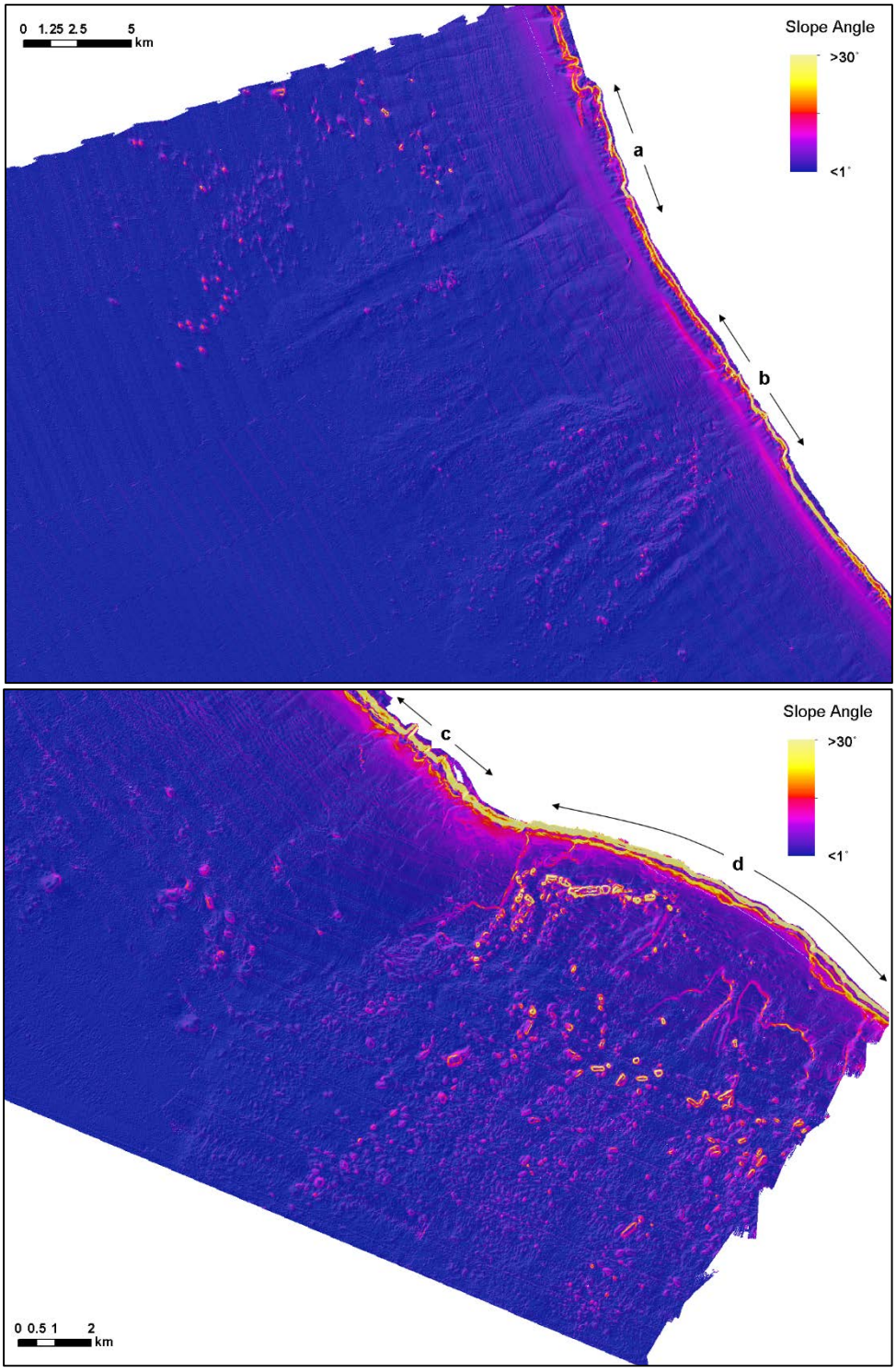

Figure 3.2. Shaded steepness map derived from bathymetric map that shows four segments (a-d) of margin with crooked and convex bankward morphology. It also shows the associated mass transport deposits on the slope and basin floor.

Margin failures

Segment a

A convex bankward morphology (segment *a*) occurs for 5 km along the margin. For this length, the platform top edge is gently sloping until it reaches the break at ~50 m water depth (Figure 3.3a). The platform edge is shallower than the adjacent non-failure affected edge, which is ~65 m. The upper slope has a mean steepness of 50˚, and a maximum of 60˚. It is carved by numerous slope perpendicular furrows. The upper margin steepness decreases to less than 30˚ at 90 m water depth. At a depth of 140-160 m, the upper slope is onlapped by a sediment wedge. At the point of onlap an irregular and discontinuous moat occurs, but does not show the ridge and moat pattern of the "normal" margin. Multiple v-shaped incisions of ~10 m deep are observed to be incised in the sediment wedge.

Downslope of the margin scar, a complex of large blocks with a slope channel and fan system occurs on a <1˚ lower slope and basin floor. This debris field extends for 13 km along strike and downslope for ~22 km from the platform margin.

Segment b

Convex margin segment *b* (Figure 3.3b) is found 9 km south from margin collapse segment *a*. This segment is 8 km long. The declivity of the upper slope is similar to segment *a* (50˚); however, the depth of platform edge ranges from 40-60 m. Several deep furrows mark the margin and upper slope. These furrows are up to 150 m deep and connect downward to v-shaped incisions on the onlapping sediment wedge. Gullies, which are common on the middle slope, are connected

to those incisions and extend downslope for ~3-4 km. The sediment wedge partly buries the blocks that are deposited on the toe-of-slope, around 5 km from the platform margin where it thins out (Figure 3.4).

A channelized debris field is found on the lower slope and basin floor beneath margin collapse segment *b*. It is 13 km wide and extends outward to 20 km from the platform margin. Massive blocks that range from 100-400 m wide and 20 m high are scattered across the debris field. The debris field is cut by several channels 800-1000 m wide, 2-5 km long, and 4-8 m deep.

Segment c

Further south, segment *c* forms a smaller embayment at 3 km long (Figure 3.3c). A reentrant, ~300 m deep, and several other smaller reentrants cut into the platform edge. The upper slope is onlapped by a thin sediment wedge. A shallow moat, ~ 5 m deep, occurs at the top of the onlap wedge.

Several large blocks occur below segment *c* on the lower slope. These blocks are located 3 -10 km downslope from the margin failure. The blocks are 200-600 m across and approximately 20 m high. There are less than 30 large blocks in the field and they are distributed over 100 m apart.

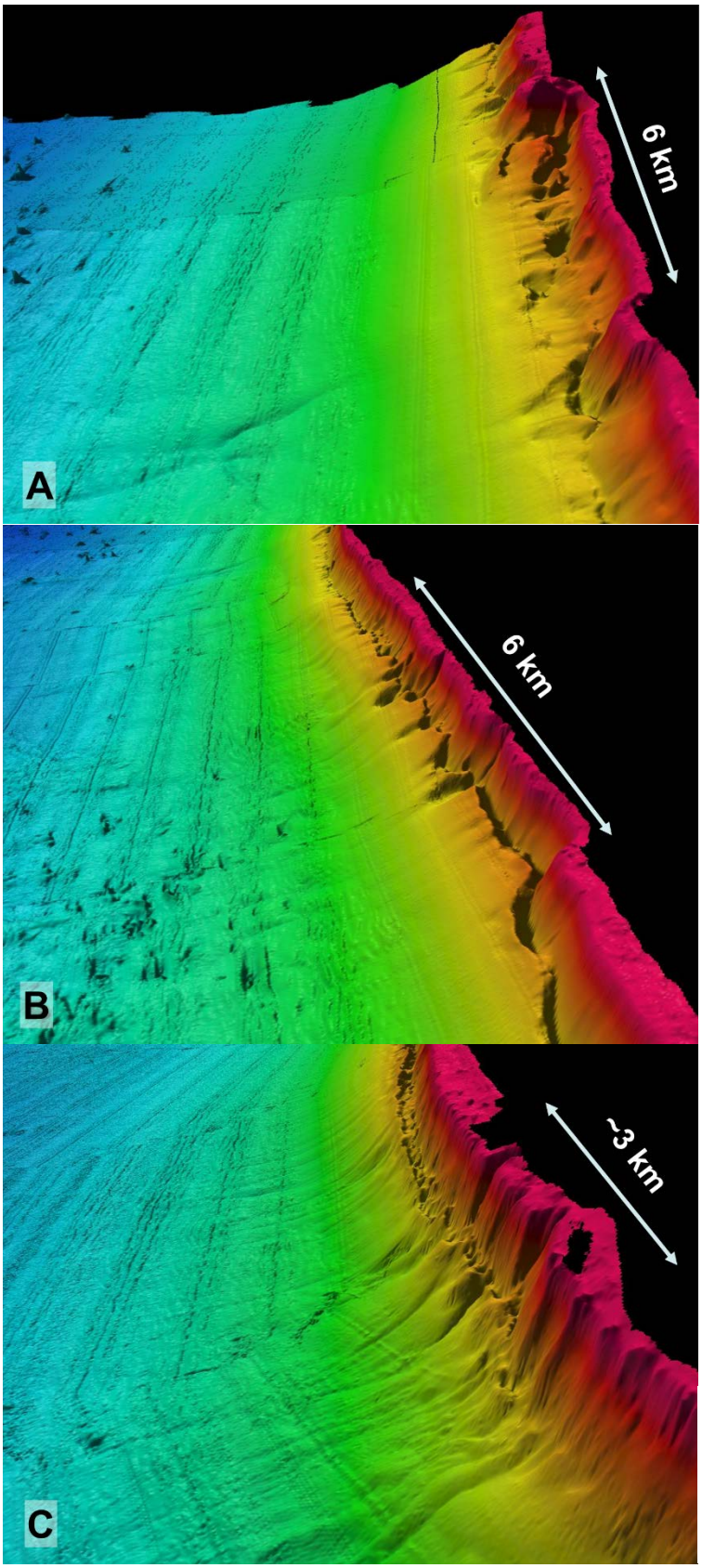

Figure 3.3. Margin scar segments *a*, *b*, and *c* that show crooked and convex bankward margin morphology

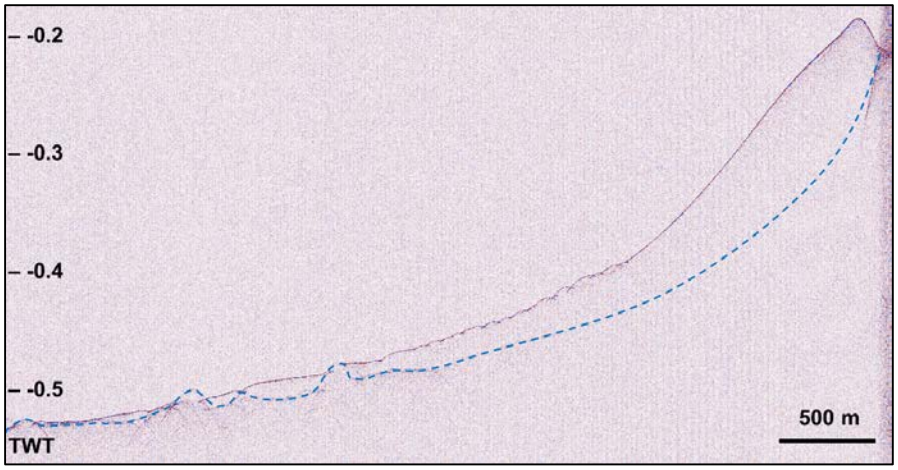

Figure 3.4. Interpreted sub-bottom profile that shows boulders partially buried by the Holocene sediment wedge. This cross-section is from margin collapse segment *b*. The Pleistocene surface is marked by the blue dashed line.

Large scale multiphase failure (segment *d*)

The platform margin of segment *d* forms a large convex bankward morphology that runs for a length of 21 km as measured on satellite imagery. The multibeam bathymetry dataset, however, only covers 12 km of the marginal scar (Figure 3.5). The upper slope has a higher declivity (60-76˚) compared to the other margin failures in the study area. The upper slope is onlapped by a thin sediment wedge with a moat up to 10 m deep. The declivity of the sediment wedge is ~20˚ at the upper part, which is also higher compared to the non-failure slope in the study area (~8˚).

Beneath segment *d*, a large mass transport complex was deposited on the slope and the basin floor. This mass transport complex is bounded by a vertical displacement (scar) that runs from the platform margin to the slope (Figure 3.5). Blocks, slope failure scars, and margin collapse deposits mark this 13 km slope to basin floor transect.

Upslope of the east of the scar, the middle slope is incised by gullies 5-10 m deep which are spaced every 200-400 m (Figure 3.5). Downslope, there is an elongated slab that is 1.5 km long, 250 m wide, 60 m high and oriented oblique to the margin (label b in Figure 3.5). It is deposited in 375 m water depth, 1.1 km away from the margin. Several large blocks, 200-300 m long and ~30-60 m high, are also emplaced in a linear fashion along the scar with size decreasing downslope. A 300 m wide and 2 km long channel occurs down the middle slope (label c in Figure 3.5). This channel starts at 320 m water depth and has incised to 15 m deep. The channel begins just below a large block (200 m wide 30 m high).

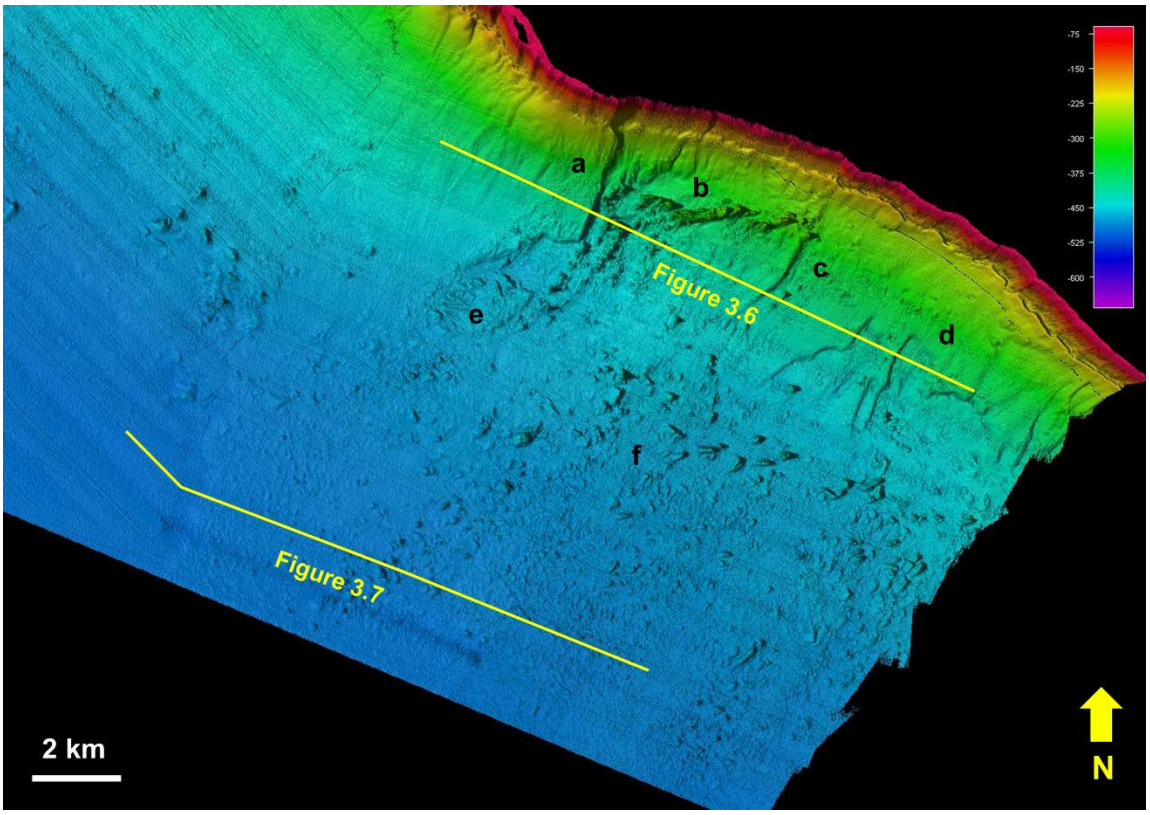

Figure 3.5. Margin failure on segment *d* with a large convex bankward morphology. a) a scar that runs from the margin to the lower slope, b) an elongated fragment of collapsed margin, c) a channel, d) a series of slump scars on the lower slope, e) a detached lithified slab, and f) debris field on the basin floor. Yellow lines indicate sub-bottom profile locations.

Lower slope failure

The lower slope experienced multiple failures. These failures left slide scars and produced large amounts of debris and blocks that were transported to the toe-of-slope and basin floor. There are four separate slide scars discussed here (label d and e in Figure 3.5).

In the west, a rectangular slab of the lower slope slides 1.2 km downslope and left a scar 750 m wide and 20 m high (label 4 in Figure 3.5). This slide scar occurs at 430 m water depth on a 2˚ slope, west of the large scar. The detached slab is 2000 x 800 m in dimension. The upper right corner (northeast) of the slab has begun to disintegrate, to produce a rafted boulder of 400 x 200 m across and 14 m high (label e in Figure 3.5). To the east, three slump scars are observed on a 2.5˚ slope at ~360-375 m water depth. Their lengths range from 600 - 1700 m across. On the floor of all three scars, a scar-bounded trench occurs. This trench is ~20 m deep and 1 km long. The sub-bottom profile shows that all slide scars are covered by Holocene sediment (Figure 3.6).

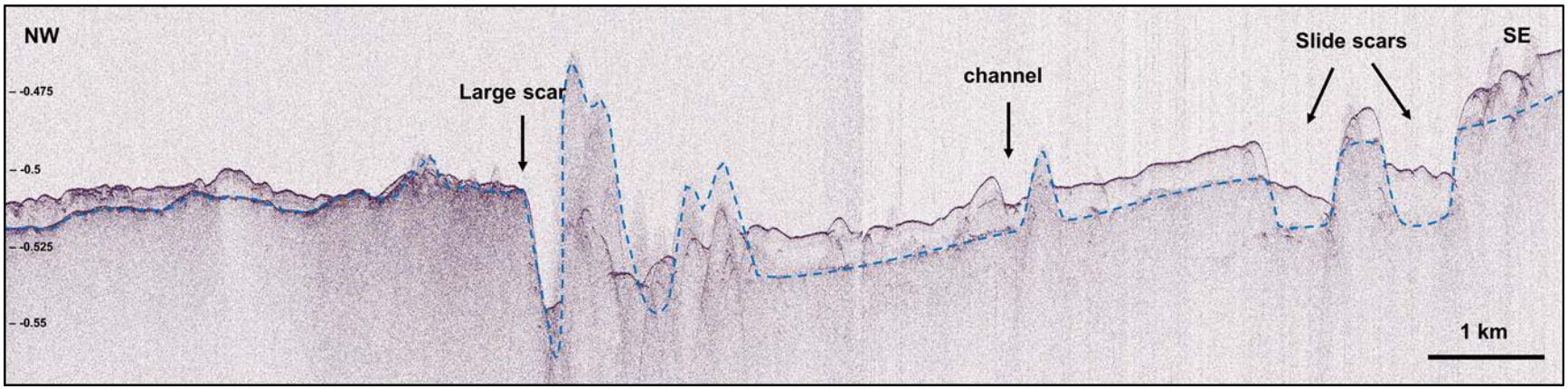

Figure 3.6. Sub bottom profile from the big scar (segment *d*) showing the slope is displaced at the Pleistocene (blue dashed line) surface which is draped by thin Holocene sediment. Boulders and blocks that resulted from the margin and upper slope collapse were also deposited on the Pleistocene surface.

Debris and block field

The toe-of-slope and basin floor are covered by downslope displaced debris and blocks (label f in Figure 3.5). One such block is ~100–600 m across and ~30 m high. Most of the larger blocks are >400 m long are scattered in water depths ranging from 450–490 m. These blocks are mostly elongate. Further downslope, blocks are smaller (<200 m in diameter) and rounded, and are deposited more closely spaced. The entire mass transport deposit creates a topographic relief of approximately 10 m on the basin floor.

Sub-bottom profiles across the debris and block field display many diffractions in the shallow subsurface, as deep as 10 ms (TWT) (Figure 3.7). The size of the blocks is comparable to those in the megabreccia debris flow deposits described from the Canning basin (Playford, 1980) and the modern Nicaraguan Rise (Hine et al., 1992).

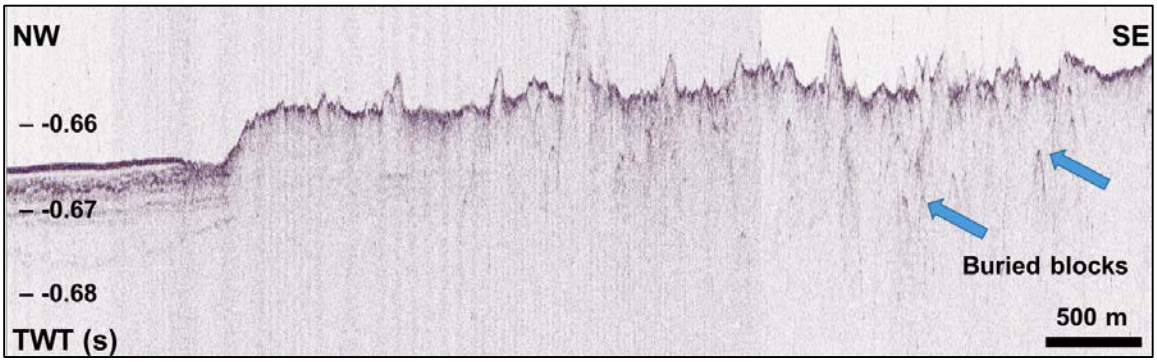

Figure 3.7. A sub-bottom profile across the mass transport deposit resulting from the margin and slope failure in segment *d*. This deposit creates 10 m relief compared to the surrounding pelagic (undisturbed) deposit. Parallel and more coherent reflections on the left are interpreted as pelagic sediments that partly bury the debris field. This cross section is located 12 km from the platform margin (see Figure 3.5 for location).

Platform margin retreat

To capture the relation between the slope morphology and the basinal debris deposit, a semi-quantitative analysis was performed. Three different parameters were measured along the strike: the upper slope angle (steepness), the depth of the margin break, and the debris density. The 100-km long length of margin that was used for this analysis is shown in Figure 3.1.

Upper slope angle (steepness)

A map of slope steepness shows a ~300 m wide band of high declivity (>25˚) on the upper slope at ~60-180 m water depth. The margin break to uppermost part of the slope typically has the highest declivity, it then shallows slightly and then gets steeper again before it is onlapped by the sediment wedge. For the analysis, the upper slope angle (steepness) parameter is also recorded at the uppermost slope in 500 m intervals along the margin strike.

Depth of margin break

The depth of margin break is the depth to the abrupt change from the platform top to the uppermost slope. The depth is measured along the margin strike in 500 m intervals.

Debris density

The debris density parameter is used to represent the quantity of debris on the toe-of-slope and basin floor. It measures the area of seafloor covered with blocks per unit area. Firstly, the debris and blocks are identified based on slope angle cut-off

criteria on the steepness map. Data points with a greater slope angle than 4˚ are treated as blocks. After a map containing the block distribution is generated, the debris density is calculated within a 1x1 km area (Figure 3.8). With an average block size of more than 200 m across, a 1x1 km area is sufficient to capture the variability without losing significant details. The debris density measurement was made on the basin floor ~8.5 km away from the platform margin, perpendicular to the data points collected on the platform edge.

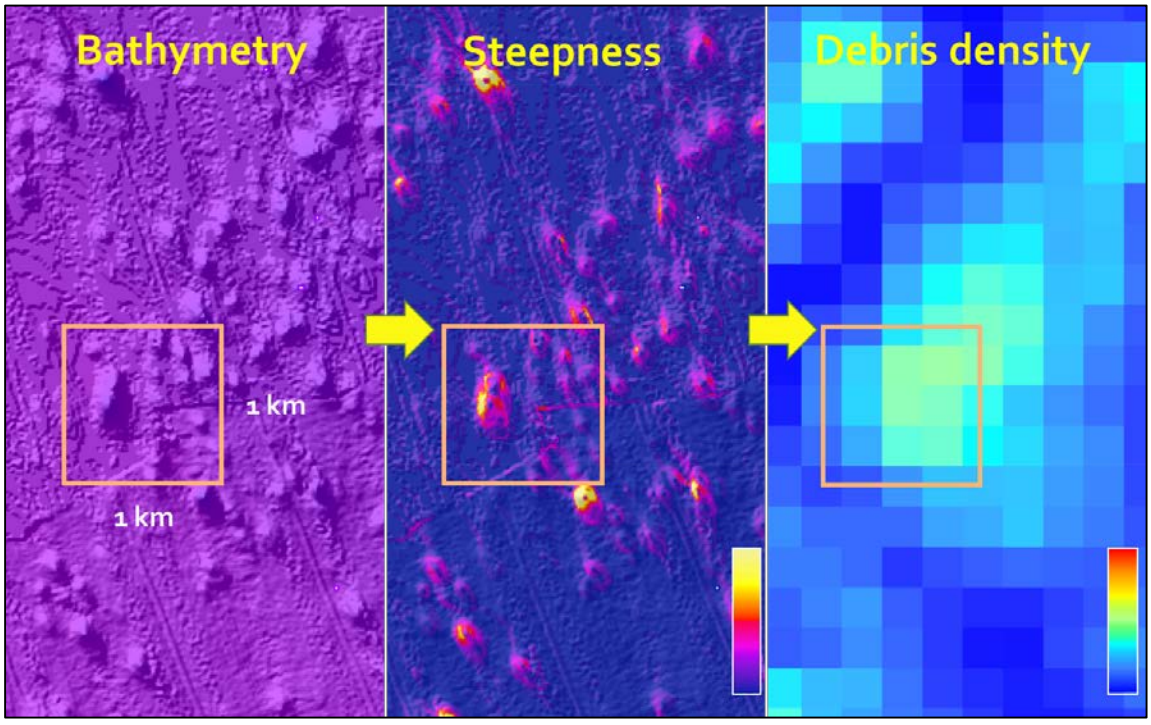

Figure 3.8. Illustration of the workflow to calculate the debris density. The steepness map is derived from the bathymetry map. The steepness of the features is calculated and, using 4˚ slope angle cut-off, the blocks are isolated. Finally, the density of the debris is computed in a 1x1 km bin size.

Analysis

In Figure 3.9 the measured parameters are plotted against the distance along the margin from north to south. The graphs show that the typical slope angle of the upper slope in southwest GBB ranges from 20-40˚ with the margin break at ~60 to 65 m water depth. In areas of margin collapse (labeled *a*-*d* in Figure 3.9) the steepness and the debris density all increase while the depth to the margin break decreases. Segment *a* and *b,* which have similar scar lengths, also have similar margin morphometrics and debris density parameters. The largest convex bankward morphology in the southernmost portion of the study area (segment *d*) reaches up to 23 km long (from satellite imagery), has a significantly higher upper slope angle (>70˚), a shallower depth of margin break (<40 m), and a large increase in amount debris on the basin floor.

Those data indicate that the margin collapse causes the platform edge to retreat and become steeper and shallower. The amount of blocks and debris being shed strongly relate to the size and extent of the collapse.

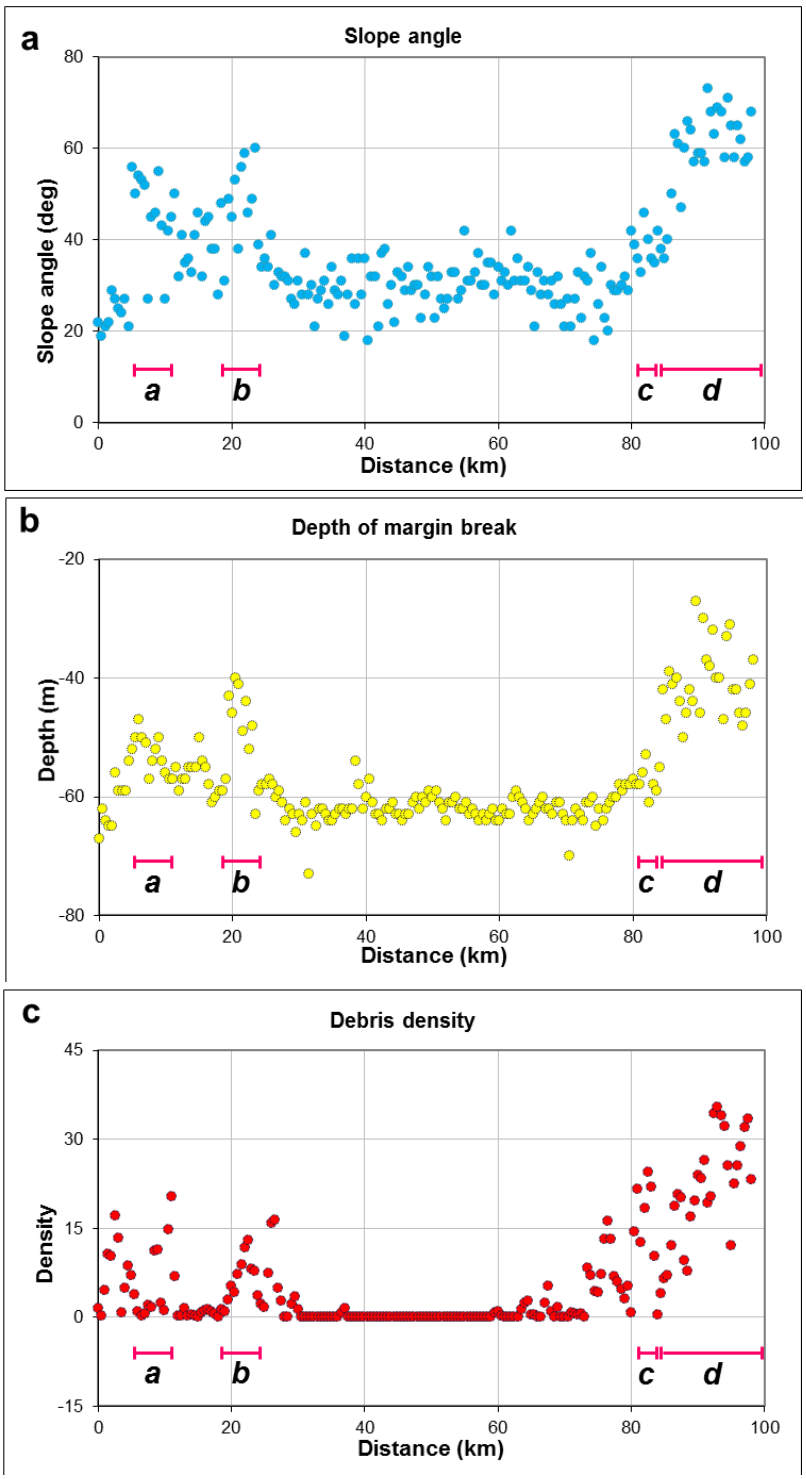

Figure 3.9. Plots of (a) upper slope angle, (b) depth of the platform margin break, and (c) the debris density along the strike. Locations of segments *a* to *d* are marked on the graphs. All three parameters display disturbances in the areas of margin collapse (segments *a*-*d*).

DISCUSSIONS

Volume of material eroded off the margin

Deviations from the average margin slope profile help in estimating the volume of margin collapse. The top of the western Great Bahama Bank slopes on average with a 3˚ declivity to a water depth of ~60 m, which is the average depth of the margin break (Figure 3.10). Along the collapsed margin of segment *d*, the largest collapse feature in the study area, the depth of margin break is shallower at ~30 m. Using the 3˚ inclination for the sloping bank margin, a margin retreat of ~400 m can be calculated. Furthermore, when using a simple wedge geometry model, the estimated volume of material that was transported to the toe-of-slope and basin floor from the 23 km long marginal scar is ~30 km^3.

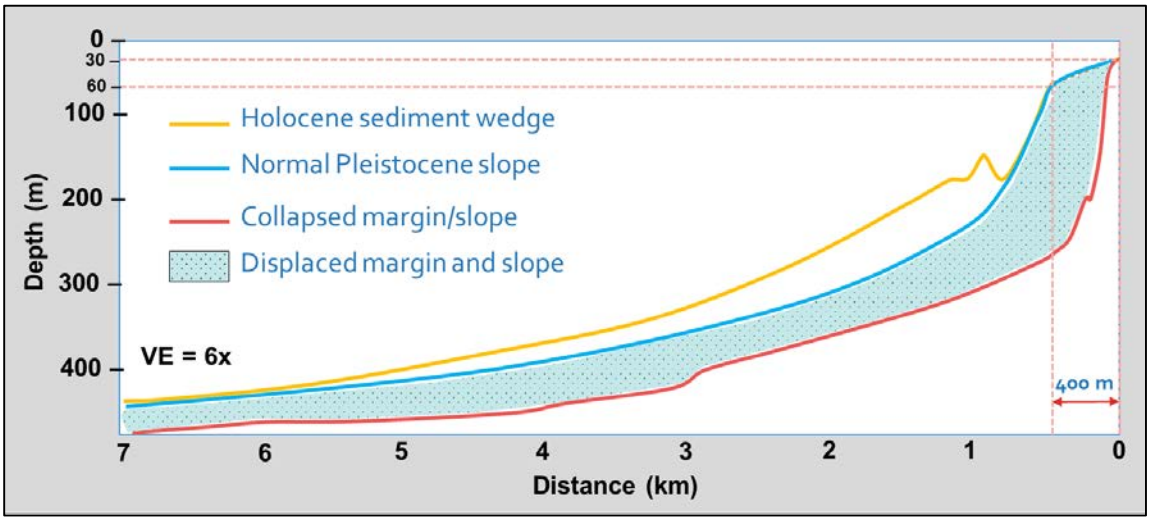

Figure 3.10. Profile of normal and failure-affected slopes. In the collapsed margin, the platform edge is shallower, at ~-30 m water depth. It suggests that the margin retreated 400 m bankward and a significant amount of margin and slope deposits was caved away.

Triggering mechanisms

Submarine landslides in siliciclastic environments have been well documented. They usually occur along specific detachment layers, e.g. a methane hydrate layer (Rothwell et al., 1998). Seismic shock and sea-level lowering are postulated to induce the release of methane and induce the instability. Others have postulated that the size and location of the submarine slides are more related to sedimentation and erosion processes rather than slope angle and seismic activity (McAdoo et al., 2000).

In the carbonate environment, the triggering mechanisms for failures are not well constrained due to a lack of modern examples. Mechanisms that could initiate mass movements include: seismic shock, storm wave, over-steepening, differential cementation, or the release of pore water pressure due to a fall in sea level (Cook et al., 1972; Hilbrecht, 1989). (Mulder et al., 2012a) describe a large slope failure on the slope of GBB further north from the study and attribute the failure to methane release based on small pockmarks visible above the slope scar.

It is commonly thought that failure is more pervasive on the uncemented lower slope than the steep cemented margin. Seismic data from northern Little Bahama Bank reveal numerous slump scars on the lower slope at water depth >550 m (Mullins et al., 1984). There the slope failure occurrence is related to the less cemented lower slope. The submarine cementation also stabilizes the sediments on the upper slope and controls the headward extension of submarine canyon. However, slide scars tens of meters across were observed on the cemented slope in the Tongue of the Ocean (Grammer and Ginsburg, 1992).

The role of sea-level fluctuations in generating instability on carbonate slope is not yet clear. Based on an outcrop study, Spence and Tucker (1997) attributed the collapse of a low-angle slope to overpressure, which is released during a relatively rapid fall in sea level. They downplay the role of oversteepening and seismic shock as trigger mechanisms for margin failure. Sarg (1988) proposed higher slope erosion during sea-level lowstands. Yet, the age of the failure scar in the upper slope of TOTO indicates that it must have taken place during the transgression (Grammer et al., 1993).

There are two types of failure in the study area: collapse that affects the platform margin and the uppermost slope, and slides on the lower slope. The breccia from the upper slope might be transported as rock-fall or slide to the base of the slope: for example a large fragment of 3 km long in Figure 3.5 (label b). These upper slope materials incorporate mud and fine sands from the slope and can get transported further as debris flows, kilometers away from the upslope source area. This type of transport might also induce turbidity current further downslope.

Failures in the lower slope occur in slides or slumps. These mass movements can occur in both the lithified and partly lithified slope. When a lithified slope breaks, the detached material can travel kilometers downslope (e.g. label e in Figure 3.5). Partly lithified slope packages are more likely to disintegrate and produce smaller debris.

The sediments and rocks in each environment have different mechanical properties and hence, their instability might be induced by different mechanisms.

Below are several possibilities for triggering mechanism of the slope failures in southwest GBB.

Earthquake/seismic shock in the Bahamas region

The northwestern Bahamas is considered a seismically inactive region today; however, its tectonic history involves an interaction with the eastward moving Caribbean plate relative to North America. Its former plate boundary, the present day Cuba, which was a Cretaceous island arc, began to collide with the North American passive margin (Bahamas) in the Paleocene. The collision ceased in the Middle Eocene. Afterward, during the Middle to Late Eocene, the Caribbean plate continued to drift east-northeastward relative to the North American plate. This continued eastward motion occurs along a new plate boundary. The Greater Antilles (Cuba) was welded to the North American plate (Pindell, 1993).

The northward termination of the collision zone is marked by the Santaren Anticline located offshore north of Cuba and southwest of Great Bahama Bank (Masaferro et al., 1999). Growth strata analysis on the Santaren Anticline has suggested that the far-field deformation is still ongoing (Masaferro et al., 1999). Seismic line BPC2011-15 (Figure 3.11) that runs NE-SW shows that there is a relatively young fault that extends up to the seafloor. This fault creates elevated topography on the seafloor along western side of this study area (Figure 3.1). On the same seismic line to the east, an anticline is deformed by a fault with normal displacement on the crest that extends up to the seafloor, suggesting a change in tectonic regime, from compressional to extensional or transtensional.

There are no modern records of seismic epicenters in the vicinity of Great Bahama Bank (USGS[1]). Earthquakes are concentrated along the Caribbean plate boundary (>350 km from the study area) and might have more impact on the eastern Bahamas. However, earthquakes in Cuba (1880) have been known to send vibrations that can be felt in Key West, Florida (USGS[2]). More recently, in September 10, 2006, an earthquake of 5.8 Magnitude in the Gulf of Mexico was felt in Miami, Florida (USGS[3]; D. F. McNeill and M. Grasmueck, personal communication).

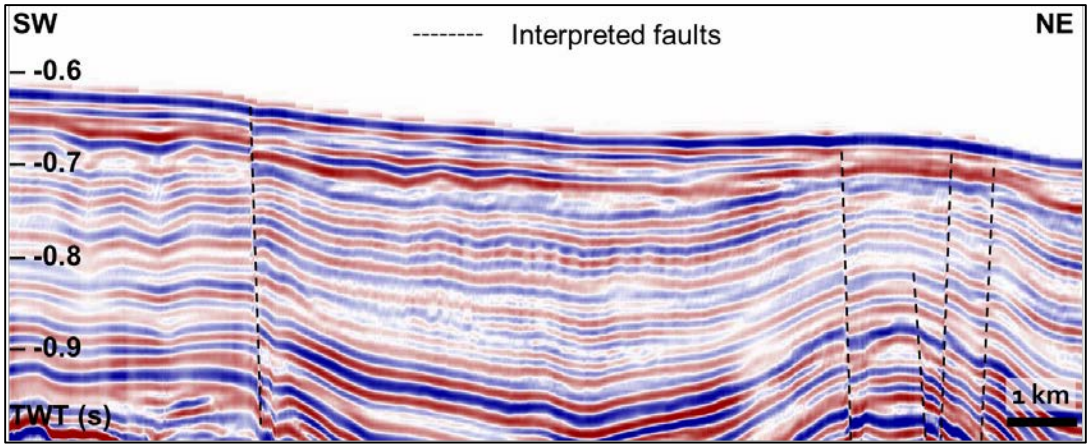

Figure 3.11. Seismic line BPC2011-15 showing relatively young faults that extend to the seafloor. The fault on the left causes higher topography on the seafloor in the west the study area (see Figure 3.1 for location).

Faults and fractures by sediment loading and compaction

A study of the syndepositional fractures in Canning Basin shows that the fracture patterns are related to the early cementation and the proximity to the platform margin (Frost and Kerans, 2010). In a Neogene slope example, McNeill and Eberli

[1] http://earthquake.usgs.gov/earthquakes/world/caribbean/seismicity.php
[2] http://earthquake.usgs.gov/earthquakes/states/florida/history.php
[3] http://earthquake.usgs.gov/earthquakes/eqinthenews/2006/usslav/

(2009) reported early fractures in a core from the western margin of Great Bahama Bank. These fractures are concentrated in Middle Pliocene cemented coarse-grained package that was loaded by the prograded margin in the late Pliocene. Seismic line BPC2011-11 (Figure 3.12) shows that the reflections of prograding slope sediment are disrupted by numerous discontinuities interpreted as faults.

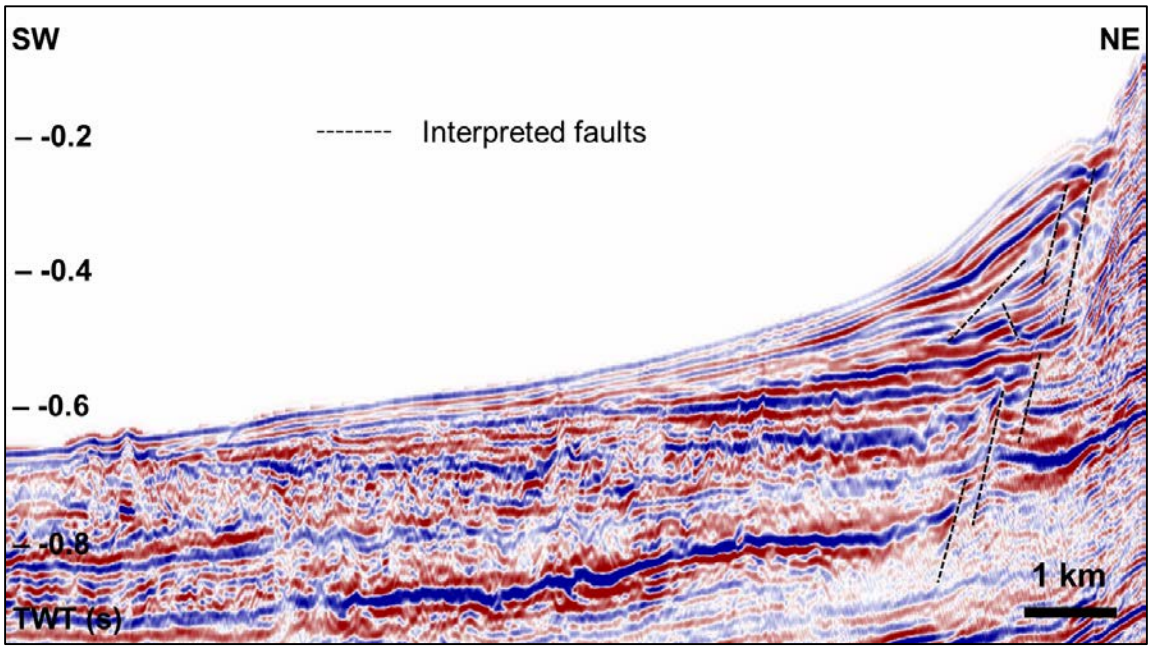

Figure 3.12. Seismic line BPC2011-11 showing interpreted faults in the slope package (see Figure 3.1 for location).

Weak detachment layer

ODP Leg 101 in the Bahamas discovered that modern slump scars are associated with the collapsed wall of the slope canyons (Austin et al., 1988). During the Pliocene however, numerous small-scale downslope movements and slump masses occurred on a detachment surface (Harwood and Towers, 1988). Turbidites within the periplatform ooze can potentially act as detachment surface based on a core study from slopes along the Great and Little Bahama Bank (Eberli,

1988). In the cores from these slopes, the bottom layer of the turbidites contains more interstitial water, which is prone to overpressure and may act as a detachment layer. Similar processes likely control the occurrence of lower slope failure in this study area.

Timing of the margin collapse and the slope failure

The lack of core material does not allow a precise age date for the margin collapse in this study. The timing of collapse is best deduced based on relative succession. The only dating on the slope failure available in the Bahamas is from the study of (Grammer et al., 1993). The radiocarbon dating of the cement and skeletal component of the upper slope in TOTO suggests that the slope failures are fairly young, about 10 kyr ago, which coincide with the rise of sea level just before the onset of platform flooding.

In the study area, morphometric analysis of the slope suggests that the debris field resulted from the margin and upper slope collapse (Figure 3.9). The sub-bottom profiles across the debris field show that the blocks were deposited on top of the inferred Pleistocene surface and onlapped by Holocene sediments (Figure 3.4 and Figure 3.6). This suggests that the margin collapse is older than the platform flooding ~7000 years ago. On a sub-bottom cross-section (Figure 3.6), a series of slide scars on the lower slope erode into the Pleistocene surface, but the scars are now draped by Holocene sediments suggesting an age equivalent with the margin collapse.

CONCLUSIONS

The margin and cemented upper slope of southwestern Great Bahama Bank are prone to collapse. Four separate segments of margin failure have been identified in the study area. Those failures are associated with mass transport deposits on the slope and the basin floor. The largest margin collapse located in the southernmost portion of the study area is followed by multiple failures on the lower slope. It is estimated that the platform margin retreated more than 400 m bankward from the collapse.

Based on sub-bottom profile data, we interpret the timing of the catastrophic collapse to have occurred before the platform flooding began 7 kyr ago. This is in agreement with the dating on the slope failures in TOTO by (Grammer et al., 1993).

There are two most likely triggering mechanisms for the margin collapse. Located in the northern edge of Cuban fold and thrust belt, seismic shock may have triggered the collapse. The other explanation is rapid slope sedimentation in the prograding leeward margin of GBB as proposed by McNeill and Eberli (2009), which might have induced fracturing and faulting and contributed to the instability of the slope.

CHAPTER 4. POCKMARKS ON THE DRIFT DEPOSITS IN THE FLORIDA STRAITS

OVERVIEW

Pockmarks are depressions in the seafloor, which are usually related to fluid flow escape from muddy sea-floor sediment (Hovland et al., 2002). They were first discovered on the Scotian Shelf (King and MacLean, 1970). The fluid expelled from a pockmark can be hydrocarbon (both thermogenic and biogenic) (Loseth et al., 2009; Vaular et al., 2010), submarine groundwater on sediment mixed with groundwater (Robb, 1990), or volcanic, i.e. hydrothermal gas (Pickrill, 1993).

The occurrence of circular depressions in carbonate environment, however, is often ambiguous as to whether they are fluid escape structures or dissolution features. Submarine sinkholes in carbonate environment were discovered in the eastern Florida region, along Pourtales and Miami Terraces (Jordan, 1954; Jordan et al., 1964; Land et al., 1995; Land and Paull, 2000). Those sinkholes (up to 960 m in diameter) were interpreted as karst features. Betzler et al. (2011) relate giant pockmarks (up to 3000 m across and 180 m deep) on the periplatform slopes in the Maldives to seepage from deep-sourced hydrocarbons, with their differing morphologies reflective of different stages of formation. On the western slope of Great Bahama Bank, a few small pockmarks (50 m in diameter) have been recently observed as the seafloor imaging has become more extensive (Mulder et al., 2012a). A recent multibeam bathymetry study from north of Cay Sal Bank also reveals a pockmark field on sediment drift deposit (Betzler et al., 2013). These

pockmarks were attributed to fluid migration through faults which extend to, and displace, the sea-floor.

In this chapter, we document the occurrence of mega-pockmarks in the Florida Straits. The pockmarks morphology is characterized using multibeam bathymetry data. Their diameter ranges from 163 m to 3235 m. The genesis of the pockmarks is analyzed using 2D seismic data and correlated with regional well data.

METHODOLOGY AND DATASET

Seafloor morphology was analyzed with high-resolution multibeam bathymetry data along the upper slope to basin floor between Great Bahama Bank (GBB) and the seafloor south of Cay Sal Bank (CSB). The data was acquired by Fugro Geoservices in 2011 using a Reson SeaBat 8160 59 kHz Multibeam Echosounder (MBES) system. This system also recorded the backscatter data. The surface bin resolution for multibeam bathymetry data is from 10 to 15 m. In addition, the top 1 s (TWT) of multichannel seismic data acquired in 2011 by Spectrum ASA were incorporated in the study. These seismic data consist of 27 densely sampled, 160-fold seismic lines. Seismic multiple attenuation was done using a combination of 2D Surface Related Multiple Elimination (SRME) and High-Resolution Radon demultiple techniques. Finally, two passes of Kirchhoff pre-stack time migration were applied to the dataset. In addition, an older seismic dataset was used that helps correlate borehole age data to the new data (Bergman, 2005).

REGIONAL SETTINGS

The highly deformed Cuban fold and thrust was formed as a result of the collision between the Cuban arc and North America during the late Cretaceous and early Tertiary (Pindell, 1993). The growth fold strata from an anticline in the Santaren Channel documents that the deformation continues until the Pliocene and maybe until the present day (Masaferro et al., 1999).

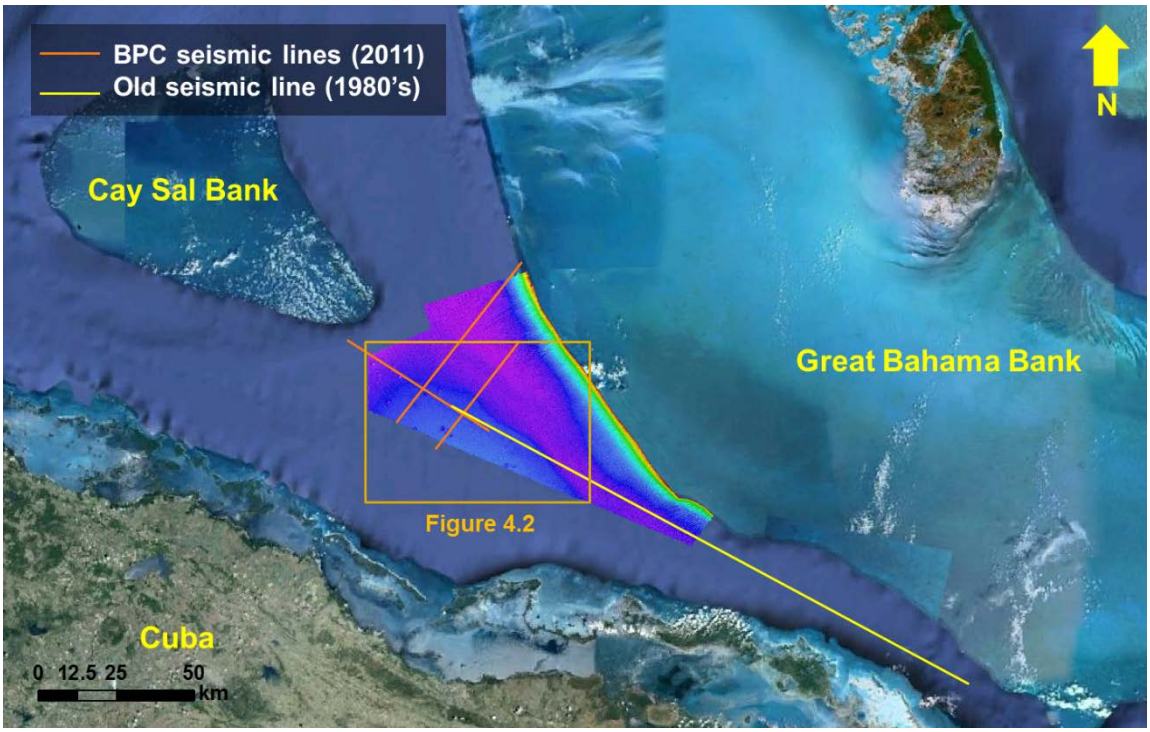

Figure 4.1. Location of study area in southwestern Great Bahama Bank. Data available for this study include multibeam bathymetry, multichannel seismic lines from 2011 and 1980's.

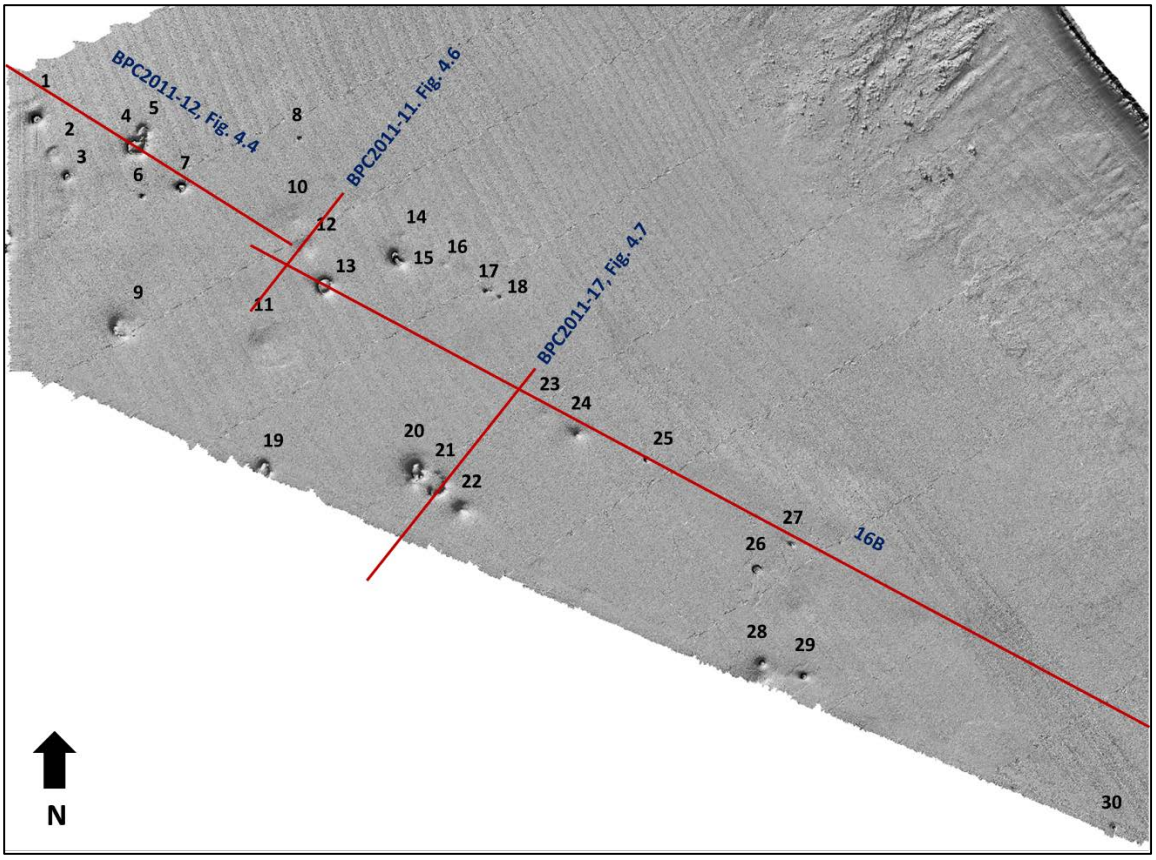

Figure 4.2. Shaded relief map showing the thirty pockmarks on the seafloor. Pockmarks which were measured are numbered.

RESULTS AND INTERPRETATION

Pockmarks morphology

Thirty pockmarks were observed on the surface of the seafloor in the west of the study area. The morphology of the pockmarks ranges from a very gentle and shallow circular depression to a deep and steep-walled sinkhole-type hole (Table 2). The average diameter and depth of the pockmarks are 980 m and 37 m respectively. The largest pockmark by diameter is 3235 m wide, and 9 m deep.

The smallest pockmark is 163 m wide and 70 m deep. The deepest pockmark is 135 m deep and 546 m wide, whereas the shallowest is 1 m deep and 646 m wide.

Morphometric analysis included measuring the width, depth, and slope angle of the pockmark's wall. These parameters were then normalized to the largest value in each category. The normalized curves show that the width and the depth of the pockmarks are not correlative, whereas the depth is positively correlated to the declivity of the wall (Figure 4.3).

Table 2. The dimension of pockmarks that were measured in this study. The pockmarks with largest and smallest diameter are shaded in blue and light blue respectively. The deepest and shallowest ones are shaded in yellow and light yellow respectively.

#	diameter (m)	gradient of the wall (deg)	depth (m)	#	diameter (m)	gradient of the wall (deg)	depth (m)
1	510	71	120	16	482	0.5	2
2	1,180	2.8	7	17	163	60	70
3	572	35	40	18	266	39	33
4	1,324	29	36	19	1,172	9	24
5	1,392	15	20	20	1,422	29	46
6	211	64	85	21	2,005	20	33
7	546	55	135	22	1,192	4	28
8	276	32	32	23	1,645	0.5	3
9	1,875	3	18	24	614	8.9	25
10	2,625	0.5	4	25	296	53	56
11	3,235	0.5	9	26	538	53	60
12	1,494	0.5	7	27	253	36	18
13	1,490	19	29	28	384	26	34
14	646	0.5	1	29	422	46	50
15	1,055	64	20	30	202	60	65

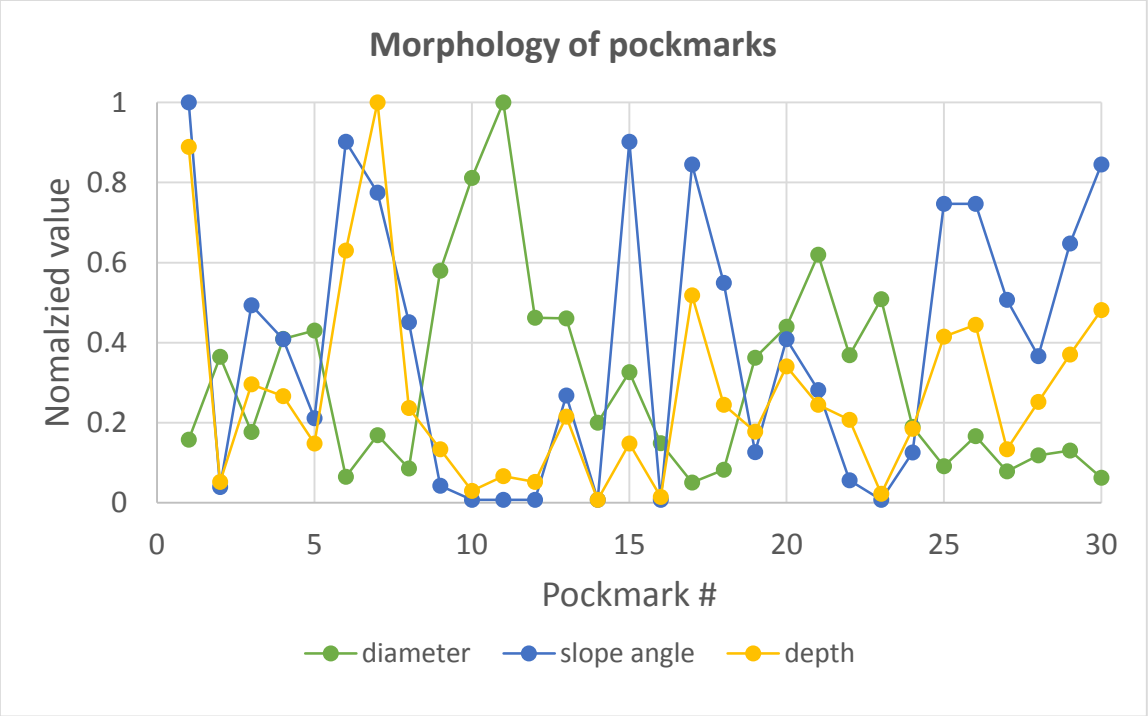

Figure 4.3. Curves that show the diameter, slope angle, and depth of the pockmarks normalized to the largest value in each category. This graph shows a correlation between the slope angle of the wall and the depth of the pockmarks, while the diameter appears to be not correlated to the other parameters.

Basinal setting

The basin deposits along southern side of Cay Sal Bank consists of a thick (300 ms TWT) package with parallel and continuous seismic reflector. The deposits thin to the north and south direction, creating a mounded morphology about 200 km long. To the east, the sediment package interfingers with the slope deposits of western Great Bahama Bank. These sediments downlap to a major seismic boundary (horizon B) to the north (Figure 4.4). This horizon B and the seismic terminations are not resolvable in the south because of poor seismic data quality, but the sediment package seems to downlap on to a lower horizon, which is assigned to horizon A (Figure 4.5). Wavy reflections are observed on all SW-NE

oriented seismic lines: BPC2011-11 (Figure 4.6) and BPC2011-17 (Figure 4.7). These wavy reflections are restricted to the basinal facies at ~650 ms (TWT). The elongated and mounded sediment package is interpreted as a drift deposit. This deposit is here called “Nicholas Drift” due to its location in the Nicholas Channel.

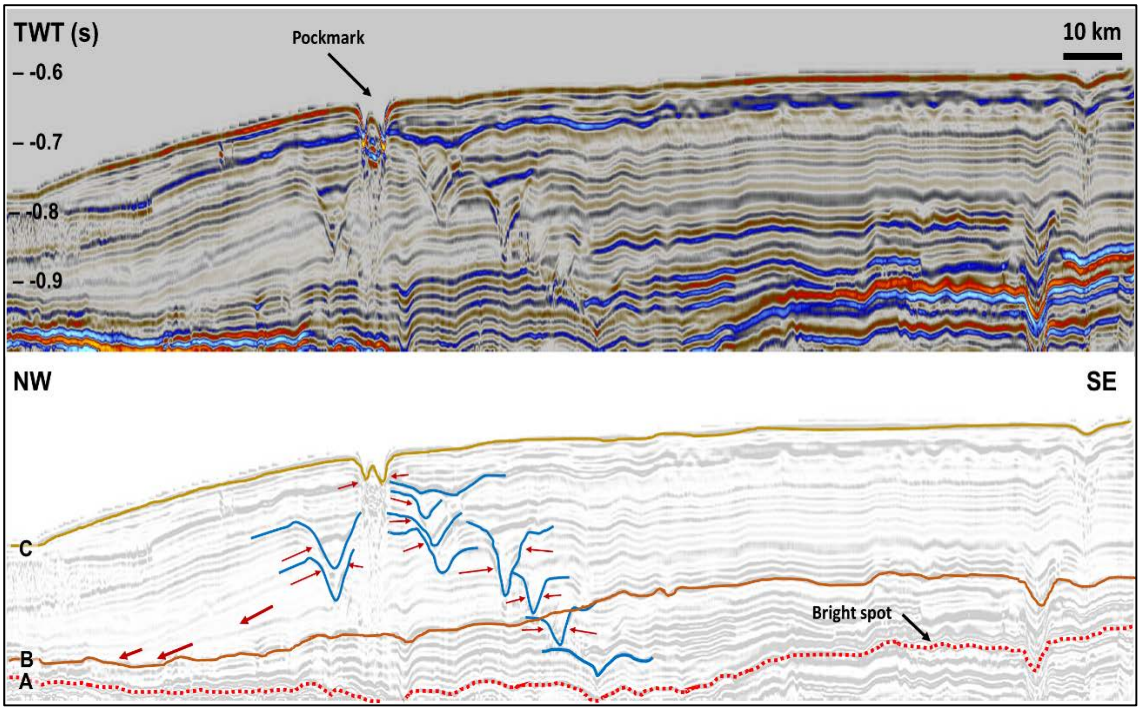

Figure 4.4. Seismic line BPC2011-12 showing the northern end of Nicholas Drift with buried pockmarks.

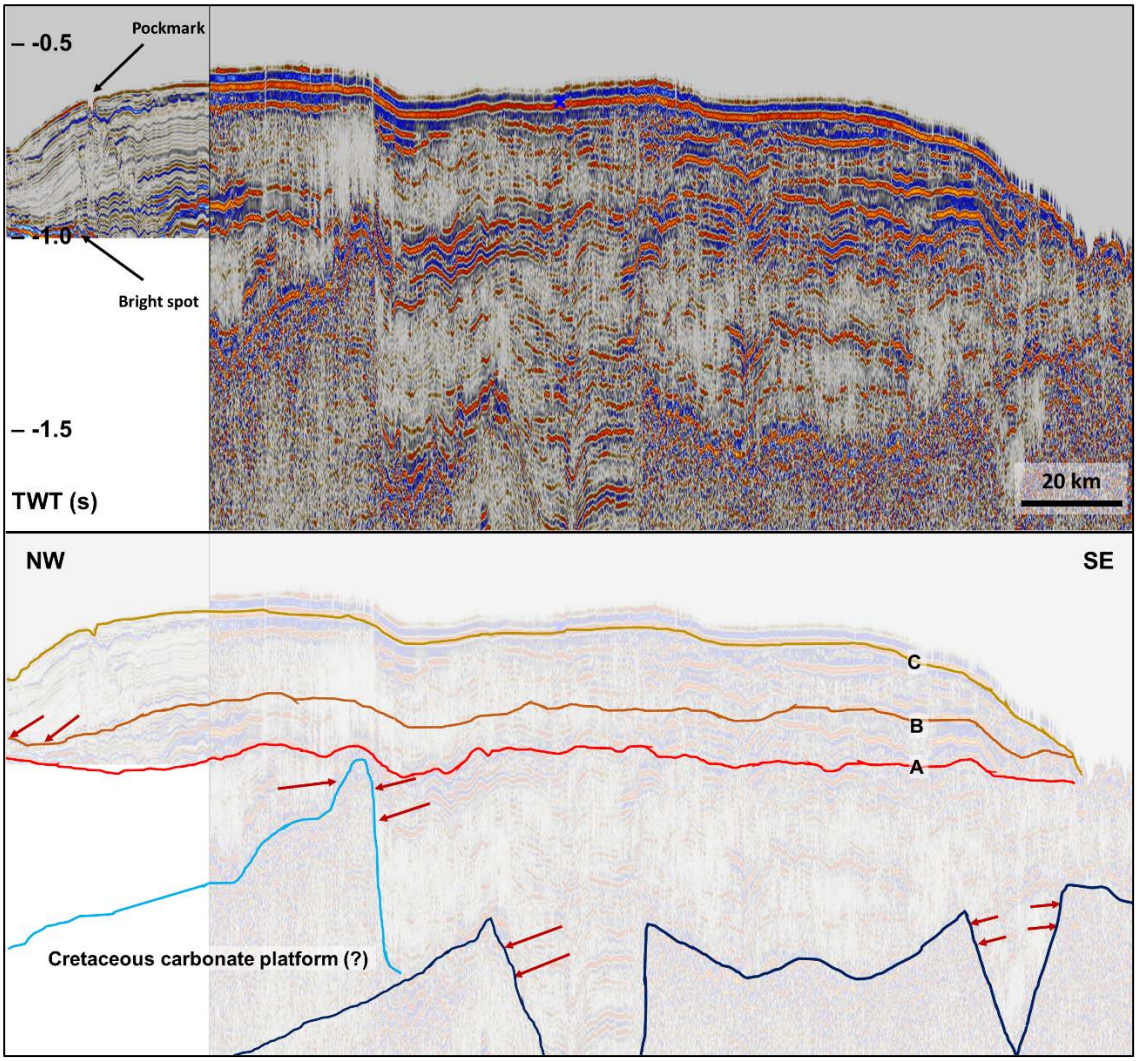

Figure 4.5. A composite figure of seismic lines BPC2011-12 and 16B showing the 200 km long Nicholas Drift that overlies a Cretaceous carbonate platform. Horizon A is the base of deposit that is also interpreted as bright spot similar to line BPC2011-11 and BPC2011-17 (Figure 4.6 and Figure 4.7). Another major seismic reflection, Horizon B, is a downlap surface (see Figure 4.4 for the expanded version). The seafloor is indicated as horizon C. See Figure 4.1 for lines location.

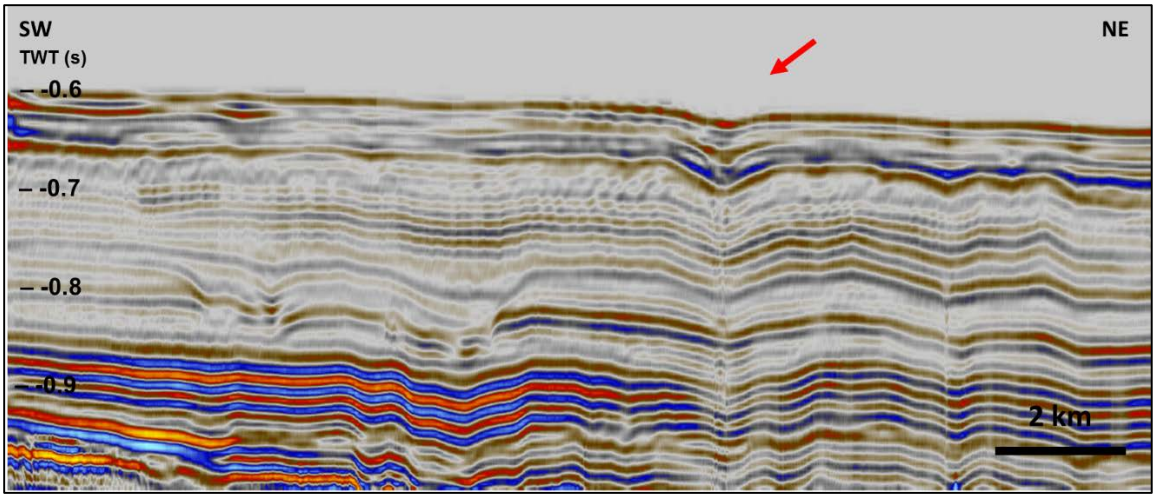

Figure 4.6. BPC2011-11 showing a gentle depression (pockmark no. 12) on the seafloor (see Figure 4.2 for location).

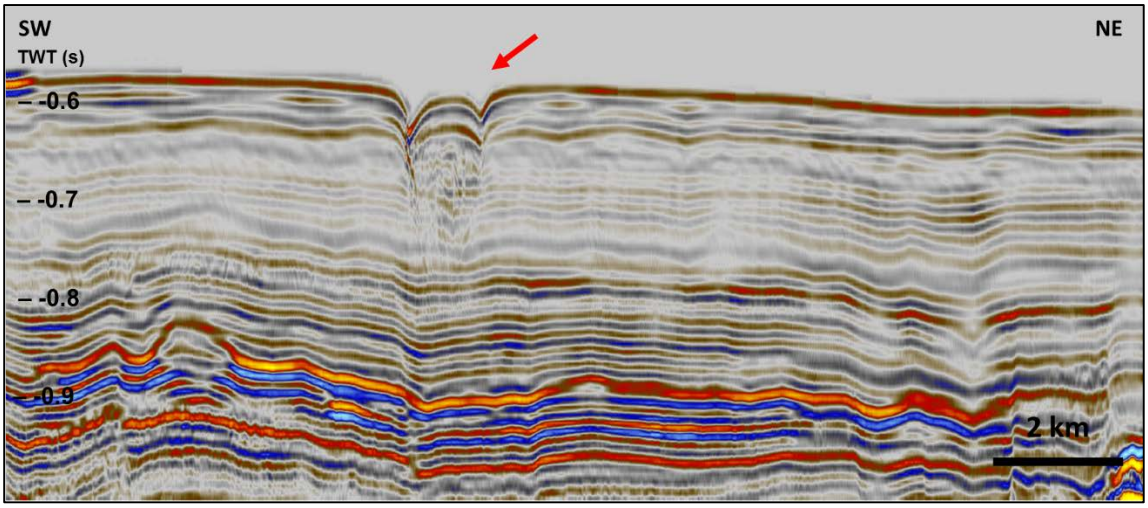

Figure 4.7. BPC2011-17 showing a pockmark (no. 21) with bright spot at ~0.9 s TWT, pull down, and gas chimney effect on a reflection indicating gas accumulation (see Figure 4.2 for location).

DISCUSSIONS

Age, sediment composition, and geochemistry of the drift deposit

The age model for the Cenozoic strata that was constructed by Masaferro et al. (1999) is used in this study. The base of Nicholas Drift deposit (Horizon A, Figure

4.4) is picked on a continuous reflection overlying an older basinal deposit that onlaps and eventually buries a shallow-water build-up. This shallow-water carbonate platform is inferred to be Cretaceous in age (Ball et al., 1985).

The inferred age of Horizon A is around 8.7 Ma. Horizon B, which is a downlap surface, is inferred to be 5.6 Ma. This horizon might be related to the hiatus that was reported by Masaferro et al. (1999). The age model shows that the Nicholas Drift is coeval with the deposition of the Santaren Drift reported by Anselmetti et al. (2000) and Bergman (2005).

The nearest information for a drift deposit from the Florida-Bahamas region is from ODP Leg 166 site 1006. The ODP slope-to-basin transect penetrated the distal part of the Santaren Drift, west of GBB. In Hole 1006, 713 m of Pleistocene to Miocene drift sediments were recovered (Eberli et al., 1997a). The sediment is composed of pelagic- and platform-derived material with variable amount of fine-grained siliciclastics and evidence of pyritization (Eberli et al., 1997a). The Pleistocene units contain nannofossil ooze interbedded with siliciclastic clays and silts. The Pliocene and Miocene age unit is dominated by nannofossil ooze and chalk.

A significant amount of methane and hydrocarbon residue was recorded in the Santaren drift sediment (Eberli et al., 1997a). Methane gas was found in sediment of late Pliocene and older (Figure 4.8). Concentrations of heavier hydrocarbon (ethane and propane) were noted in the early Pliocene section. A higher ratio between the concentration of methane and ethane is suggestive of the presence of microbial activity. The interval with higher biogenic gas generation coincides

with the higher seismic reflection (bright spot) at ~900 ms (TWT) (Figure 4.4, Figure 4.6, and Figure 4.7). Rock-eval pyrolysis indicates that the organic matter is not thermally mature. However, a heavier hydrocarbon chain is present, suggesting a migration from a deeper source (Eberli et al., 1997a).

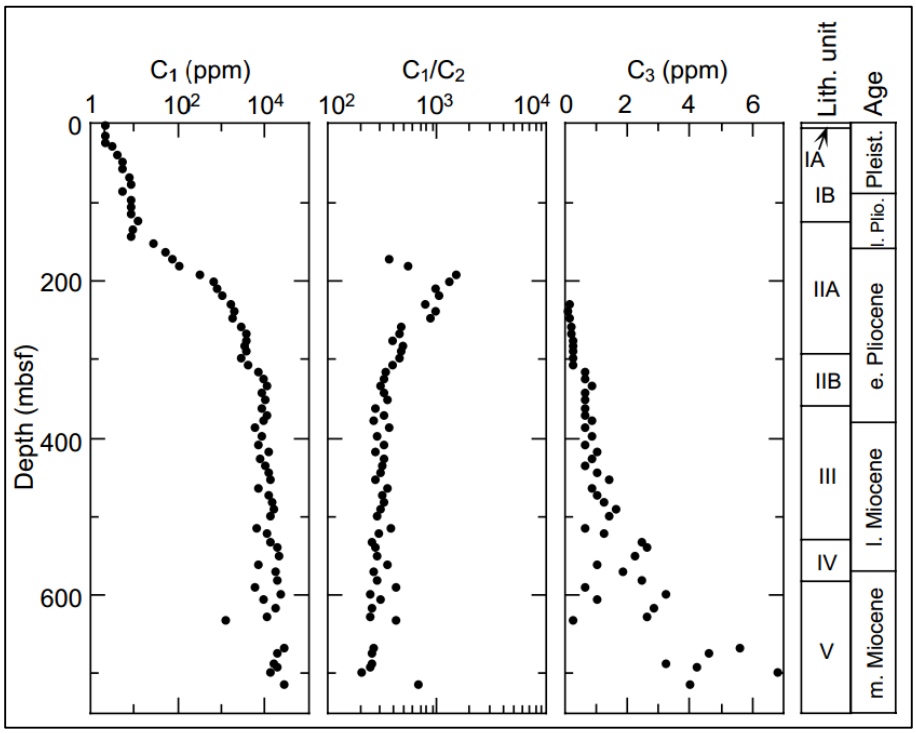

Figure 4.8. Concentration of methane, ratio of methane and ethane, and concentration of propane in ODP Leg 166 borehole 1006 on the drift deposit (Eberli et al., 1997a).

Compaction and overpressure

The focused expulsion of subsurface fluid to the sea-floor is controlled by many factors. The fluid may migrate through faults (e.g. Betzler et al., 2011) or diffuse through more permeable layers. Gay et al. (2006) proposed that the pockmarks in the Lower Congo Basin are closely related to the type of stratigraphic trap (e.g. turbidite channels) in the underlying strata.

Pockmarks in the study area are distributed in a northwest – southeast direction along the northern edge of Cuban thrust and fold belt. The sea floor where the pockmark field is located has a broad and broadly mounded topography. To the east, it is bounded by a ~70 m deeper sea-bottom in the axis of Old Bahama Channel. This elevated sea-floor is caused by the compression of a carbonate platform (see previous section).

There is a widespread occurrence of biogenic gas in the subsurface along the western GBB slope to basin floor transect. The amount of total organic carbon (TOC) generally decreases basinward (Eberli et al., 1997a). The biogenic gas is generated from organic matter oxidation through sulfate reduction, which is evident from the presence of H_2S gas (Kramer et al., 2000). They also suggested methane oxidation as an important mechanism for organic matters degradation. Low C_1/C_2 ratio in all ODP Leg 166 sites suggests the presence of thermogenic gas, although there are zones of high biogenic gas concentration in Site 1006 (drift deposit) and Site 1005 (upper slope) (Eberli et al., 1997a).

Despite of the gas accumulation across the slope to basin transect, mega-pockmarks in southwest GBB are restricted along the Cuban fold and thrust belt. This suggests that regional tectonics play an important role in their formation and distribution. We propose that the pockmarks genesis is related to overpressure caused by tectonic-generated stress.

Overpressure in sedimentary basin usually happens when sedimentation rate is high and permeability is low (i.e. fine-grained sediments), where the rate of porosity loss is higher than the compaction rate (Zoback, 2007). This leads to the

accumulation of pressure in the pore fluids. Many researchers have also shown that overpressure can be generated in compressional tectonic settings (e.g. Luo et al., 2007). The effect of tectonic stress which causes the rock to compact and prevents the fluid to escape is similar to the effect of overburden (Swarbrick and Osborne, 1998; Luo et al., 2007). For example, in 1983, an increase in groundwater discharge during an earthquake in Idaho was attributed to the release of stress which increased the pore pressure (Wood et al., 1985).

Unlike siliciclastic rocks, shallow-water carbonate rocks are known to have a non-linear relationship between sonic velocity, porosity, and depth. This relation is mainly controlled by the depositional lithology and diagenetic alteration (Anselmetti and Eberli, 2001). The same holds true for the permeability trend where pore type is the main controlling factor (Melim et al., 2001). Permeability of the Cretaceous chalk from the North Sea behaves similarly, where the onset of overpressure occurs at a depth 1200 to 1800 (Mallon et al., 2005).

CONCLUSIONS

This research reports the first discovery of mega-pockmarks in the Florida Straits. How exactly the local pore-pressure relation influences their distribution in the Bahamas is not yet understood. Episodic folding during the growth of Santaren anticline (Masaferro et al., 2002) might have induced the overpressure of biogenic gas within in the drift deposit. These pockmarks are likely the expression of hydrodynamic and pressure regime in the Cuba-Bahamas collision zone.

The occurrence of pockmarks is important in many aspects. Pockmarks have been linked to the slope instability (Dalla Valle and Gamberi, 2011). Slope failures along western slope of GBB might also be related to some type of fluid escape phenomenon.

CHAPTER 5. SUMMARY

The Bahamas is one of the best-studied modern carbonate platforms. The work presented here has contributed to new insights into the controls on the development of a carbonate slope. More specifically, the aim of this study was to characterize the modern slope morphology along southwestern Great Bahama Bank using high-resolution multibeam bathymetry and sub-bottom profile data and interpret the sedimentary processes.

The deep-water off southwestern Great Bahama Bank is divided into four physiographic environments: slope covered with off-bank sediment, toe-of-slope dominated by redeposited carbonates, basin floor with pelagic and drift deposits, and an elevated seafloor with pockmarks. The upper slope is characterized by a steep and furrowed wall, and onlapped by a sediment wedge. The wedge is composed of bank-top sediments that are transported through downslope currents. These currents erode the sediment wedge at its point of onlap and create a moat. Coarser-grained sediments bypass the slope through gullies and are deposited as slope apron and sediment lobes on the lower slope. This is known as line-sourced deposition in carbonates, that differentiates it from siliciclastics.

However, the spatial variability of the slope is mainly controlled by the instability of the margin and slope. The margin collapse feature is characterized by crooked and convex bankward margin morphology. In southwest Great Bahama Bank, 50% of the margin has collapsed, depositing mass transport complexes to the toe-of-slope

and basin floor. The mass transport complexes include mound and block fields, a channel-levee and fan system, and a channelized debris field. Failures on the lower slope are also observed. The margin and slope failures are likely triggered by both external and internal processes: earthquake and seismic shock, fracturing by sediment loading and compaction, and the presence of weak detachment layers. Based on relative succession, the margin collapse occurred before the platform flooding 7 kyr ago.

Ocean currents play an important role in the sedimentation of basinal sediments. Fluid movement and circulation promotes early cementation that produces hardgrounds and also winnows out finer sediments. Ocean currents that flow in the Old Bahama Channel carry sediment from the upstream and deposits them as contourites. Mega-pockmarks are embedded in the contourite. The pockmarks distribution is likely controlled by the subsurface pressure regime that is influenced by regional tectonics along the Cuba-Bahamas collision zone.

Sea level also plays an important role in the slope sedimentation. Platform-top sediment production is high during sea-level highstands. During previous sea-level highstands, high export of bank-top sediment to the adjacent deep-water may have promoted channelization. In the subsequent sea-level lowstand, the channels were starved and cemented in the marine environment. During the last seal-level highstand, channel deposition has reactivated, producing cut-and-fill morphology. The highstand deposits have also partly buried other previous lowstand deposits, such as the mass transport complexes. The variability of the carbonate slope is depicted in Figure 5.1.

The interplay of these sedimentary processes (downslope turbidity current, margin collapse, ocean current) produce a consistent sediment distribution pattern. The slope is covered with a 6 to 7 km-wide tract of homogeneous and muddy sediments. On the toe-of-slope, redeposited carbonates and coarse-grained sediments dominate. The toe-of-slope sediments transition into a muddy basin floor.

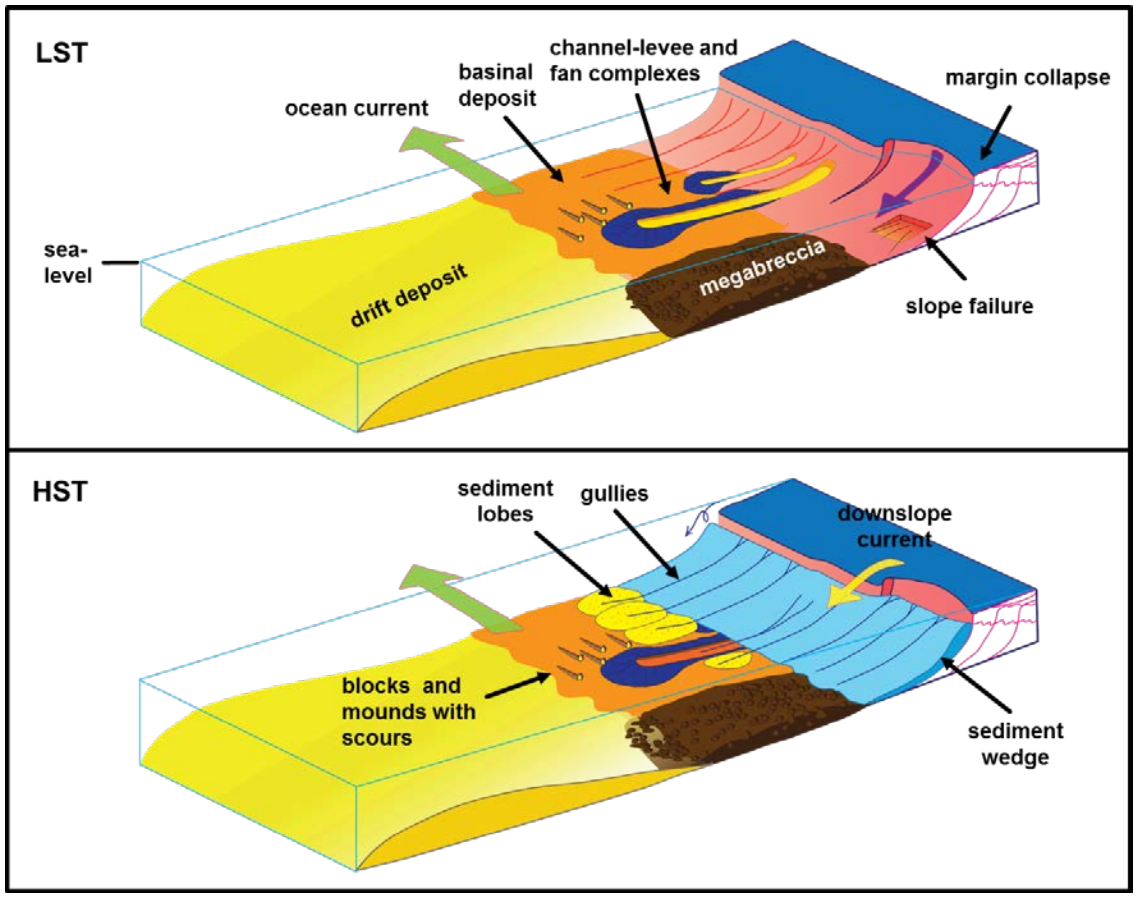

Figure 5.1. Slope development during sea-level lowstand (LST) and highstand (HST). During the LST, the slope experienced more erosion. Margin collapse caved off a large portion of the upper slope and produced megabreccia on the toe-of-slope. On the lower slope, slope failures and channel-levee and fan complexes formed. After the platform was flooded, sediments produced on the bank-top were exported to the adjacent slope and deposited as a sediment wedge. Coarse-grained sediments were bypassed and deposited as lobes. On the basin floor, ocean current winnows out the fines. The ocean current direction is indicated by scours adjacent to the mounds and the asymmetry of the channel levee. The ocean currents also carried sediments from the upstream and deposited them as a drift deposit.

REFERENCES

Anselmetti, F. S., and Eberli, G. P., 2001, Sonic velocity in carbonates; a combined product of depositional lithology and diagenetic alterations: Special Publication - Society for Sedimentary Geology, v. 70, p. 193-216.

Anselmetti, F. S., Eberli, G. P., and Ding, Z.-D., 2000, From the Great Bahama Bank into the Straits of Florida; a margin architecture controlled by sea-level fluctuations and ocean currents: Geological Society of America Bulletin, v. 112, no. 6, p. 829-844.

Atkinson, L. P., Berger, T., Hamilton, P., Waddell, E., Leaman, K., and Lee, T. N., 1995, Current meter observations in the Old Bahama Channel: Journal of Geophysical Research: Oceans, v. 100, no. C5, p. 8555-8560.

Austin, J. A., Jr., Schlager, W., Comet, P. A., Droxler, A. W., Eberli, G. P., Fourcade, E., Freeman-Lynde, R. P., Fulthorpe, C. S., Harwood, G., Kuhn, G., Lavoie, D., Leckie, R. M., Melillo, A. J., Moore, A., Mullins, H. T., Ravenne, C., Sager, W. W., Swart, P., Verbeek, J. W., Watkins, D. K., Williams, C., and Palmer, A. A., 1988, Leg 101; an overview: Proceedings of the Ocean Drilling Program, Scientific Results, v. 101, p. 455-472.

Ball, M. M., Martin, R. G., Bock, W. D., Sylwester, R. E., Bowles, R. M., Taylor, D., Coward, E. L., Dodd, J. E., and Gilbert, L., 1985, Seismic structure and stratigraphy of northern edge of Bahaman-Cuban collision zone: AAPG Bulletin, v. 69, no. 8, p. 1275-1294.

Bergman, K. L., 2005, Seismic analysis of paleocurrent features in the Florida Straits; insights into the paleo-Florida Current, upstream tectonics, and the Atlantic-Caribbean connection.

Bernet, K. H., Eberli, G. P., and Gilli, A., 2000, Turbidite frequency and composition in the distal part of the Bahamas transect: Proceedings of the Ocean Drilling Program, Scientific Results, v. 166, p. 45-60.

Betzler, C., Lindhorst, S., Huebscher, C., Luedmann, T., Fuerstenau, J., and Reijmer, J., 2011, Giant pockmarks in a carbonate platform (Maldives, Indian Ocean): Marine Geology, v. 289, no. 1-4, p. 1-16.

Betzler, C., Lindhorst, S., Lüdmann, T., Borstel v., F., Büld, M., Djamlan, E., Eberli, G., Eggers, D., Eversheim, J., Jentzen, A., Keizer, F., Ludwig, J., Möbius, J., Paulat, M., Reiche, S., Reijmer, J., Reolid, J., Schiebel, L., Schutter, I., Ulferts, L., Winter, S., Wolf, D., Wunsch, M., Rentsch, H., and Raeke, A., 2013, METEOR-Berichte Cruise Report CICARB

Blomeier, D. P. G., and Reijmer, J. J. G., 2002, Facies architecture of an Early Jurassic carbonate platform slope (Jbel Bou Dahar, High Atlas, Morocco): Journal of Sedimentary Research, v. 72, no. 4, p. 462-475.

Boardman, M. R., and Neumann, A. C., 1984, Sources of periplatform carbonates; Northwest Providence Channel, Bahamas: Journal of Sedimentary Petrology, v. 54, no. 4, p. 1110-1123.

Chakraborty, B., Schenke, H. W., Kodagali, V., and Hagen, R., 2000, Seabottom characterization using multibeam echosounder angular backscatter; an application of the composite roughness theory: IEEE Transactions on Geoscience and Remote Sensing, v. 38, no. 5, Part 2, p. 2419-2422.

Collins, J. F., Kenter, J. A. M., Harris, P. M., Kuanysheva, G., Fischer, D. J., and Steffen, K. L., 2006, Facies and reservoir-quality variations in the late Visean to Bashkirian outer platform, rim, and flank of the Tengiz buildup, Precaspian Basin, Kazakhstan, *in* Harris, P. M., and Weber, L. J., eds., Giant hydrocarbon reservoirs of the world: From rocks to reservoir characterization and modeling, Volume AAPG Memoir 88/SEPM Special Publication, p. 55-95.

Coniglio, M., and Dix, G. R., 1992, Carbonate slopes: Canada, Geological Association of Canada : St. Johns, NL, Canada, p. 349-373.

Cook, H. E., McDaniel, P. N., Mountjoy, E. W., and Pray, L. C., 1972, Allochthonous carbonate debris flows at Devonian bank ('reef') margins, Alberta, Canada: Bulletin of Canadian Petroleum Geology, v. 20, no. 3, p. 439-486.

Correa, T. B. S., Eberli, G. P., Grasmueck, M., Reed, J. K., and Correa, A. M. S., 2012a, Genesis and morphology of cold-water coral ridges in a unidirectional current regime: Marine Geology, v. 326, p. 14-27.

Correa, T. B. S., Grasmueck, M., Eberli, G. P., Reed, J. K., Verwer, K., and Purkis, S., 2012b, Variability of cold-water coral mounds in a high sediment input and tidal current regime, Straits of Florida: Sedimentology, v. 59, no. 4, p. 1278-1304.

Crevello, P. D., and Schlager, W., 1980, Carbonate debris sheets and turbidites, Exuma Sound, Bahamas: Journal of Sedimentary Petrology, v. 50, no. 4, p. 1121-1147.

Dalla Valle, G., and Gamberi, F., 2011, Pockmarks and seafloor instability in the Olbia continental slope (northeastern Sardinian margin, Tyrrhenian Sea): Marine Geophysical Research, v. 32, no. 1-2, p. 193-205.

Davis, R. A., 1983, Sediment gravity flow deposition on a modern carbonate slope apron; northern Little Bahama Bank: AAPG Bulletin, v. 67, no. 3, p. 447-447.

Droxler, A. W., and Schlager, W., 1985, Glacial versus interglacial sedimentation rates and turbidite frequency in the Bahamas: Geology [Boulder], v. 13, no. 11, p. 799-802.

Droxler, A. W., Schlager, W., and Whallon, C. C., 1983, Quaternary aragonite cycles and oxygen-isotope record in Bahamian carbonate ooze: Geology [Boulder], v. 11, no. 4, p. 235-239.

Eberli, G. P., 1988, Physical properties of carbonate turbidite sequences surrounding the Bahamas; implications for slope stability and fluid movements: Proceedings of the Ocean Drilling Program, Scientific Results, v. 101, p. 305-314.

Eberli, G. P., and Ginsburg, R. N., 1987, Segmentation and coalescence of Cenozoic carbonate platforms, northwestern Great Bahama Bank: Geology [Boulder], v. 15, no. 1, p. 75-79.

-, 1989, Cenozoic progradation of northwestern Great Bahama Bank, a record of lateral platform growth and sea-level fluctuations: Special Publication - Society of Economic Paleontologists and Mineralogists, v. 44, p. 339-351.

Eberli, G. P., Swart, P. K., Malone, M. J., Anselmetti, F. S., Arai, K., Bernet, K. H., Betzler, C., Christensen, B. A., De Carlo, E., Dejardin, P. M., Emmanuel, L., Frank, T. D., Haddad, G. A., Isern, A. R., Katz, M. E., Kenter, J. A. M., Kramer, P. A., Kroon, D., McKenzie, J. A., McNeill, D. F., Montgomery, P., Nagihara, S., Pirmez, C., Reijmer, J. J. G., Sato, T., Schovsbo, N. H., Williams, T., Wright, J. D., and Marin, J. A., 1997a, Proceedings of the Ocean Drilling Program, initial reports; Bahamas Transect, covering Leg 166 of the cruises of the Drilling Vessel JOIDES Resolution, San Juan, Puerto Rico, to Balboa Harbor, Panama, sites 1003-1009, 17 February-10 April 1, Volume 166: United States, Texas A & M University, Ocean Drilling Program : College Station, TX, United States.

Eberli, G. P., Swart, P. K., Malone, M. J., Anselmetti, F. S., Arai, K., Bernet, K. H., Betzler, C., Christensen, B. A., De Carlo, E. H., Dejardin, P. M., Emmanuel, L., Frank, T. D., Haddad, G. A., Isern, A. R., Katz, M. E., Kenter, J. A. M., Kramer, P. A., Kroon, D., McKenzie, J. A., McNeill, D. F., Montgomery, P., Nagihara, S., Pirmez, C., Reijmer, J. J. G., Sato, T., Schovsbo, N. H., Williams, T., and Wright, J. D., 1997b, Site 1005: Proceedings of the Ocean Drilling Program, Part A: Initial Reports, v. 166, p. 171-232.

Enos, P., 1973, Channelized submarine carbonate-debris flow, Cretaceous, Mexico: American Association of Petroleum Geologists Bulletin, v. 57, no. 4, p. 777-777.

Frost, E. L., and Kerans, C., 2010, Controls on syndepositional fracture patterns, Devonian reef complexes, Canning Basin, Western Australia: Journal of Structural Geology, v. 32, no. 9, p. 1231-1249.

Gay, A., Lopez, M., Cochonat, P., Levache, D., Sermondadaz, G., and Seranne, M., 2006, Evidences of early to late fluid migration from an upper Miocene turbiditic channel revealed by 3D seismic coupled to geochemical sampling within seafloor pockmarks, Lower Congo Basin: Marine and Petroleum Geology, v. 23, no. 3, p. 387-399.

Ginsburg, R. N., Harris, P., Eberli, G., and Swart, P. K., 1991, The growth potential of a bypass margin, Great Bahama Bank: Journal of Sedimentary Research, v. 61, no. 6, p. 976-987.

Grammer, G. M., Crescini, C. M., McNeill, D. F., and Taylor, L. H., 1999, Quantifying rates of syndepositional marine cementation in deeper platform environments-new

insight into a fundamental process: Journal of Sedimentary Research, v. 69, no. 1, p. 202-207.

Grammer, G. M., and Ginsburg, R. N., 1992, Highstand versus lowstand deposition on carbonate platform margins; insight from Quaternary foreslopes in the Bahamas: Marine Geology, v. 103, no. 1-3, p. 125-136.

Grammer, G. M., Ginsburg, R. N., and Harris, P. M., 1993, Timing of deposition, diagenesis, and failure of steep carbonate slopes in response to a high-amplitude/high-frequency fluctuation in sea level, Tongue of the Ocean, Bahamas: AAPG Memoir, v. 57, p. 107-131.

Grammer, G. M., Harris, P. M., and Eberli, G. P., 2001, Carbonate platforms; exploration- and production-scale insight from modern analogs in the Bahamas: Leading Edge [Tulsa, OK], v. 20, no. 3, p. 252.

Grasmueck, M., Eberli, G. P., Viggiano, D. A., Correa, T., Rathwell, G., and Luo, J., 2006, Autonomous underwater vehicle (AUV) mapping reveals coral mound distribution, morphology, and oceanography in deep water of the Straits of Florida: Geophysical Research Letters, v. 33, no. 23.

Hamilton, P., Larsen, J. C., Leaman, K. D., Lee, T. N., and Waddell, E., 2005, Transports through the Straits of Florida: Journal of Physical Oceanography, v. 35, no. 3, p. 308-322.

Harwood, G. M., and Towers, P. A., 1988, Seismic sedimentologic interpretation of a carbonate slope, north margin of Little Bahama Bank: Proceedings of the Ocean Drilling Program, Scientific Results, v. 101, p. 263-277.

Hilbrecht, H., 1989, Redeposition of Late Cretaceous pelagic sediments controlled by sea-level fluctuations: Geology [Boulder], v. 17, no. 12, p. 1072-1075.

Hine, A. C., Locker, S. D., Tedesco, L. P., Mullins, H. T., Hallock, P., Belknap, D. F., Gonzales, J. L., Neumann, A. C., and Snyder, S. W., 1992, Megabreccia shedding from modern, low-relief carbonate platforms, Nicaraguan Rise: Geological Society of America Bulletin, v. 104, no. 8, p. 928-943.

Hovland, M., Gardner, J. V., and Judd, A. G., 2002, The significance of pockmarks to understanding fluid flow processes and geohazards: Geofluids, v. 2, no. 2, p. 127-136.

James, N. P., 1981, Megablocks of calcified algae in the Cow Head breccia, western Newfoundland; vestiges of a Cambro-Ordovician platform margin: Geological Society of America Bulletin, v. 92, no. 11, p. I799-i811.

Janson, X., Kerans, C., Loucks, R., Marhx, M. A., Reyes, C., and Murguia, F., 2011, Seismic architecture of a Lower Cretaceous platform-to-slope system, Santa Agueda and Poza Rica Fields, Mexico: AAPG Bulletin, v. 95, no. 1, p. 105-146.

Jordan, G. F., 1954, Large sink holes in Straits of Florida: Bulletin of the American Association of Petroleum Geologists, v. 38, no. 8, p. 1810-1817.

Jordan, G. F., Malloy, R. J., and Kofoed, J. W., 1964, Bathymetry and geology of Pourtales Terrace, Florida: Marine Geology, v. 1, no. 3, p. 259-287.

Kenter, J. A. M., 1990, Carbonate platform flanks; slope angle and sediment fabric: Sedimentology, v. 37, no. 5, p. 777-794.

Kenter, J. A. M., Ginsburg, R. N., and Troelstra, S. R., 2001, Sea-level-driven sedimentation patterns on the slope and margin: Special Publication - Society for Sedimentary Geology, v. 70, p. 61-100.

King, L. H., and MacLean, B., 1970, Pockmarks on the Scotian shelf: Geological Society of America Bulletin, v. 81, no. 10, p. 3141-3148.

Kramer, P. A., Swart, P. K., De Carlo, E. H., and Schovsbo, N. H., 2000, Overview of interstitial fluid and sediment geochemistry, sites 1003-1007 (Bahamas Transect): Proceedings of the Ocean Drilling Program, Scientific Results, v. 166, p. 179-195.

Ladd, J. W., and Sheridan, R. E., 1987, Seismic stratigraphy of the Bahamas: AAPG Bulletin, v. 71, no. 6, p. 719-736.

Land, L. A., and Paull, C. K., 2000, Submarine karst belt rimming the continental slope in the Straits of Florida: Geo-Marine Letters, v. 20, no. 2, p. 123-132.

Land, L. A., Paull, C. K., and Hobson, B., 1995, Genesis of a submarine sinkhole without subaerial exposure; Straits of Florida: Geology [Boulder], v. 23, no. 10, p. 949-951.

Leaman, K. D., Molinari, R. L., and Vertes, P. S., 1987, Structure and Variability of the Florida Current at 27°N: April 1982–July 1984: Journal of Physical Oceanography, v. 17, no. 5, p. 565-583.

Loseth, H., Gading, M., and Wensaas, L., 2009, Hydrocarbon leakage interpreted on seismic data: Marine and Petroleum Geology, v. 26, no. 7, p. 1304-1319.

Luo, X., Wang, Z., Zhang, L., Yang, W., and Liu, L., 2007, Overpressure generation and evolution in a compressional tectonic setting, the southern margin of Junggar Basin, northwestern China: AAPG Bulletin, v. 91, no. 8, p. 1123-1139.

Mallon, A. J., Swarbrick, R. E., and Katsube, T. J., 2005, Permeability of fine-grained rocks; new evidence from chalks: Geology [Boulder], v. 33, no. 1, p. 21-24.

Malone, M. J., Slowey, N. C., and Henderson, G. M., 2001, Early diagenesis of shallow-water periplatform carbonate sediments, leeward margin, Great Bahama Bank (Ocean Drilling Program Leg 166): Geological Society of America Bulletin, v. 113, no. 7, p. 881-894.

Masaferro, J. L., Bulnes, M., Poblet, J., and Eberli, G. P., 2002, Episodic folding inferred from syntectonic carbonate sedimentation; the Santaren Anticline, Bahamas Foreland: Sedimentary Geology, v. 146, no. 1-2, p. 11-24.

Masaferro, J. L., and Eberli, G. P., 1999, Jurassic-Cenozoic structural evolution of the southern Great Bahama Bank: Sedimentary Basins of the World, v. 4, p. 167-193.

Masaferro, J. L., Poblet, J., Bulnes, M., Eberli, G. P., Dixon, T. H., and McClay, K., 1999, Palaeogene-Neogene/present day(?) growth folding in the Bahamian foreland of the Cuban fold and thrust belt: Journal of the Geological Society of London, v. 156, Part 3, p. 617-631.

McAdoo, B. G., Pratson, L. F., and Orange, D. L., 2000, Submarine landslide geomorphology, US continental slope: Marine Geology, v. 169, no. 1-2, p. 103-136.

McIlreath, I. A., and James, N. P., 1978, Facies models; 13, Carbonate slopes: Geoscience Canada, v. 5, no. 4, p. 189-199.

McNeill, D. F., and Eberli, G. P., 2009, Early load-induced fracturing in a prograding carbonate margin: Special Publication of the International Association of Sedimentologists, v. 41, p. 327-336.

Melim, L. A., Anselmetti, F. S., and Eberli, G. P., 2001, The importance of pore type on permeability of Neogene carbonates, Great Bahama Bank: Special Publication - Society for Sedimentary Geology, v. 70, p. 217-238.

Meyerhoff, A. A., and Hatten, C. W., 1973, Bahamas Salient of North America; Tectonic Framework, Stratigraphy, and Petroleum Potential: American Association of Petroleum Geologists Bulletin, v. 57, no. 10, p. 2148-2148.

Morsilli, M., Rusciadelli, G., and Bosellini, A., 2002, Large-scale gravity-driven structures; control on margin architecture and related deposits of a Cretaceous carbonate platform (Montagna della Maiella, Central Apennines, Italy): Bollettino della Societa Geologica Italiana. Volume Speciale, v. 1, Part II, p. 619-628.

Mulder, T., Ducassou, E., Eberli, G. P., Hanquiez, V., Gonthier, E., Kindler, P., Principaud, M., Fournier, F., Leonide, P., Billeaud, I., Marsset, B., Reijmer, J. J. G., Bondu, C., Joussiaume, R., and Pakiades, M., 2012a, New insights into the morphology and sedimentary processes along the western slope of Great Bahama Bank: Geology [Boulder], v. 40, no. 7, p. 603-606.

Mulder, T., Ducassou, E., Gillet, H., Hanquiez, V., Tournadour, E., Combes, J., Eberli, G. P., Kindler, P., Gonthier, E., Conesa, G., Robin, C., Sianipar, R., Reijmer, J. J. G., and Francois, A., 2012b, Canyon morphology on a modern carbonate slope of the Bahamas; evidence of regional tectonic tilting: Geology [Boulder], v. 40, no. 9, p. 771-774.

Mullins, H. T., Dolan, J. F., Breen, N. A., Andersen, C. B., Gaylord, M., Petruccione, J. L., Wellner, R. W., Melillo, A. J., and Jurgens, A. D., 1991, Retreat of carbonate platforms; response to tectonic processes: Geology [Boulder], v. 19, no. 11, p. 1089-1092.

Mullins, H. T., Gardulski, A. F., and Hine, A. C., 1986, Catastrophic collapse of the West Florida carbonate platform margin: Geology [Boulder], v. 14, no. 2, p. 167-170.

Mullins, H. T., Heath, K. C., Van Buren, H. M., and Newton, C. R., 1984, Anatomy of a modern open-ocean carbonate slope; northern Little Bahama Bank: Sedimentology, v. 31, no. 2, p. 141-168.

Mullins, H. T., and Hine, A. C., 1989, Scalloped bank margins; begining of the end for carbonate platforms?: Geology [Boulder], v. 17, no. 1, p. 30-33.

Mullins, H. T., and Neumann, A. C., 1979, Deep carbonate bank margin structure and sedimentation in the northern Bahamas: Special Publication - Society of Economic Paleontologists and Mineralogists, no. 27, p. 165-192.

Mullins, H. T., Neumann, A. C., Wilber, R. J., and Boardman, M. R., 1980a, Nodular carbonate sediment on Bahamian slopes; possible precursors to nodular limestones: Journal of Sedimentary Petrology, v. 50, no. 1, p. 117-131.

Mullins, H. T., Neumann, A. C., Wilber, R. J., Hine, A. C., and Chinburg, S. J., 1980b, Carbonate sediment drifts in northern Straits of Florida: AAPG Bulletin, v. 64, no. 10, p. 1701-1717.

Neumann, A. C., and Land, L. S., 1975, Lime mud deposition and calcareous algae in the Bight of Abaco, Bahamas; a budget: Journal of Sedimentary Petrology, v. 45, no. 4, p. 763-786.

Normark, W. R., Hess, G. R., Stow, D. A. V., and Bowen, A. J., 1980, Sediment waves on the Monterey Fan levee; a preliminary physical interpretation: Marine Geology, v. 37, no. 1-2, p. 1-18.

Payros, A., and Pujalte, V., 2008, Calciclastic submarine fans; an integrated overview: Earth-Science Reviews, v. 86, no. 1-4, p. 203-246.

Pickrill, R. A., 1993, Shallow seismic stratigraphy and pockmarks of a hydrothermally influenced lake, Lake Rotoiti, New Zealand: Sedimentology, v. 40, no. 5, p. 813-828.

Pilskaln, C. H., Neumann, A. C., and Bane, J. M., 1989, Periplatform carbonate flux in the northern Bahamas: Deep-Sea Research. Part A: Oceanographic Research Papers, v. 36, no. 9, p. 1391-1406.

Pindell, J. L., 1993, Regional synopsis of Gulf of Mexico and Caribbean evolution: Program and Abstracts - Society of Economic Paleontologists. Gulf Coast Section. Research Conference, v. 13, p. 251-274.

Playford, P. E., 1980, Devonian 'great barrier reef' of Canning Basin, Western Australia: AAPG Bulletin, v. 64, no. 6, p. 814-840.

Playton, T. E., Janson, X., and Kerans, C., 2010, Carbonate Slopes, *in* James, N. P., and Dalrymple, R. W., eds., Facies Models 4: St. Johns, Newfoundland, Canada, Geological Association of Canada, p. 449-476.

Rankey, E. C., and Doolittle, D. F., 2012, Geomorphology of carbonate platform-marginal uppermost slopes; insights from a Holocene analogue, Little Bahama Bank, Bahamas: Sedimentology, v. 59, no. 7, p. 2146-2171.

Rendle, R. H., and Reijmer, J. J. G., 2002, Quaternary slope development of the western, leeward margin of the Great Bahama Bank: Marine Geology, v. 185, no. 1-2, p. 143-164.

Richardson, W. S., Schmitz, W. J., Jr, and Niiler, P. P., 1969, The velocity Structure of the Florida Current from the Straits of Florida to Cape Fear: Deep Sea Research, v. 16, p. 225-231.

Robb, J. M., 1990, Groundwater processes in the submarine environment: Special Paper - Geological Society of America, v. 252, p. 267-281.

Roth, S., and Reijmer, J. J. G., 2004, Holocene Atlantic climate variations deduced from carbonate periplatform sediments (leeward margin, Great Bahama Bank): Paleoceanography, v. 19, no. 1.

Rothwell, R. G., Thomas, J., and Kaehler, G., 1998, Low-sea-level emplacement of very large late Pleistocene 'megaturbidite' in the Western Mediterranean Sea: Nature [London], v. 392, no. 6674, p. 377-380.

Sarg, J., 1988, Carbonate sequence stratigraphy: Sea-Level Changes: An Integrated Approach: SEPM, Special Publication, v. 42, p. 155-181.

Schlager, W., and Camber, O., 1986, Submarine slope angles, drowning unconformities, and self-erosion of limestone escarpments: Geology [Boulder], v. 14, no. 9, p. 762-765.

Schlager, W., and Chermak, A., 1979, Sediment facies of platform-basin transition, Tongue of the Ocean, Bahamas: Special Publication - Society of Economic Paleontologists and Mineralogists, no. 27, p. 193-208.

Schlager, W., and Ginsburg, R. N., 1981, Bahama carbonate platforms; the deep and the past: Marine Geology, v. 44, no. 1-2, p. 1-24.

Schlager, W., Reijmer, J. J. G., and Droxler, A., 1994, Highstand shedding of carbonate platforms: Journal of Sedimentary Research, Section B: Stratigraphy and Global Studies, v. 64, no. 3, p. 270-281.

Slowey, N. C., Wilber, R. J., Haddad, G. A., and Henderson, G. M., 2002, Glacial-to-Holocene sedimentation on the western slope of Great Bahama Bank: Marine Geology, v. 185, no. 1-2, p. 165-176.

Spence, G. H., and Tucker, M. E., 1997, Genesis of limestone megabreccias and their significance in carbonate sequence stratigraphic models; a review: Sedimentary Geology, v. 112, no. 3-4, p. 163-193.

Swarbrick, R. E., and Osborne, M. J., 1998, Mechanisms that generate abnormal pressures; an overview: AAPG Memoir, v. 70, p. 13-34.

Vaular, E. N., Barth, T., and Haflidason, H., 2010, The geochemical characteristics of the hydrate-bound gases from the Nyegga pockmark field, Norwegian Sea: Organic Geochemistry, v. 41, no. 5, p. 437-444.

Walles, F. E., 1993, Tectonic and diagenetically induced seal failure within the south-western Great Bahamas Bank: Marine and Petroleum Geology, v. 10, no. 1, p. 14-28.

Wilber, R. J., Milliman, J. D., and Halley, R. B., 1990, Accumulation of bank-top sediment on the western slope of Great Bahama Bank; rapid progradation of a carbonate megabank: Geology [Boulder], v. 18, no. 10, p. 970-974.

Wilber, R. J., Whitehead, J. A., Halley, R. B., and Milliman, J. D., 1993, Carbonate-periplatform sedimentation by density flows; a mechanism for rapid off-bank and vertical transport of shallow-water fines: Comment: Geology [Boulder], v. 21, no. 7, p. 667-668.

Wilson, P. A., and Roberts, H. H., 1992, Carbonate-periplatform sedimentation by density flows; a mechanism for rapid off-bank and vertical transport of shallow-water fines: Geology [Boulder], v. 20, no. 8, p. 713-716.

-, 1993, Carbonate-periplatform sedimentation by density flows; a mechanism for rapid off-bank and vertical transport of shallow-water fines: Reply: Geology [Boulder], v. 21, no. 7, p. 668-669.

-, 1995, Density cascading; off-shelf sediment transport, evidence and implications, Bahama Banks: Journal of Sedimentary Research, Section A: Sedimentary Petrology and Processes, v. 65, no. 1, p. 45-56.

Wood, S. H., Wurts, C., Lane, T. G., Ballenger, N., Shalleen, M., Totorica, D., and Waag, C., 1985, Increased groundwater discharge caused by the 1983 Idaho (USA) earthquake: Memoires - Association Internationale des Hydrogeologues = Memoires - International Association of Hydrogeologists, v. 17, no. 1, p. 741-751.

Wynn, R. B., and Stow, D. A. V., 2002, Classification and characterisation of deep-water sediment waves: Marine Geology, v. 192, no. 1-3, p. 7-22.

Zoback, M. D., 2007, Reservoir geomechanics, United States, Cambridge University Press : New York, NY, United States.